Journal Pre-proof

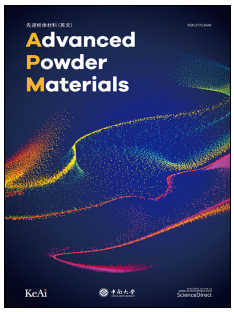

Process–Structure–Property Relationships in Low-Temperature Microwave Dielectric Ceramics: From Glass-Assisted Sintering to Cold Sintering for 5G/6G Devices.

Phieraya Pulphol, Ying Tang, Liang Fang, Wanwilai Vittayakorn, Usa Sukkha, Sugato Hajra, Hoe Joon Kim, Naratip Vittayakorn, Tosapol Maluangnont

PII: S2772-834X(26)00052-7

DOI: https://doi.org/10.1016/j.apmate.2026.100444

Reference: APMATE 100444

To appear in: *Advanced Powder Materials*

Received Date: 31 March 2026

Revised Date: 13 June 2026

Accepted Date: 15 June 2026

Please cite this article as: P. Pulphol, Y. Tang, L. Fang, W. Vittayakorn, U. Sukkha, S. Hajra, H.J. Kim, N. Vittayakorn, T. Maluangnont, Process–Structure–Property Relationships in Low-Temperature Microwave Dielectric Ceramics: From Glass-Assisted Sintering to Cold Sintering for 5G/6G Devices., *Advanced Powder Materials*, https://doi.org/10.1016/j.apmate.2026.100444.

Process–Structure–Property Relationships in Low-Temperature Microwave Dielectric Ceramics: From Glass-Assisted Sintering to Cold Sintering for 5G/6G Devices.

Phieraya Pulphol[a,b,c], Ying Tang[c], Liang Fang[c], Wanwilai Vittayakorn[b,d], Usa Sukkha[b,e], Sugato Hajra[f], Hoe Joon Kim[g], Naratip Vittayakorn[b,h]* and Tosapol Maluangnont[b,d]

[a]Department of Materials Science, Faculty of Science, Srinakharinwirot University, Bangkok 10110, Thailand

[b]Advanced Materials Research Unit, School of Science, King Mongkut's Institute of Technology Ladkrabang, Bangkok 10520, Thailand

[c]Guangxi Universities Key Laboratory of Non-Ferrous Metal Oxide Electronic Functional Materials and Devices, Guangxi Key Laboratory of Optical and Electronic Materials and Devices, College of Material Science and Engineering, Guilin University of Technology, Guilin 541004, China

[d]Department of Nanoscience and Nanotechnology, School of Integrated Innovative Technology, King Mongkut's Institute of Technology Ladkrabang, Bangkok 10520, Thailand

[e]Department of General Science and Liberal Arts, King Mongkut's Institute of Technology Ladkrabang, Prince of Chumphon Campus, Chumphon, 86160, Thailand

[f]Department of Electrical Engineering and Computer Science, Daegu Gyeongbuk Institute of Science & Technology (DGIST), Daegu 42988, South Korea

[g]Department of Robotics and Mechatronics Engineering, Daegu Gyeongbuk Institute of Science & Technology (DGIST), Daegu, South Korea

[h]Department of Chemistry, School of Science, King Mongkut's Institute of Technology Ladkrabang, Bangkok 10520, Thailand

* Corresponding author. E-mail: *naratip.vi@kmitl.ac.th*

Author(s) information

	**Dr. Phieraya Pulphol** is a Lecturer in the Department of Materials Science at Srinakharinwirot University, Thailand. She received her Ph.D. in Nanoscience and Nanotechnology from King Mongkut's Institute of Technology Ladkrabang in 2021. Her research focuses on microwave dielectric ceramics, cold sintering processes, and composite ceramics. She has published extensively on dielectric ceramics and functional materials.
	**Dr. Ying Tang** is a Professor at the School of Physics and Electronic Information Engineering, Guilin University of Technology, China. She received her Ph.D. in Metallurgical Engineering from University of Science and Technology Beijing in 2021. Her research focuses on microwave dielectric ceramics, particularly composition design, structure–property relationships, dielectric polarization mechanisms, and temperature-stable materials for advanced communication technologies. She has led several research projects supported by national and regional funding agencies. Dr. Tang has published extensively and contributed to the development of high-performance microwave dielectric materials for next-generation electronic applications.
	**Dr. Liang Fang** is a Professor at Guilin University of Technology, China, and holds a joint appointment at the State Key Laboratory of Advanced Technology for Materials Synthesis and Processing, Wuhan University of Technology. His research focuses on microwave dielectric ceramics, lead-free ferroelectric materials, and composite microwave absorbing materials. He has led numerous projects funded by the National Natural Science Foundation of China and has published extensively on structure-property relationships in dielectric ceramics and garnet materials.
	**Dr. Wanwilai Vittayakorn** is an Associate Professor in the Department of Nanoscience and Nanotechnology, School of Integrated Innovative Technology, King Mongkut's Institute of Technology Ladkrabang, Bangkok, Thailand. She received her Ph.D. from Chiang Mai University, Thailand, and is currently a lecturer in the Department of Nanoscience and Nanotechnology, School of Integrated Innovative Technology, King Mongkut's Institute of Technology Ladkrabang, Bangkok, Thailand. Her research focuses on composite and nanocomposite materials with enhanced functional performance in magnetics, dielectrics, piezoelectrics, and ferroelectrics for advanced applications.

	**Dr. Usa Sukkha** is an Assistant Professor in the Department of General Science and Liberal Arts at King Mongkut's Institute of Technology Ladkrabang, Prince of Chumphon Campus, Thailand. Her research focuses on lead-free ferroelectric ceramics, phase transition behavior, and perovskite-structured materials. Her current work emphasizes the synthesis and characterization of functional ceramics, including dielectric and piezoelectric materials.
	**Dr. Naratip Vittayakorn** is a Professor of Materials Science at the Department of Chemistry, Faculty of Science, King Mongkut's Institute of Technology Ladkrabang (KMITL), Thailand. His research focuses on energy-harvesting materials, triboelectric and piezoelectric nanogenerators, flexible triboelectric–piezoelectric hybrid systems, lead-free piezoelectric materials based on perovskite structures, microwave dielectric ceramics, transparent flexible sensors, and contact electrification at liquid–solid interfaces. He has published more than 300 peer-reviewed articles and has contributed extensively to advanced functional materials for self-powered electronics, sensing, and next-generation energy devices.
	**Dr Sugato Hajra** is currently a postdoctoral researcher at Daegu Gyeongbuk Institute of Science and Technology (DGIST) South Korea. He received a Bachelor in Technology degree from Siksha O Anusandhan University, India, in 2017. He pursued his M. Tech. degree with a specialization in VLSI and Embedded Systems at Siksha O Anusandhan University, and also served as a joint researcher at the Advanced Multifunctional and Materials Laboratory in the Institute of Technical Education and Research, Bhubaneswar, India in 2019. He received the Ph.D. degree in the Department of Robotics and Mecharonics Engineering in 2024 from DGIST, South Korea. His research interests mainly include lead-free piezoelectric/ multiferroics materials, metal–organic frameworks, solid-state electronic devices, and hybrid energy harvesters
	**Dr Hoe Joon Kim** is currently an Associate Professor in Robotics and Mechatronics Engineering with the Daegu Gyeongbuk Institute of Science and Technology (DGIST), Daegu, South Korea, and also holds a courtesy appointment in the Information and Communication Engineering Department at DGIST. He received the B.S. degree from Johns Hopkins University, Baltimore, MD, USA, in 2009, and the M.S. and Ph.D. degrees from the University of Illinois at Urbana–Champaign, Urbana, IL, USA, in 2011 and 2015, respectively, all in mechanical engineering. His research interests focus on piezoelectric MEMS resonators for RF wireless communication, nanogenerators, chemical/physical sensing, environmental monitoring, and emerging nanomaterials.

Dr. Tosapol Maluangnont is an Associate Professor in the Department of Nanoscience and Nanotechnology, School of Integrated Innovative Technology, King Mongkut's Institute of Technology Ladkrabang, Bangkok, Thailand. His research focuses on layered materials, dielectric spectroscopy, and the development of functional ceramics and composites. He has extensive expertise in the structural characterization and gamma-irradiation modification of layered alkali titanates and their corresponding nanosheet-containing nanocomposites.

Acknowledgments

This project is funded by National Research Council of Thailand (NRCT) and King Mongkut's Institute of Technology Ladkrabang (N42A690584). The work of Phieraya Pulphol was financially supported by the Guangxi ASEAN Outstanding Young Scientists Program (Grant No. ATYSP2025010). S. Hajra and H.J Kim received funding support from National Research Foundation of Korea (NRF) grant funded by the Ministry of Science and ICT (MSIT) (No. RS-2024-00346135).

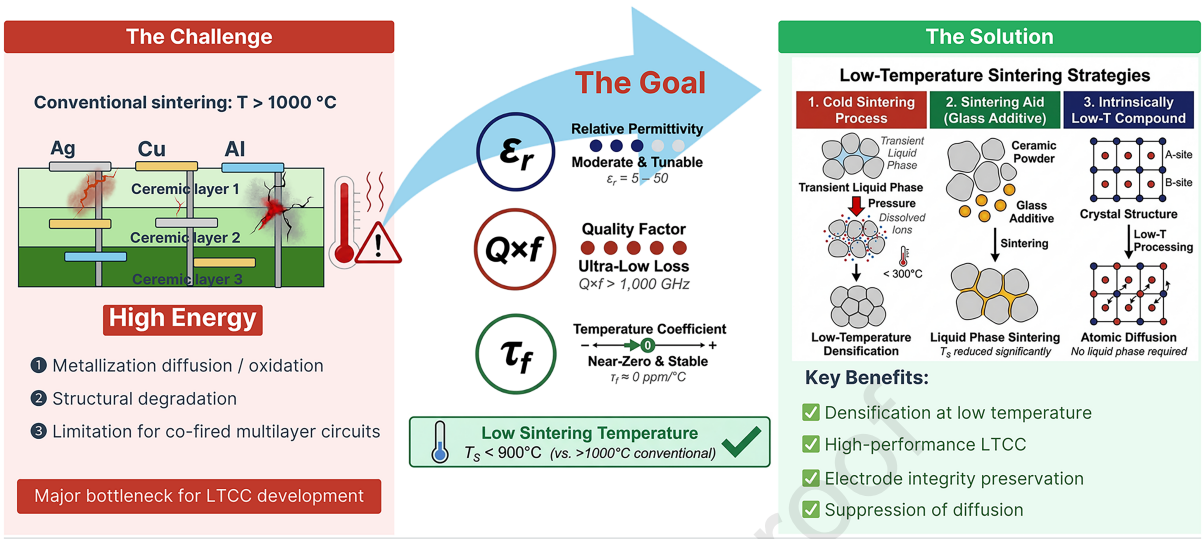

Emerging low-temperature sintering approaches for microwave dielectric ceramics were critically reviewed from a process-structure-properties perspective. Sintering additives, intrinsically low-temperature compounds, and cold sintering strategies enable reduced processing temperatures while preserving dielectric performance and LTCC compatibility.

Process-Structure-Property Relationships in Low-Temperature Microwave Dielectric Ceramics: From Glass-Assisted Sintering to Cold Sintering for 5G/6G Devices.

Abstract: With the rapid advancement of wireless communication from 5G to 6G, a pressing need has emerged for microwave dielectric ceramics with excellent performance at reduced processing temperatures, compatible with low-temperature Co-fired ceramic (LTCC) technology. This review traces historical milestones and highlights modern design strategies for achieving optimum dielectric constant, ultra-low dielectric loss, and near-zero temperature coefficient of resonant frequency. Special emphasis is placed on recent advances in low-temperature densification routes, including sintering aids, intrinsically low-sintering-temperature ceramic families, and novel techniques like the cold sintering process (CSP). This review provides a critical analysis of the performance trade-offs inherent to each strategy, addressing the persistent challenges in achieving ultra-low loss. Furthermore, we highlight the paradigm shift toward a holistic, multifunctional design imperative for 6G systems. Finally, the transformative potential of cross-disciplinary approaches, particularly AI-assisted discovery and computational modeling, is discussed as a key enabler for accelerating the design of next-generation, high-performance, and sustainable LTCC-compatible materials.

Keywords: Microwave dielectric ceramic; Low-temperature co-fired ceramic (LTCC); Cold sintering process (CSP); 5G/6G communication; Low dielectric loss; Sintering aid.

1. Introduction

The ongoing evolution of wireless technology, from 4G to 5G and now towards 6G, is driving increasingly strict demands for microwave component performance. To meet the needs of higher data rates, lower latency, massive connectivity, and device miniaturization, dielectric materials must possess precisely engineered properties: a high quality factor ($Q \times f$), a suitable dielectric permittivity (ε_r) and a near-zero temperature coefficient of resonant frequency (τ_f) [1]. These requirements are becoming even more critical as operating frequencies extend from sub-6 GHz into the millimeter-wave (mm-wave) and sub-terahertz ranges [2]. However, achieving these properties often requires high-temperature processing, which conflicts with the manufacturing demands for cost-effective, co-firable technologies like low-temperature Co-fired ceramic (LTCC). This creates a fundamental dilemma: how to reduce processing temperatures without sacrificing performance. This review critically analyzes this core trade-off by exploring the three dominant paradigms being pursued to resolve it: (i) extrinsic modification through sintering aids, (ii) the design of intrinsically low-sintering-temperature compounds, and (iii) radical process innovation via cold sintering process (CSP). Figure 1 provides a schematic overview of the key challenges and strategies discussed in this review, starting from the increasing technological demands, the limitations of conventional ceramic sintering, and the emerging strategies developed to overcome these issues, ultimately leading to the realization of LTCC.

In these higher frequency bands, designers face severe constraints due to greater signal attenuation, reduced propagation distances, and the need for denser base station deployment. Microwave dielectric ceramics are crucial for meeting these demands, serving as the foundation for essential passive components like resonators, filters, and antennas in modern communication systems [3, 4]. There are numerous studies reported on the development of microwave dielectric

properties. For example, minimizing intrinsic and extrinsic loss to achieve high $Q \times f$ [5-8], tuning temperature coefficient of resonant frequency (τ_f) by making the crystal structure distorted [9] or compensated by opposite sign of τ_f [10, 11]. Intrinsic losses are inherent to the material's crystal lattice and its atomic vibrations called phonons. Materials with highly symmetrical, ordered, and rigid crystal structures tend to have lower intrinsic losses [12]. The theory of intrinsic dielectric loss in perfect crystals, developed by Gurevich and Tagantsev [12, 13], describes how anharmonic interaction of an alternating electric field with the phonon system leads to energy dissipation; this intrinsic loss is strongly dependent on crystal symmetry, with higher symmetry generally resulting in lower loss. Disruptions in the crystal lattice, such as cation or anion vacancies, interstitials, or lattice distortions, increase phonon scattering and lead to higher loss. Any deviations in the stoichiometric ratio can create defects. Thus, precise material preparation is necessary [14]. Moreover, another technique to minimize intrinsic loss is finding materials composed of light ions with strong ionic or covalent bonds. These materials tend to have high intrinsic phonon frequencies, typically in the infrared range. Because these frequencies are much higher than microwave frequencies, there is a poor energy coupling between the electromagnetic wave and the lattice vibrations. This inefficiency in absorbing microwave energy results in very low dielectric loss. [15-17]. Extrinsic losses are related to imperfections and non-idealities introduced during the ceramic processing, such as density of samples, impurities, second phases, defects, and microstructures [1, 4, 18-20]. These are often more controllable than intrinsic losses.

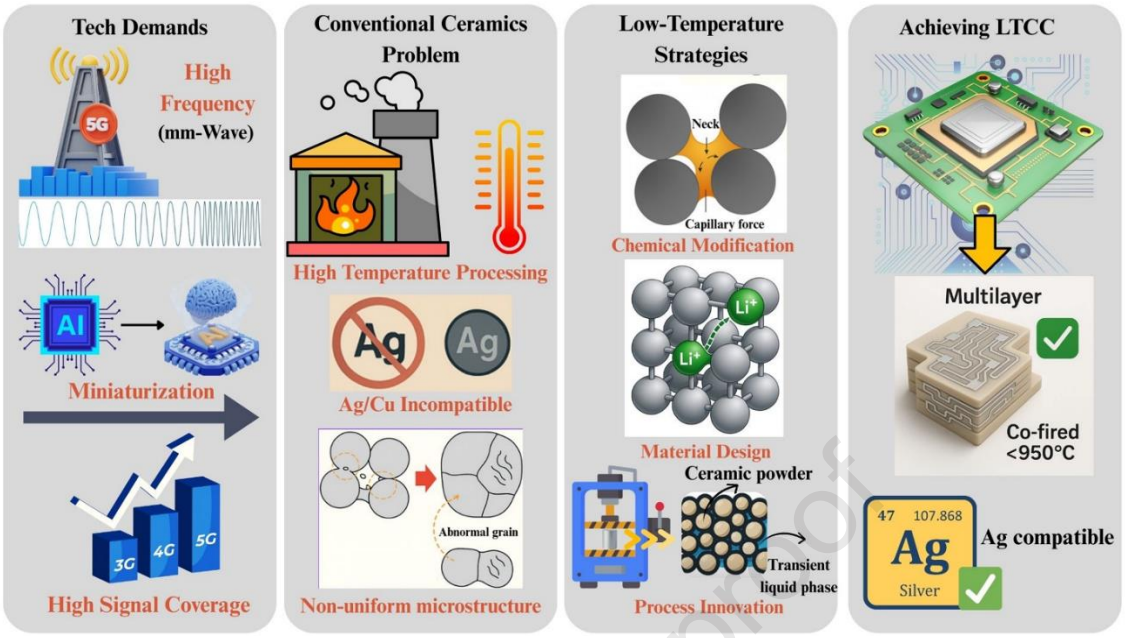

Fig. 1 A schematic overview illustrating the progression from the technological demands of 5G/6G communication to the development of LTCC. The figure highlights the challenges of conventional high-temperature sintering and presents the advanced strategies including chemical modification, material design, and process innovation that enable the integration of ceramics with low-cost metal electrodes.

State-of-the-art microwave dielectric ceramics such as $BaZn_{1/3}Ta_{2/3}O_3$, $Ba(Mg_{1/3}Ta_{2/3})O_3$, and other perovskites can achieve outstanding dielectric performance [21-23]. Yet, they require sintering temperatures above 1200°C–1500°C [24, 25]. High sintering temperatures pose three critical challenges to ceramic manufacturing. First, the prolonged firing at high temperatures consumes substantial energy and extends processing cycles, which directly raises production costs. Second, these high temperatures exceed the melting points of widely used conductors like silver (Ag) [4, 26-30]. This can result in preventing the ceramics from being co-fired with metal electrodes. This forces manufacturers to use more costly, multi-step post-metallization processes. Finally, high-temperature processing can compromise the material itself. It may cause the

volatilization of constituent elements (such as Li, Pb, Te, and V), lead to phase decomposition, and result in excessive grain growth and other microstructural defects, all of which ultimately degrade the ceramic's dielectric properties.

Recent comprehensive reviews have further consolidated our understanding of CSP. H. Palneedi *et al.* [31] systematically examined the effects of CSP process parameters (temperature, pressure, dwell time, solvent type) on densification and grain growth, providing a quantitative framework for process optimization. C. Liu *et al.* [32] reviewed recent advances in LTCC, ULTCC, and CSP technologies for next-generation electronics, highlighting how these ultra-low-temperature processing routes enable co-integration with silicon chips, aluminum electrodes, and polymers. In response to these challenges, significant research has focused on developing low-temperature processing strategies for microwave dielectric ceramics that do not compromise their dielectric properties. This review examines three major routes that have emerged to achieve this goal. First, the use of sintering aids and glass additives promotes liquid-phase densification at lower temperatures, though this requires a careful balance to avoid introducing unwanted secondary phases and increasing dielectric loss. Second, the development of intrinsically low-sintering-temperature ceramic compounds such as those with lithium-based rock-salt, spinel, and olivine structures. These systems can provide low densification temperatures below 950°C which makes them compatible with silver co-firing. The third and final approach is the CSP. This process is an ultra-low-temperature consolidation technique that uses transient liquid phase and applied external pressure to achieve high density through dissolution-precipitation mechanisms. Across these three categories, we address the fundamental mechanisms by which the sintering temperature is reduced, the critical trade-offs between densification temperature and key dielectric properties ($Q\times f$, ε_r and τ_f). and the detailed relationships among processing,

103 microstructure, and properties that inform effective material design. Finally, we discuss the
104 industrial implications of these methods for scalability, reliability, and cost-effectiveness.

105 **2. Fundamental principles of microwave dielectric ceramics**

106 The required properties for microwave dielectric materials are determined by three important
107 factors: a) the dielectric permittivity (ε_r), b) the quality factor ($Q\times f$), and c) the temperature
108 coefficient of resonant frequency (τ_f) (Fig. 2). The roles and property enhancements of the
109 materials will be described in the following sections.

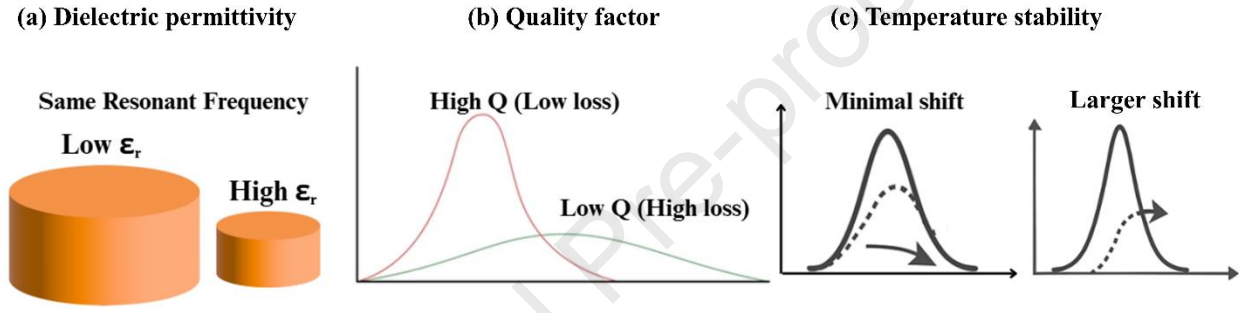

110

111 **Fig. 2** Conceptual illustration of the three key requirements for high-performance microwave
112 dielectric ceramics. (a) Dielectric permittivity (ε_r): a high ε_r allows for device miniaturization, as
113 a smaller resonator can achieve the same resonant frequency. (b) Quality factor ($Q\times f$): a high
114 $Q\times f$ value, corresponding to low dielectric loss, is represented by a sharp and narrow resonant
115 peak, indicating high frequency selectivity. (c) Temperature coefficient of resonant frequency
116 (τ_f): a near-zero τ_f is required for thermal stability, ensuring a minimal shift of the resonant peak
117 with temperature changes.

118 **2.1 Dielectric permittivity (ε_r)**

119 When a dielectric material is exposed to electromagnetic waves, the oscillating electric field
120 induces a corresponding polarization within the material. This interaction can cause the material
121 to resonate at specific frequencies, depending on its dielectric properties. The dielectric

permittivity of the material influences the propagation velocity of electromagnetic waves through it, which can effectively shorten the wavelength within the material. The wavelength inside dielectric material is the reciprocal of the square root of dielectric permittivity as the given equation.

$$\lambda_{\mathrm{d}} = \frac{\lambda_0}{\sqrt{\varepsilon_r}} \tag{1}$$

where λ_{d} is the wavelength in dielectric material, λ_0 is the wavelength in vacuum and ε_r is the dielectric permittivity of the material. By increasing the permittivity of a resonator, its physical size can be reduced without compromising its resonant frequency. This property allows for the miniaturization of microwave components. The dielectric permittivity determines the propagation velocity of electric signals through a dielectric material. Materials with low dielectric permittivity enable high-speed signal transmission, while those with high permittivity are advantageous for miniaturization. It is important to note that dielectric permittivity is frequency dependent. At microwave frequencies, the net dipole moment and polarization are primarily influenced by ionic and electronic polarization mechanisms. The dielectric constant is a function of relative density, which is influenced by porosity. Furthermore, the unit cell volume, which determines the polarizability of the material, also contributes to the dielectric constant.

2.2 Quality factor ($Q \times f$)

The quality factor, often expressed as $Q \times f$ (Q multiplied by resonant frequency in GHz), is a function of resonant frequency. This frequency is determined by the puck's dimensions and the material's permittivity and surrounding environment. It is determined from the shape of the resonant peak and can be measured by calculating the ratio between the resonant frequency (f_0) to the width of resonant frequency peak (Δf). The high Q materials are represented as the sharp resonant frequency peak which provide the quality factor can be represented by the inversely

proportional to the loss tangent (tan δ) of the dielectric materials, where a higher Q indicates lower energy loss. To obtain high Q for the millimeter wave application, it is necessary to use the ultra-low loss materials. The correlation between loss tangent and the resonant frequency can be ascribed in the term of $Q \times f$ product and it should be high ($Q \times f > 100$ THz) for the 5G technology.

The dielectric loss of the materials is the sum between intrinsic and extrinsic losses. Intrinsic dielectric losses occur within perfect crystals due to the interaction between the phonon system and the alternating electric field. When the ac field come to dielectric crystal, it alters the equilibrium of the crystal system leading to the energy dissipation [12]. The extrinsic losses originate from the quality of the specimens include the relative density, microstructure, impurities, and defects [20, 21]. To obtain ultra-low loss materials, starting materials with minimal dipole and charge carrier concentrations, as well as low carrier mobility, are essential. Additionally, minimizing crystal lattice disorder, which arises from deviations in charge distribution, helps reduce dielectric loss [33, 34]. Microwave dielectric ceramics are conventionally fabricated through solid-state reaction. Sintering parameters, such as temperature and time, also influence the microstructure and densification of the ceramic which affects its microwave dielectric performance. The dielectric loss is frequency dependent, generally increasing as frequency is elevated. This behavior is governed by two main mechanisms: intrinsic loss from the interaction with lattice phonons, and extrinsic loss introduced by crystal defects and impurities. Both mechanisms typically contribute more to the total loss at higher frequencies [35]. The ($Q \times f$) of a dielectric material is fundamentally limited by its defect density. In practice, low-frequency resonators require larger sample dimensions. These larger samples have a higher statistical probability of containing performance-limiting defects, making it more challenging to consistently achieve the material's intrinsic $Q \times f$ during production and measurement. Conversely,

168 smaller, high-frequency resonators are less susceptible to these volume-dependent statistical
169 variations, often resulting in more reliable and consistent measurement outcomes.

170 **2.3 Temperature stability**

171 Microwave dielectric materials must operate reliably over a wide temperature range, typically
172 from −40 °C to +110 °C, under various environmental conditions. τ_f is a critical parameter that
173 quantifies the stability of the resonant frequency against these temperature variations. Materials
174 with a large τ_f value are unsuitable for most microwave applications as they fail to maintain
175 frequency stability under thermal fluctuations [36]. To achieve a near-zero τ_f, it is necessary to
176 understand its origin. The τ_f value is determined by the net effect of two competing factors: the
177 coefficient of thermal expansion (α_L), which alters the resonator's physical dimensions, and the
178 temperature coefficient of the dielectric constant (τ_ε) which describes the change in permittivity
179 with temperature. Their combined influence is expressed in the following equation:

180 $$\tau_f = -(\alpha_L + \frac{\tau_\varepsilon}{2}) \quad (2)$$

181 Oxide ceramics play a pivotal role in the performance of microwave devices. A thorough
182 understanding of their crystal chemistry is essential for ongoing research and development. The
183 properties of microwave ceramics are influenced by several factors, including processing
184 conditions, the purity of starting materials, and the final density achieved through sintering. The
185 design of optimized heating and cooling schedules requires a deep understanding of the formation
186 mechanisms of different phases within complex multicomponent systems. Furthermore, the
187 properties tuning such as the permittivity, quality factor and temperature coefficient of resonant
188 frequency is achievable by adding some elements into the crystal structure. There are several
189 ceramic compounds that have been paid attention to. They can be categorized by the crystal
190 structure, for example, perovskite, tungsten bronze, and, cubic rock salt [18, 37].

The pursuit of low-temperature densification is fundamentally governed by thermodynamic and kinetic drivers, namely, grain-boundary energy minimization and the reduction of diffusion activation barriers, and by defect chemistry that controls dielectric loss and τ_f stability. In practice, these physical levers map directly onto material-design choices: liquid-phase routes (*e.g.*, glass or sintering aids) lower the effective sintering barrier via capillary-assisted rearrangement and solution-reprecipitation; intrinsically low- T_S chemistries (*e.g.*, Li-containing rock-salt, spinel, olivine families) exploit fast ionic mobility and weaker lattice bonding to accelerate solid-state diffusion while preserving high $Q\times f$; and CSP invokes a transient solvent under pressure to enable dissolution-precipitation at <200°C, followed by targeted post-anneals to heal defects and suppress residual OH^--related loss. Framed in the process–structure–property logic, each route engineer grain-boundary complexion and point-defect populations to achieve the same objective: high density with clean interfaces and minimal extrinsic losses at the lowest possible thermal budget. The following sections apply this mechanistic lens to compare these strategies and to articulate the design trade-offs among Ts–$Q\times f$–ε_r–τ_f and co-firing compatibility.

3. A brief history of microwave dielectric ceramics

The development of microwave dielectric ceramics has been inextricably linked to the evolution of wireless communication technologies over the past five decades. The progression from analog to digital networks, and from lower to higher operating frequencies, has continuously driven innovation in materials with increasingly demanding performance specifications.

3.1 Early developments and the foundation period (1960s–1970s)

The origins of microwave dielectric research can be traced to the 1960s and 1970s, when the first-generation (1G) analog mobile communication systems began to emerge. During this pioneering era, researchers explored fundamental ceramic systems that would later become commercially significant. Among the earliest materials investigated were titanates and simple binary oxide systems. The BaO-TiO_2 system received particular attention, with comprehensive phase diagram studies in the 1970s revealing multiple stable compounds, including $BaTi_4O_9$ and $Ba_2Ti_9O_{20}$ [38, 39]. These barium polytitanates would eventually become cornerstone materials for commercial microwave devices due to their moderate dielectric constants (ε_r~37–40) and acceptable quality factors ($Q\times f$~30,000–40,000 GHz), though their high sintering temperatures exceeding 1300°C presented significant manufacturing challenges [40, 41].

Parallel investigations during this period examined the $ZrTiO_4$ system, which demonstrated promising microwave characteristics with ε_r~40-42 and $Q\times f$~28,000–31,000 GHz at 7 GHz [42, 43]. However, its large positive temperature coefficient (τ_f=+58 ppm/°C) and extremely high sintering temperature (~1600°C) limited immediate practical applications. Researchers discovered that partial substitution of Zr^{4+} with Sn^{4+} to form $(Zr,Sn)TiO_4$ (ZST) ceramics successfully achieved near-zero temperature coefficients while maintaining excellent microwave properties, with $Q\times f$ values reaching 53,000–61,000 GHz [44].

3.2 The breakthrough era: complex perovskites (late 1970s-1980s)

In 1977, Kawashima *et al*. reported that $Ba(Zn_{1/3}Ta_{2/3})O_3$ (BZT) exhibited exceptionally high $Q\times f$ at microwave frequencies [44]. This discovery triggered intensive research into complex perovskites (ABO_3) with B-site cation ordering. Throughout the 1980s, "super Q" materials such as BZT and $Ba(Mg_{1/3}Ta_{2/3})O_3$ (BMT) achieved $Q\times f$ exceeding 150,000 GHz, among the highest

ever reported. These 1:2 ordered perovskites (trigonal, space group *P-3m1*) offered ε_r~28–30 and good thermal stability [45-47].

However, practical implementation faced severe obstacles. Achieving optimal cation ordering required prolonged annealing at 1400–1450°C after initial sintering at 1600–1650°C, causing high energy consumption, B-site cation volatilization, and incompatibility with low-melting-point electrode metals such as silver (melting point=961°C) [45, 46, 48].

3.3 Adaptation to digital networks (1990s-early 2000s)

The transition from 1G analog to 2G/3G digital networks demanded better frequency selectivity [49]. Materials research diversified to tungstates, niobates, and BaO-Ln_2O_3–TiO_2 systems [39].

Three main strategies emerged to reduce sintering temperatures while preserving dielectric performance: (i) liquid-phase sintering using additives (CuO, Bi_2O_3, B_2O_3, V_2O_5, or low-melting glasses), (ii) chemical processing (sol-gel, co-precipitation, hydrothermal) to enhance powder reactivity, and (iii) the development of LTCC technology (pioneered in 1982, commercialized in the 1990s), which lowered firing temperatures below 900–1000 °C by incorporating glassy phases, enabling co-firing with silver and copper electrodes [38, 47, 50]. Furthermore, the challenge of achieving near-zero temperature coefficients of resonant frequency received systematic attention. Researchers established that τ_f could be engineered through composite approaches combining materials with opposing temperature coefficients or through solid solution formation, exploiting the relationship $\tau_f = -(\alpha_L + \frac{1}{2}\tau_\varepsilon)$ where α_L represents linear thermal expansion and τ_ε is the temperature coefficient of permittivity. These strategies enabled optimization of temperature stability without sacrificing other critical properties [51-53].

3.4 Modern era: toward 4G, 5G, and beyond (2000s-present)

4G LTE (operating above 3 GHz) accelerated the need for smaller components with higher $Q \times f$ and improved temperature stability [54]. The arrival of 5G expanded the spectrum into sub-6 GHz and millimeter-wave bands (20–40 GHz), demanding ceramics that are compact, ultra-low loss ($\tan \delta < 10^{-4}$), thermally stable ($\tau_f \sim 0$ ppm/°C), and cost-effective for mass production. Looking ahead, 6G systems will operate in the sub-terahertz range (0.1–1 THz), requiring not only superior intrinsic properties but also compatibility with heterogeneous material integration and energy-efficient manufacturing [54, 55]. The detailed technological evolution and development pathways from 4G toward 6G networks, characterized by shifting operational frequencies, changing cell site densities, and structural modifications, are illustrated in Fig. 3.

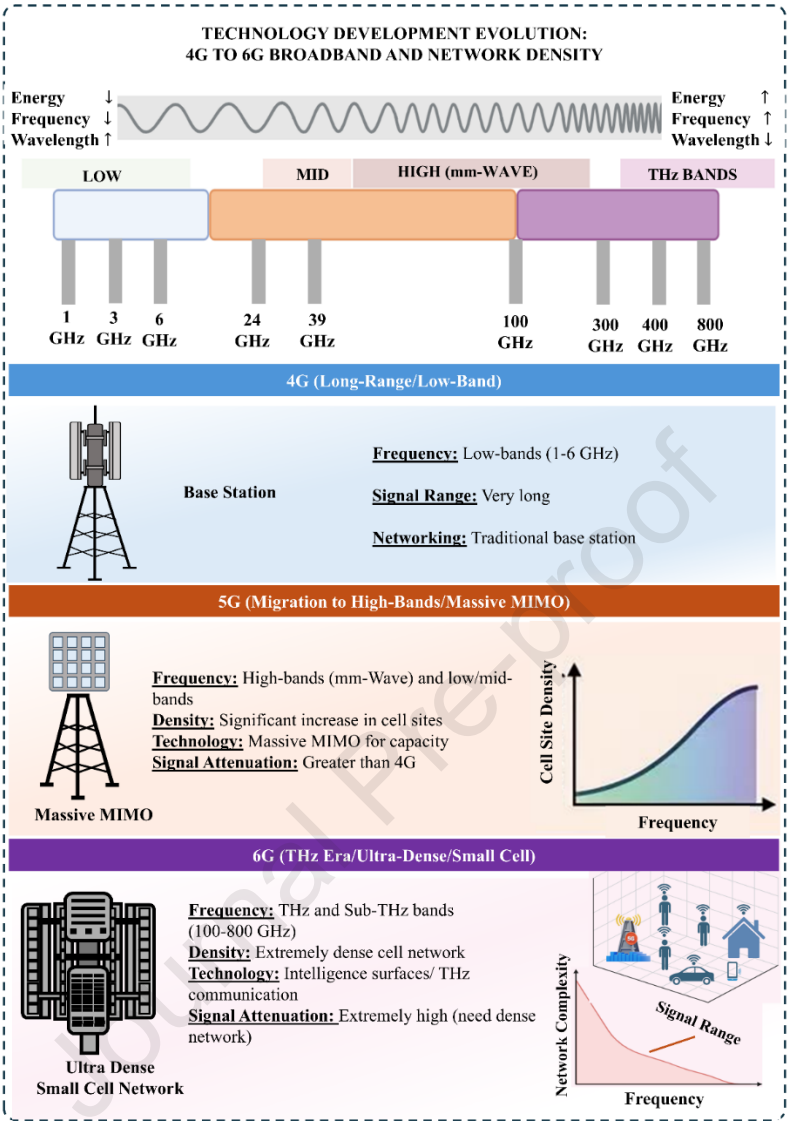

Fig. 3 An overview of the progression of wireless communication technologies and their associated frequency bands, from 4G, 5G and 6G spectrum. The figure also represents the inverse relationship between frequency and wavelength, alongside the typical base station designs and the increasing signal attenuation challenges at higher frequencies.

3.5 The Paradigm Shift: Ultra-Low Temperature Processing

While conventional high-temperature sintering (1200–1600 °C) yields excellent dielectric properties, it suffers from high energy consumption, volatile element loss, and incompatibility

with low-melting-point electrodes such as silver (melting point 961 °C). A major breakthrough came in 2016 when Randall and co-workers introduced CSP [56, 57]. This technique achieves ceramic densification at temperatures below 300 °C (often as low as room temperature) by applying a transient aqueous solution under uniaxial pressure, enabling dissolution-precipitation without high thermal energy. CSP dramatically reduces energy consumption and allows co-sintering with polymers and low-melting-point metals, opening new avenues for multifunctional devices [58].

Meanwhile, LTCC technology (sintering below 900–1000 °C) has matured commercially, becoming the mainstream platform for miniaturized multilayer RF modules [59]. The detailed mechanisms, material examples, and performance trade-offs of these low-temperature strategies are examined in Sections 4 and 8.

4. Low-temperature sintering techniques: materials and mechanisms

In addition to optimizing intrinsic dielectric properties, reducing the sintering temperature is a critical factor for enabling cost-effective manufacturing and co-integration with low-cost metal electrodes like silver (< 961 °C). Conventional ceramic processing, often requiring temperatures exceeding 1200 °C, is energy-intensive and can lead to detrimental effects such as the volatilization of constituent elements. Consequently, significant research has focused on three primary strategies to lower the densification temperature, as illustrated in Fig. 4: (a) the utilization of external sintering aids, (b) the design of intrinsically low-sintering-temperature compounds, and (c) the application of innovative pressure-assisted cold sintering processes. This section provides a detailed review of the materials and mechanisms central to each of these approaches [29, 46, 60].

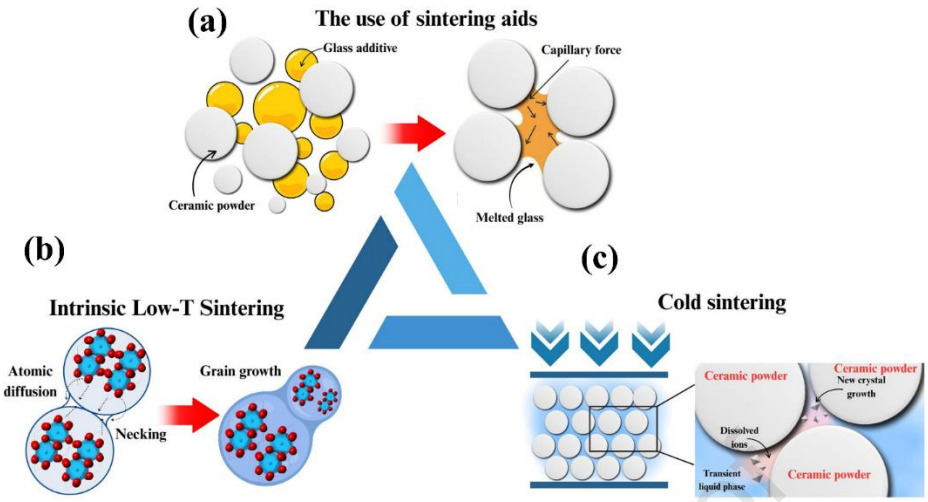

Fig. 4 An overview of the three primary strategies for achieving low-temperature densification of microwave dielectric ceramics, as discussed in this review. (a) The use of sintering aids, such as glass additives, which form a liquid phase to facilitate particle rearrangement via capillary forces. (b) Intrinsic low-temperature sintering, where materials possess inherent properties (*e.g.*, high atomic mobility) that allow for solid-state densification at lower temperatures. (c) CSP, an innovative technique that utilizes a transient liquid phase and external pressure to achieve densification at ultra-low temperatures through a dissolution-precipitation mechanism.

4.1 Sintering aids: the liquid-phase sintering approach

4.1.1 Mechanism of liquid-phase sintering

Several approaches have been employed to reduce the sintering temperature of low-loss microwave dielectric materials. These strategies can be broadly categorized: some focus on modifying the primary ceramic powder, such as using chemical synthesis to produce fine-grained starting particles [61] or the use of smaller starting particles [62], while others involve incorporating a low-melting-point additive. Among the latter, the addition of glass is a particularly

effective and economical strategy. This approach utilizes a mechanism known as liquid-phase sintering (LPS). Depending on the glass composition, two main outcomes are possible: the additive can either remain as a residual amorphous phase in the final sintered ceramic, or it can be designed to crystallize during the sintering process. Due to its versatility and cost-effectiveness, the glass addition method is one of the most widely investigated strategies. Glasses are selected as sintering aids due to their significantly lower softening and melting temperatures compared to crystalline ceramics. During heating, the glass additive melts to form a liquid phase that wets and surrounds the solid ceramic particles. This liquid phase dramatically accelerates the densification process, which is much slower in conventional solid-state sintering where densification relies solely on atomic diffusion within the solid. The mechanism of liquid-phase sintering proceeds through several stages. Initially, the capillary force generated at the liquid-solid interface pulls the particles together into a denser arrangement, reducing interparticle porosity [63]. Following this, the liquid acts as a rapid transport medium for a process known as solution-reprecipitation. This stage involves several distinct steps. First, atoms from the surface of the primary ceramic particles dissolve into the liquid phase. These dissolved atoms then diffuse through the liquid. Finally, they precipitate onto the contact points, or 'necks', between adjacent particles. This precipitation causes the necks to grow, pulling the particles closer and leading to further densification. In some systems, this can also lead to significant grain growth. Finally, the remaining liquid flows into and fills the residual pores, resulting in a highly densified ceramic product.

4.1.2 Primary and multi-component glass systems

Multi-component glasses have been shown to be an alternative way in reducing the sintering temperature of ceramics, while minimizing the detrimental effects on the matrix properties [4].

Choosing the right glass phase is crucial for the sintering process, as its liquification plays a dominant role in the viscous flow mechanism that governs densification. Simple binary oxide glasses, particularly borate (B_2O_3) and silicate (SiO_2) glasses, are the most widely used additives in microwave dielectric ceramics. However, their effectiveness is dictated by their distinct thermophysical properties. B_2O_3 glass, with its very low glass transition temperature (T_g ~ 230–325°C) and low viscosity, forms a pervasive liquid phase at a much lower temperature compared to SiO_2-based glasses (T_g>1000°C). This low-viscosity liquid phase significantly enhances particle rearrangement through strong capillary forces and accelerates mass transport via dissolution-precipitation, leading to a substantial reduction in the required sintering temperature [63, 64].

For example, in the $Ca_5Nb_2TiO_{12}$ system, the addition of borate glass was shown to promote densification without forming secondary phases at 1 wt% loading [65]. However, the effectiveness of these additives is a delicate balance. The degradation of dielectric properties, particularly the $Q\times f$ value, with excessive glass content is attributed to two primary loss mechanisms. First, the residual amorphous glass phase, which tends to segregate at grain boundaries, is inherently lossier than the crystalline ceramic matrix. Its disordered structure increases phonon scattering and introduces a continuum of energy states that dissipate microwave energy. Second, when the solubility limit of the ceramic matrix in the molten glass is exceeded, secondary phases such as $Ca_3B_2O_6$ or Ca_2SiO_4 can precipitate [66, 67]. The addition of a sintering aid, such as glass, is an effective strategy to reduce the high sintering temperatures of ceramics from 1500 °C–1650 °C down to around 1350 °C [68]. However, this benefit comes with a trade-off, as these additive phases also degrade the microwave dielectric properties. They introduce additional interfaces and potentially lossy crystal structures, which disrupt the overall lattice

perfection and increase the intrinsic dielectric loss. Therefore, the amount of the additive must be carefully optimized, confirming why a precise, often small, quantity is crucial for achieving optimal performance.

For a well-known $Ba(Mg_{1/3}Ta_{2/3})O_3$ (BMT) ceramic, glass addition has also been proposed as a method to decrease its sintering temperature. It is recognized that the microwave dielectric properties of BMT are influenced by ordered-disordered effects. Specifically, B-site cation ordering of Mg^{2+} and Ta^{5+} is the fundamental requirement for high quality-factor in complex perovskite BMT ceramics. The primary challenge with solid-state sintering of BMT is its exceptionally high sintering temperature which is higher than 1600 °C. Moreover, achieving an ordered phase of BMT necessitates prolonged annealing, often extending to several days which may lead to the volatilization of some elements in the compound. Thus, secondary phases are possibly formed, for example, $BaTa_2O_6$ and $Ba_5Ta_4O_{15}$ [69, 70]. Borate glass (B_2O_3) can be used for lowering the sintering temperature of BMT ceramics from 1600°C to 1325°C. The addition of silica does not lower the sintering temperature like in borate glass because its softening point is relatively high [71]. Although silica has high melting temperature (T_m∼1700 °C) [71] which making it unsuitable as a standalone sintering aid. However, it can form stable low-melting temperature glass compounds when blended with other oxides (*e.g.*, B_2O_3, ZnO, PbO, BaO, Bi_2O_3, Li_2O_3, MgO, etc). These resultant glass compounds can then be effectively employed as sintering aids [72-75]. In BMT ceramics, silica can promote the abnormal grain growth of the sintered ceramic as reported by Felgner [76]. This abnormal grain growth leads to the high porosity in the sintered ceramics. The degree of ordering is minimally influenced by the borate-added system, while the substantial impact is observed in the silicate system. This results in the deterioration of microwave dielectric properties of BMT ceramics as the silicate glass is added (Fig. 5) [77].

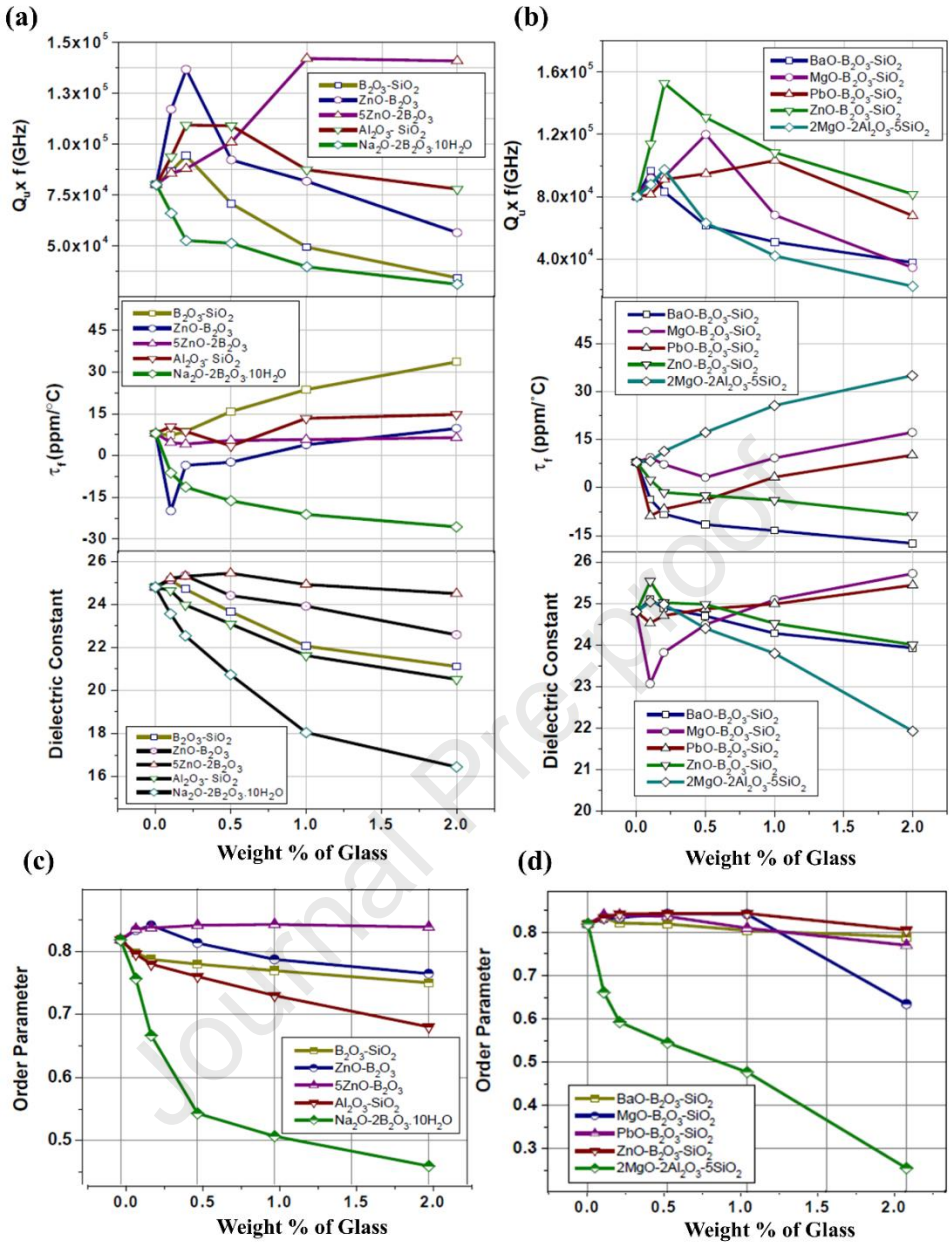

Fig. 5 Microwave dielectric properties of BMT ceramics as a function of weight% of glass additives. (a) two-component glass compounds, (b) three-component glass compounds. Variation of cation ordering of BMT ceramics as a function of glass additive amount of (c) two-component glass compounds, and (d) three-component glass compounds [77].

Takada *et al.* demonstrated the effects of two primary glasses contents (B_2O_3 and SiO_2) on BaO-TiO_2-WO_3 [78] and (Zr, Sn)TiO_4 [79] microwave ceramics. As the glass content has risen

from 5wt% to 30wt%, the density of ceramic also increases. Sintering temperature of the ceramics decreases to around 1000 °C–1100 °C with 80%–85% of relative density. However, the added glass phases react with the ceramic phase leading to the lowering in microwave dielectric features. As a reminder, the sintering temperature for LTCC technology must not exceed the melting point of the metal electrodes. This limitation makes determining the appropriate glass compounds to lower the sintering temperature of such ceramics a persistent challenge.

Some ceramic compounds can approach the low sintering temperature by the addition of glasses, for example, the τ_f compensator $Ba_5Nb_4O_{15}$ (BNO) ceramic. It was reported that borate glass can reduce the sintering temperature of BNO from 1450 °C down to 925 °C [80]. Furthermore, boric acid (H_3BO_3), a form of boron-containing compound, serves as a B_2O_3 sintering aid for various ceramic compounds. It can lower the sintering temperature of various ceramics such as, $Li_2Mg_3Ti_{0.95}(Mg_{1/3}Nd_{2/3})_{0.05}O_6$ (from 1550 °C to 1000 °C) [81], $Li_2ZnTi_3O_8$ (from 1075 °C to 880 °C) [82] and composite $0.8BaSi_2O_5$-$0.2Ba_3(VO_4)_2$ (from 1140 °C to 950 °C) [83]. Several reports indicate that the reduction in densification temperature is most practically attributed to enhanced liquid-phase diffusion through grain boundaries. This liquid phase facilitates grain recrystallization and rearrangement, which in turn eases the diffusion of trapped gases. Thus, it ultimately leads to a more compact microstructure [84, 85]. Like mostly glass additives, after the amount of H_3BO_3 increases, the quality factor of the sintered ceramics also decreases. Achieving a high $Q \times f$ and a low sintering temperature simultaneously was thus a challenging task. Yan *et al.* tried to lower the sintering temperature of $Co_{1.1}Zn_{0.9}TiO_4$ ceramics by adding H_3BO_3. The sintering temperature could be reduced from 1200 °C to 900 °C using 4 wt% of H_3BO_3 as a sintering aid. They suggested that an excessive amount of glass additive leads to abnormal grain growth which affected the quality factor of the ceramic (see Fig. 6) [86].

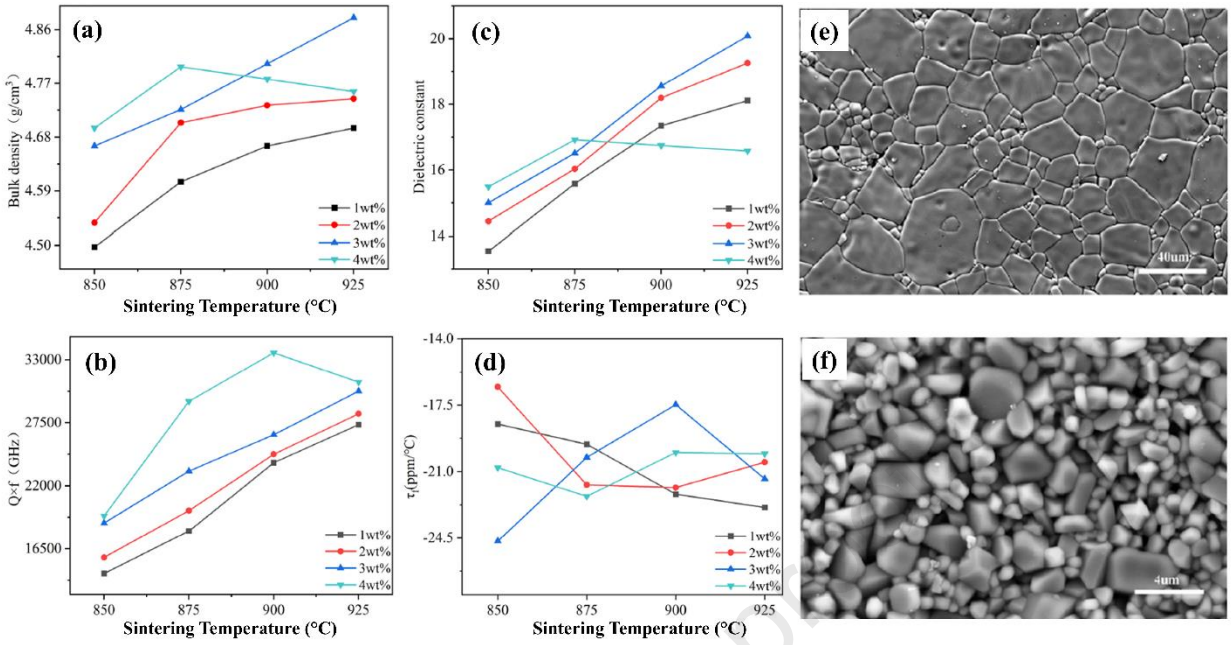

Fig. 6 (a-d) Microwave dielectric properties and bulk density of $Co_{1.1}Zn_{0.9}TiO_4$ ceramic at various contents of H_3BO_3 as a function of sintering temperature. (e,f) Microstructure of (e) traditional sintered $Co_{1.1}Zn_{0.9}TiO_4$ ceramic and (f) 4 wt% of H_3BO_3 addition [86].

It is noted that the sintering temperatures of the compounds mentioned earlier remain within a critical threshold (within 900 °C), which could lead to reactions with the silver electrodes. The microwave dielectric properties also deteriorated as secondary phases were detected. This observation is consistent with other borate-based compounds, even when sintering temperatures were lowered to less than 900 °C [87-92].

Glass additives with more than one component have been proposed to lower the sintering temperature of ceramics with high density products [60-61, 76]. Borosilicate glasses (B_2O_3-SiO_2) generally exhibit lower dielectric losses than alkali-containing glasses. In alkali-containing glasses (*e.g.*, Li-, Na-, K-containing glass compounds), weakly bonded alkali ions can absorb energy, leading to increased dielectric loss. In contrast, borosilicate glasses possess a continuous network of SiO_4 and BO_3 units linked by strong Si–O–B bonds, resulting in higher electrical

resistance and lower dielectric loss which is reported by Navias [77]. Moreover, additional glass as a sintering aid can lead to the existence of secondary phases. For the famous BMT ceramics, the addition of MCAS glass to BMT lowered the sintering temperature to 1300 °C. However, this resulted in a significant decrease in the $Q \times f$ value to 9700 GHz, making it unsuitable for industrial production [78, 79]. Excessive glass addition can induce thermal stress during soldering, leading to cracking due to the differential thermal expansion between the glass and ceramic phases. Multi-component glass compounds are mostly based on the primary borate and silica glasses. A small amount of glass compounds such as $ZnO\text{-}B_2O_3$, $5ZnO\text{-}2B_2O_3$, $ZnO\text{-}B_2O_3\text{-}SiO_2$ can reduce sintering temperature for BMT ceramics from 1650 °C down to 1300 °C with desired relative density ($\rho \sim 98.7\%$) without any secondary phases. Furthermore, these glass compounds enhance the degree of ordering of the B-site cations which improve the quality factor of the BMT ceramics. The glass compound that promotes very good microwave dielectric features in BMT ceramic is the ternary $ZnO\text{-}B_2O_3\text{-}SiO_2$ (ZBS) glass. It acts as a perfect liquid-phase medium for the sintering of BMT when added just 0.2 wt% (ε_r=25.5 and $Q \times f$=152,800 GHz, τ_f=−1.5 ppm/°C) [77].

Kim *et al*. demonstrated the use of B_2O_3 as a sintering aid to lower the processing temperature of $Ba_5Nb_4O_{15}$ (BNO) ceramics. While this additive successfully reduced the sintering temperature from 1450 °C to 925 °C, it also led to the formation of a secondary phase at a glass concentration of 1 wt% [80]. A similar limitation was observed when using a ZnB_2O_4 glass system, where additions exceeding 1 wt% resulted in the formation of secondary phases such as ZnB_2O_4, $Ba_3B_2O_6$ and $ZnNb_2O_6$ [92]. J. Tang [91] utilized $BaO\text{-}B_2O_3\text{-}ZnO$ as a sintering aid for $Ba_5Nb_4O_{15}$ ceramic. The study found that adding 6 wt% of $BaO\text{-}B_2O_3\text{-}ZnO$ can lower the sintering temperature from 1450°C to 850°C with relative density of 94.5%. The glass-added

452 ceramic showed $Ba(Zn_{0.33}Nb_{0.67})O_3$ phase as the secondary phase along with $Ba_5Nb_4O_{15}$ and the
453 microwave dielectric properties were slightly deteriorated from the glass-free system (ε_r=37.1
454 and $Q\times f$=13,820 GHz) [91]. Thus, the amount of glass is required to optimize. However, using
455 ternary glass additive such as $BaCu(B_2O_5)$ can lower the sintering temperature of $Ba_5Nb_4O_{15}$
456 ceramic (T_S from 1450 °C to 875 °C) without any secondary phases while its microwave
457 dielectric properties were improved [90]. The ternary $MgO\text{-}B_2O_3\text{-}SiO_2$ (MBS) is used as sintering
458 aid in various ceramic compounds. Zhang *et al.* reported the effect of MBS glass content on the
459 sintering temperature and microwave dielectric features of rock-salt $Li_3Mg_2NbO_6$ ceramic [75].
460 $Li_3Mg_2NbO_6$ ceramic achieved satisfying microwave dielectric properties with the addition of
461 0.5 wt% MBS glass. The sintering temperature decreased from 1250 °C to 925 °C, they displayed
462 an ε_r of 14.5, a $Q\times f$ of 80,759 GHz, and a τ_f of −20.7 ppm/°C.

463

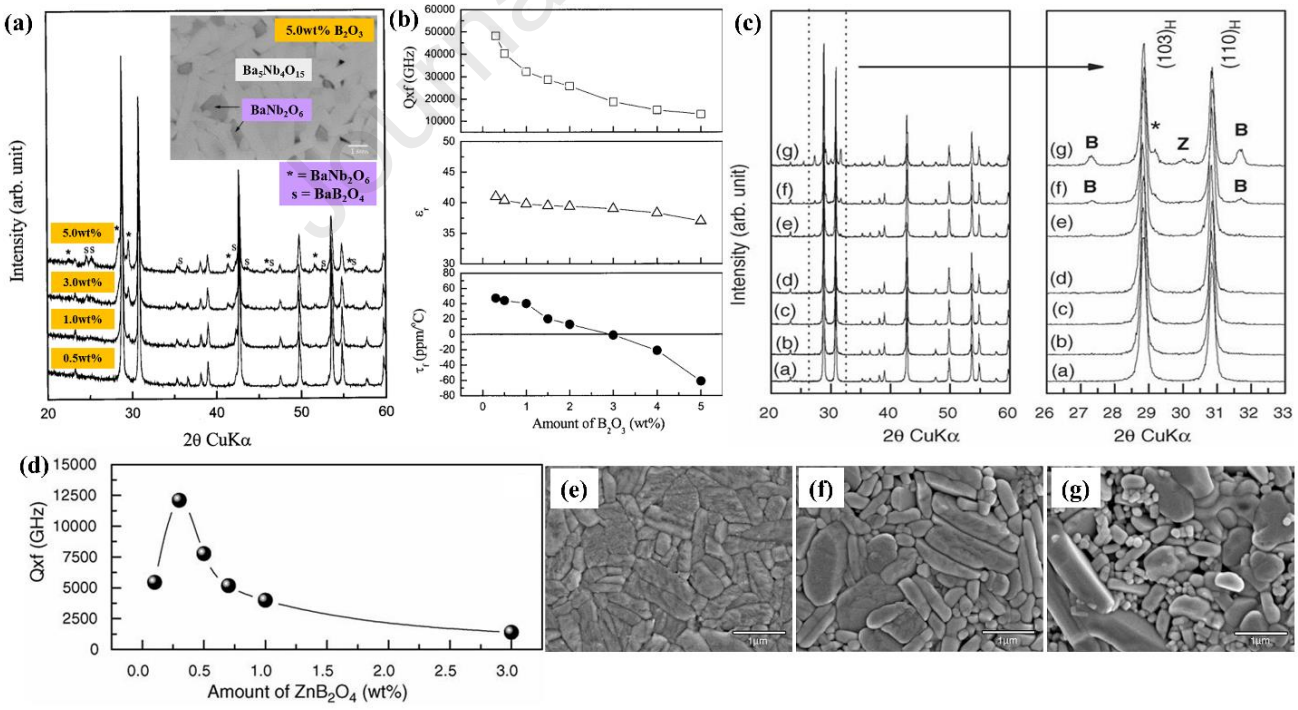

464

Fig. 7 Low sintered $Ba_5Nb_4O_{15}$ ceramics using two types of glass additives (B_2O_3 and ZnB_2O_4). (a) Phase formation and (b) microwave dielectric properties ($Q\times f$, ε_r, and τ_f) of sintered $Ba_5Nb_4O_{15}$ ceramics as a function of B_2O_3 glass content (the inset of Figure 7(a) shows the backscattered image of $BaNb_2O_6$ secondary phase). (c) Influence of ZnB_2O_4 glass content on $Ba_5Nb_4O_{15}$ phase formation (where: *=ZnB_2O_4, B=$Ba_3B_2O_6$ and Z=$ZnNb_2O_6$ secondary phases) and (d) $Q\times f$ values. (e-g) Microstructure of 0.3 wt%, 3 wt%, and 10 wt% of ZnB_2O_4 content, respectively. (Adapted from D.W. Kim *et al*. [80] and J.R. Kim *et al*. [92])

While glass additives are effective in reducing sintering temperature, their impact on the final microwave dielectric properties needs to be considered. As the glass phases themselves still maintain in the ceramic or they can react with the pristine ceramic compound forming secondary phases. These glasses and secondary phases directly affect microwave dielectric properties especially to the quality factor. Some glass systems, the glass additive can aid for recrystallization during the sintering process. This phenomenon forms a glass-ceramic composite. In the work by J.Y. Qiu [93], they fabricated the borosilicate-based glass-ceramic. The results reveal that as the amount of Li_2O is promoted into borosilicate glass, it acts as the crystallization catalysts [94]. The effects of glass additives on ceramic compounds are summarized in Table 1. While these case studies demonstrate the potential of multi-component glass systems, the sheer complexity of these systems, often involving three, four, or even more oxide components, presents a significant challenge for traditional trial-and-error experimental approaches. This is where computational materials science, particularly through the use of thermodynamic databases like CALPHAD (calculation of phase diagrams), is becoming indispensable [95, 96]. By predicting phase stability and the melting behavior of complex glass compositions, researchers can rapidly screen and identify promising candidates for sintering aids before undertaking extensive experimental work.

Moreover, machine learning models trained on existing experimental data are now being employed to predict the optimal glass composition that minimizes sintering temperature while preserving the high $Q \times f$ value of the ceramic matrix, accelerating the discovery cycle for new LTCC materials.

492 **Table 1** Effects of glass additives on sintering temperature (T_S), microwave dielectric properties and limitations.

Type of sintering aid	ΔT_S (°C)	ε_r	$Q \times f$ (GHz)	τ_f (ppm/°C)	Advantages	Limitation
Borate glass	100-400	Slightly decreased	Slightly–moderately decreased	Can shift significantly (±)	Small amount of glass can provide dense ceramics without forming any second phases	Thermal instability
Silicate glass	50-200	Stable or slightly increased	Slightly decreased	Minor changes	Good chemical stability, adjustable composition	Limited solubility in some systems Increase dielectric loss from the residual glass
ZnO-B_2O_3-SiO_2 (ZBS) glass	200-400	Stable	Slightly decreased	Stable or adjusted toward zero	Good match with Ag/Pt with stable τ_f	ZnO volatility Moisture susceptibility
Li_2O-B_2O_3-SiO_2 (LBS) glass	200-300	Slightly decreased	Moderately decreased	Negligible	Good glass-ceramic compatibility, promotes densification	Li volatilization during sintering
Aluminosilicate glass	150-250	Stable	Slightly decreased	Minor changes	Good mechanical strength, chemical durability	Higher T_S than borate-based glass
Phosphate glass	250-350	Slightly decreased	Decreased	Can shift toward positive	Very low T_S, fast densification	Poor water resistance, limited thermal stability
Fluoroborate glass	300-400	Slightly decreased	Decreased	Minor changes	Low T_S, fluoride addition aids densification	Possible fluorine loss, phase instability
Bi_2O_3-based glass	300-400	Increased	Decreased	Shift toward negative	Very low T_S, improves liquid-phase sintering	Bi volatility, reaction with electrodes

493

4.2 Intrinsically low-sintering-temperature compounds

Beyond the use of external additives, a significant research thrust focuses on developing ceramic compounds that inherently possess low sintering temperatures due to their unique crystal chemistry and bonding characteristics.

4.2.1 Lithium-containing systems: rock-salts and spinels

The sintering temperature of a material is correlated with its melting point, which is a function of the cohesive energy of the crystal lattice. The cohesive energy is influenced by factors such as crystal structure, bond strength, and bond polarity [97]. Materials with weaker bonds and higher bond polarity tend to have lower melting points and, consequently, lower sintering temperatures.

Lithium (Li)-containing compounds are vital in LTCC technology, distinct from the role of glass additives. This ability stems from intrinsic properties related to lithium's unique characteristics within specific crystal frameworks. The fundamental reason for their ability to promote low-temperature densification lies in the enhanced solid-state diffusion kinetics enabled by the Li^+ ion.

Unlike liquid-phase sintering, densification in these systems is primarily driven by atomic diffusion. The small ionic radius (0.76 Å for CN=6) and low charge (+1) of the Li^+ ion facilitate a remarkably high diffusion coefficient, even at moderate temperatures [97]. This high mobility allows lithium ions to act as an "internal fluxing agent," effectively lowering the activation energy for the rate-limiting mass transport mechanisms, such as grain boundary and volume diffusion. In essence, the mobile Li^+ ions promote the necessary atomic rearrangement for neck growth and pore elimination without requiring the formation of a pervasive liquid phase. This localized "weakening" or increased dynamism in specific bond environments contributes to easier bond breaking and reforming, reducing the overall thermal energy required for sintering.

517 This is why lithium-based compounds with structures like rock salt (*e.g.*, Li_2TiO_3, $Li_3Mg_2NbO_6$)
518 and spinel (*e.g.*, $Li_3Mg_4NbO_8$) have emerged as promising materials for high-performance
519 microwave applications, often achieving high $Q \times f$ values (>50,000 GHz) at sintering
520 temperatures below 950°C [37, 98-100].

521 The presence of mobile Li ions contributes to densification at lower temperatures. According
522 to the relationship between cohesive energy and melting point proposed by Van Uitert [97],
523 materials with lower packing fractions (typically <60%) tend to have lower sintering
524 temperatures. However, exceptions exist: Li_3NbO_4 exhibits a packing fraction >65% but can be
525 sintered below 950°C due to its weak Li–O bonds and high bond polarity, which reduce the
526 activation energy for solid-state diffusion [29]. This is consistent with the Shannon's ionic radius
527 rules [101] and has been experimentally confirmed by Zhou *et al*. [97] Another striking exception
528 is Li_2WO_4, which adopts a phenacite-type structure (space group $I4_1/amd$). Despite its relatively
529 high packing fraction arising from a dense framework of WO_6 octahedra, Li_2WO_4 can be
530 densified at only 640-660 °C with a remarkable $Q \times f$ value of ~ 62,000 GHz, as reported by Zhou
531 *et al*. [27]. Its ultra-low sintering temperature is attributed to the weak Li–O bonding and the high
532 polarizability of the phenacite structure, which facilitates Li^+ diffusion even at moderate
533 temperatures. Moreover, Li_2WO_4 exhibits excellent chemical compatibility with both Ag and Al
534 electrodes at its sintering temperature, making it a promising ULTCC candidate for millimeter-
535 wave and terahertz applications [27, 102].

536 Recent investigations have revealed that partial substitution of O^{2-} anions with F^- anions can
537 significantly reduce the sintering temperature of rock salt-structured materials. This strategy
538 operates on a fundamental crystal chemistry principle: the substitution of a divalent O^{2-} anion
539 with a monovalent F^- anion introduces charge-compensating vacancies (either cation or anion

vacancies, depending on the system) and locally alters the Madelung energy of the lattice. This disruption can weaken the overall cohesive energy of the crystal, effectively lowering its melting point and, consequently, the sintering temperature. Moreover, the presence of fluorides can lead to the formation of low-melting eutectic phases with the oxide matrix, introducing a localized liquid phase at lower temperatures that further enhances densification kinetics. This dual mechanism is evident in the properties of several low-temperature sintered fluorides. For example, LiF exhibits a very negative τ_f microwave dielectric ceramic with high $Q\times f$ of 73,800 GHz, ε_r=9 and τ_f=−118 ppm/°C when sintered at 800 °C [103]. Although LiF itself has good microwave dielectric properties, it can be used as a dopant for properties tuning. Yang *et al.* incorporated LiF into $Zn_{1.8}SiO_{3.8}$ ceramics. Just 2 wt% of LiF was required to form a sufficient liquid phase capable of filling the pores to improve relative density and no secondary phases were detected in the XRD patterns. However, due to the volatilization of Li during sintering, ceramics with higher LiF content did not achieve further densification. The microwave dielectric properties were reported to be ε_r=6.3, $Q\times f$=64,200 GHz, and τ_f=−21.1 ppm/°C with the sintering temperature decreased from 1325°C to 950°C [104]. Zhang *et al*. reported a significant reduction in the sintering temperature of $Li_2Mg_3TiO_6$ from 1280°C to 950°C through the partial substitution of 8% O^{2-} with F^- [105]. Li_4NbO_4F ceramics can be sintered at low temperatures (750 °C–875 °C) to achieve high $Q\times f$ values up to 61,111 GHz and τ_f of −51 ppm/°C [106], $Li_7Ti_3O_9F$ at 950 ◦C, having $Q\times f$=88,200 GHz, ε_r=22.5, and τ_f=−24.2 ppm/°C [107].

Apart from the rock-salt structure, spinel structure $Li_2MTi_3O_8$ (M=Zn, Mg, Co, Cu, etc.) has been paid attention since 2010. Microwave dielectric features of $Li_2ZnTi_3O_8$ ceramic with cubic structure were firstly investigated by the research group of Zhou [30]. It was reported that there is some relevance between the degree of ordering and the microwave dielectric properties of

563 $Li_2ZnTi_3O_8$ ceramic. This compound is normally sintered at temperature around 1050°C-1125°C
564 using traditional sintering ($Q \times f$=62,000 GHz, ε_r=26.2, and τ_f=−15 ppm/°C) [30]. For the
565 occupation of Mg at M-site, the sintering temperature of $Li_2MgTi_3O_8$ shows similar to those used
566 for the $Li_2ZnTi_3O_8$ system which is 1075 °C [108]. However, the sintering temperatures required
567 to densify the material are typically too high for co-firing with metal electrodes. It has been
568 reported that substituting ions at the M-site with ions of similar ionic radii can effectively reduce
569 the sintering temperature while also improving the microwave dielectric properties [109-111].
570 This strategy has been significantly enhanced by first-principles calculations based on Density
571 Functional Theory (DFT), which can predict the energetic favorability of specific substitutions
572 and their resulting effect on the lattice dynamics and dielectric properties. Such computational
573 screening allows for a more targeted and efficient approach to material design, moving beyond
574 simple ionic radii rules to a more fundamental understanding of structure-property relationships.
575 The difference between the substituted cations and the host cations should be less than 10% to
576 induce the ordering effect in the system [101, 112].

577 **4.2.2 Tellurate-Based Systems**

578 Tellurate-based ceramics, such as $BaTe_4O_9$, $Bi_2Te_2O_8$, and $Zn_2Te_3O_8$, $MgTeMoO_6$,
579 ZnTeMoO6, $Li_3Y_3Te_2O_{12}$ and $Li_3Yb_3Te_2O_{12}$, present good microwave dielectric feature with low
580 sintering temperature [113-117]. Tellurate-based compounds are particularly interesting because
581 tellurium can adopt two distinct oxidation states: Te^{4+} and Te^{6+}. It is noted that Te^{4+} is prone to
582 reaction with silver metal.

583

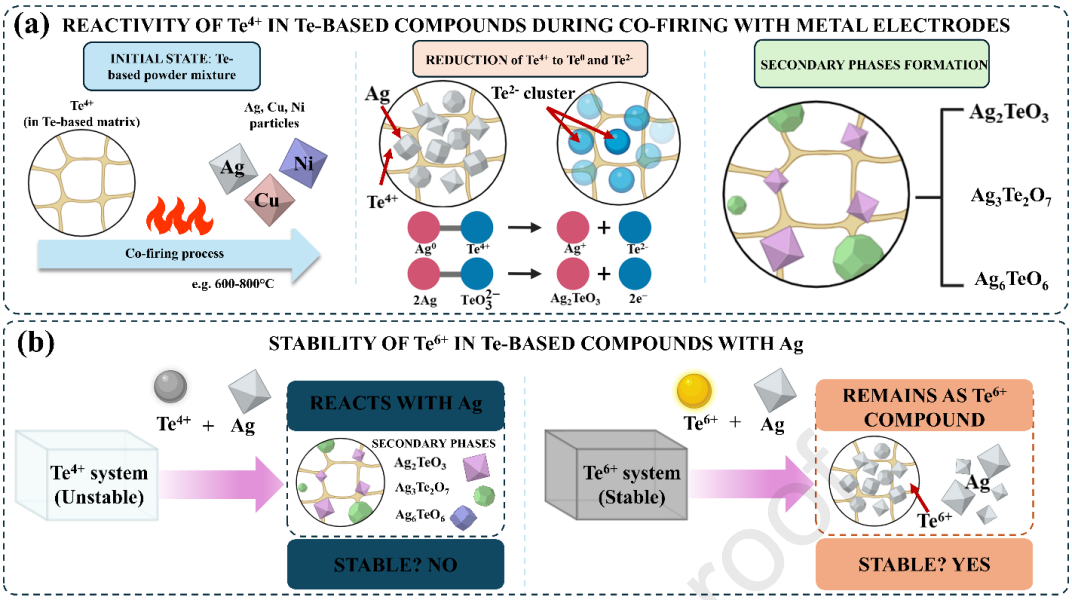

Fig. 8 A schematic diagram illustrating the redox reaction between tellurate-based ceramics containing Te^{4+} ions and metal electrodes (*e.g.*, Ag, Cu). (a) At elevated co-firing temperatures, the Te^{4+} ions are reduced to elemental tellurium (Te^0, Te^{2-}), which subsequently reacts with the metal electrode to form undesirable secondary phases such as Ag_2Te and other tellurides, compromising the device performance. (b) Comparison of the stability of Te^{6+} and Te^{4+} during co-firing with Ag.

Te^{4+} ions are susceptible to redox reactions at elevated temperatures, especially during co-firing with metal electrodes such as Ag, Cu, or Ni (see Fig. 8). The Te^{4+} species can be reduced to Te^0 (elemental Te) or even further to Te^{2-} [118]. This reaction leads to the undesirable formation of secondary phases like Ag_6TeO_6, Ag_2TeO_3, and $Ag_3Te_2O_7$ [119]. In contrast, Te^{6+} is considerably more stable and shows no reactivity with silver. The rational design of novel Te^{6+}-based compounds with low sintering temperatures is an active area of research, increasingly guided by high-throughput computational screening. By combining DFT calculations with crystal structure prediction algorithms, researchers are systematically exploring the vast compositional space to identify new, thermodynamically stable Te^{6+} garnets and perovskites that are predicted to exhibit

excellent microwave dielectric properties and chemical compatibility with silver, paving the way for the next generation of tellurate-based LTCCs. For example, recent studies have used DFT to compute the electronic structure, lattice dynamics, and phonon behavior of garnet-type tellurates such as $Li_3Y_3Te_2O_{12}$ and $Li_3Yb_3Te_2O_{12}$ [117, 120]. By calculating key properties such as band gap, dielectric permittivity, and phonon dispersion, DFT enables rapid prescreening of candidate compositions before experimental synthesis. This computational pre-selection drastically reduces the number of experimental iterations required to achieve a target microwave performance. Furthermore, machine learning models employing physically meaningful descriptors, notably bond ionicity, packing fraction, and cation polarizability, have been trained on existing tellurate and perovskite databases [121]. These models can rapidly screen thousands of hypothetical compositions and predict key microwave properties such as $Q\times f$ and ε_r. The synergy of DFT-calculated ground-state properties and ML-driven high-throughput screening is now being applied to identify new tellurate variants with predicted $Q\times f$ exceeding 150,000 GHz and sintering temperatures below 700 °C, thereby accelerating the development of next-generation ULTCC materials.

For the Te^{6+} compounds (see Fig. 9), Y. Tang *et al.* simply prepared the compounds via conventional sintering. The resulting $Li_3Y_3Te_2O_{12}$ displayed good microwave dielectric properties after sintered at 940°C (ε_r=7.83±0.2, $Q\times f$=47,800±500 GHz and τ_f=−47±3.0 ppm/°C), while $Li_3Yb_3Te_2O_{12}$ ceramic shows the best microwave dielectric properties after sintered at 950 °C (ε_r=5.94±0.2, $Q\times f$=41,800±500 GHz and τ_f=−76±3.0 ppm/°C). These compounds also show good compatibility with silver which makes them a good candidate for LTCC technology.

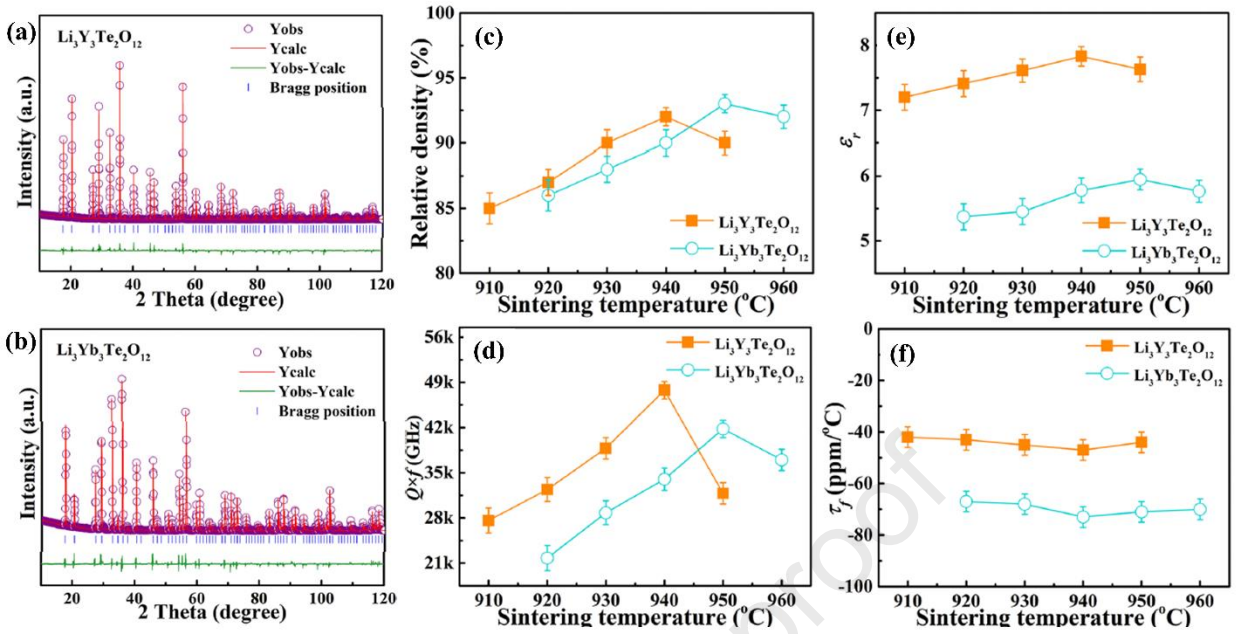

621

622 **Fig. 9** (a-b) XRD patterns of $Li_3Yb_3Te_2O_{12}$ and $Li_3Y_3Te_2O_{12}$ ceramics, respectively. (c-f) Relative
623 density and microwave dielectric of $Li_3Yb_3Te_2O_{12}$ and $Li_3Y_3Te_2O_{12}$ ceramics as a function of
624 sintering temperature [117].

625 **4.2.3 Vanadate and Silicate Systems**

626 A wide range of V_2O_5-based microwave dielectric compounds has been extensively
627 investigated and reported, owing to their low synthesis temperatures and superior chemical
628 compatibility with Ag electrodes [122-124]. $LiVO_3$ is one of the vanadate-based compounds that
629 show very low sintering temperature. C. Yin *et al.* demonstrated the microwave dielectric
630 properties of $LiVO_3$ ceramics. It shows a pure monoclinic single phase with a *C*2/*c* space group.
631 Optimal sintering conditions of 520°C for 8 hours yielded excellent microwave dielectric
632 properties (ε_r=8.78, $Q\times f$=16,900 GHz and τ_f=−117 ppm/°C) (see Fig. 10) [125].

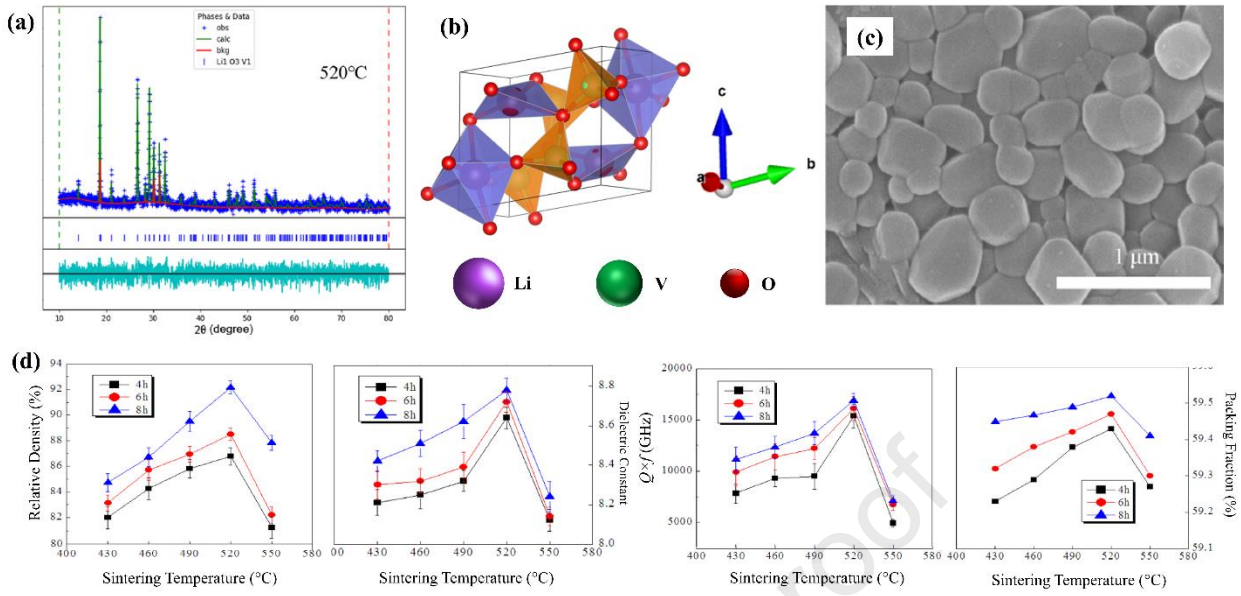

Fig. 10 $LiVO_3$ ceramics prepared by conventional sintering. (a,b) XRD pattern and microstructure of ceramic sintered at 520°C for 8 h. (c) Density and microwave dielectric properties as a function of sintering temperature [125].

Silicate-based olivine crystal structure was reported as another interesting LTCC system. It possesses a relatively high covalent bonding which is known as high sintering temperature microwave dielectric system (T_s~1300–1500°C). The high bond strength of the SiO_4 tetrahedral leads to low permittivity and high $Q\times f$. Substitution of Li^+ onto the A-site of the olivine structure can reduce the sintering temperature by 200–500 °C. Li_2SrSiO_4, when sintered at 880 °C, it exhibited microwave dielectric properties of ε_r=7.4, $Q\times f$=100,700 GHz, and τ_f=−85.4 ppm/°C (Fig. 11) [126].

Li-containing compounds are one of the keys for LTCC. However, there are some factors that might be determined. The presence of lithium and the resulting sintering mechanisms can have complex effects on the microwave dielectric properties. If the Li-containing liquid phase does not fully crystallize or is not completely incorporated into the main ceramic grains, a residual glassy phase at grain boundaries can act as a significant source of dielectric loss, especially if it contains

mobile Li^+ ions. Mobile ions contribute to relaxation losses at microwave frequencies, substantially lowering the $Q \times f$. Uncontrolled reactions leading to highly lossy secondary phases can also occur. Conversely, if the liquid phase perfectly aids densification by eliminating porosity (a major source of extrinsic loss) and facilitates the formation of a highly ordered, defect-free main phase, the $Q \times f$ can be optimized. Some Li-containing compounds are also intrinsically low-loss.

Moreover, the τ_f is a composite property affected by the thermal expansion and temperature dependence of the permittivity of all phases present. The thermal expansion and dielectric temperature characteristics of the Li-containing glassy or crystalline phases can significantly shift the τ_f of the composite, requiring careful tuning to achieve a near-zero value for temperature-stable devices. Optimizing these systems requires a delicate balance: maximizing densification and Ag-compatibility while simultaneously ensuring that the inherent advantages of low-temperature processing do not compromise the critical microwave dielectric properties, particularly the indispensable high $Q \times f$.

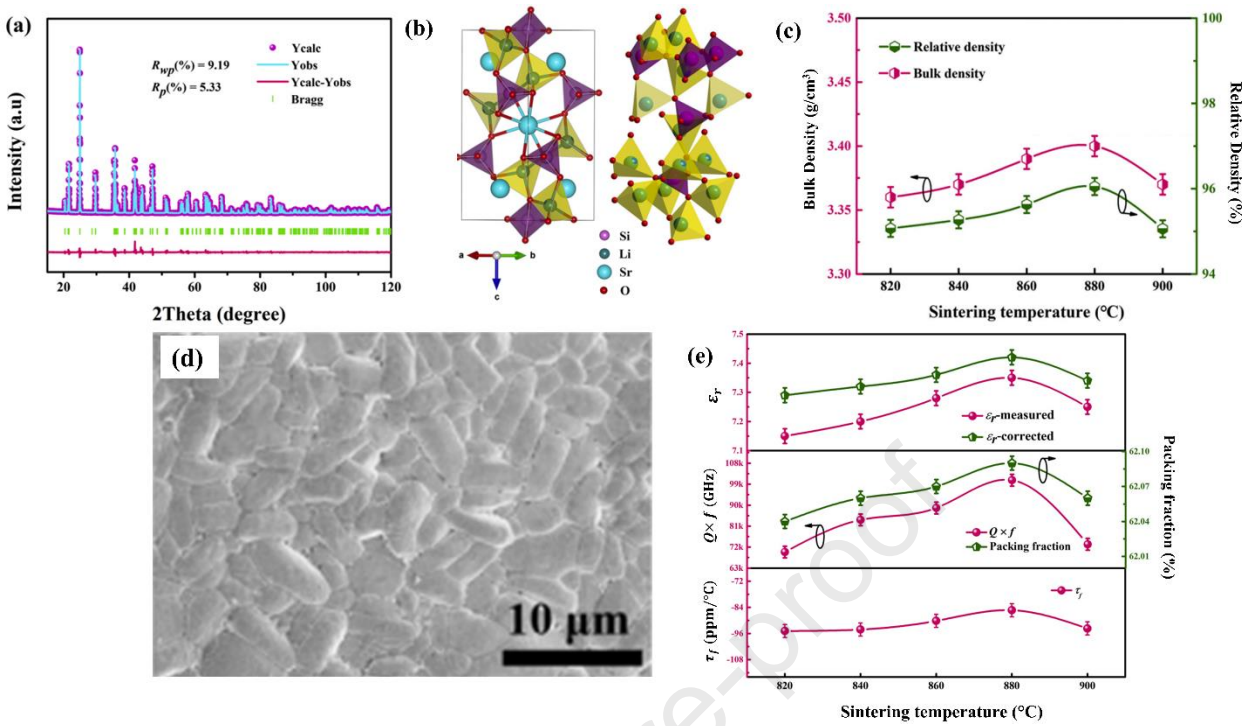

663

664 **Fig. 11** (a) XRD pattern of Li_2SrSiO_4 ceramic sintered at 880°C, (b) crystal structure of Li_2SrSiO_4

665 ceramic, (c) density of Li_2SrSiO_4 as a function of sintering temperature, (d) microstructure of

666 Li_2SrSiO_4 ceramic, and (e) microwave dielectric properties as a function of sintering temperature

667 [126].

668 **Table 2** Microwave dielectric properties and sintering temperature low-temperature firing

669 compounds

Family	Compound	T_s (°C)	ε_r	$Q\times f$ (GHz)	τ_f (ppm/°C)	Limitations	Ref.
Li-rock salt	Li_2TiO_3, Li_2ZrO_3	900–1000	20–30	Medium-high	Positive (large)	Requires dopants for $Q\times f$ improvement	[127, 128]
Li-spinel	$Li_2MgTi_3O_8$, $Li_4Mg_3Ti_5O_{18}$	800–900	13–16	High	Near zero	Li volatilization, atmosphere sensitivity	[30], [108]
Tellurate	$BaTe_4O_9$, $Bi_2Te_2O_8$, $Zn_2Te_3O_8$,	650–750	15–20	High	± tunable	Toxicity of Te, high raw material cost	[113-117]

	$MgTeMoO_6$, ZnTeMoO6, $Li_3Y_3Te_2O_{12}$ $Li_3Yb_3Te_2O_{12}$						
Vanadate	$Ba_3(VO_4)_2$, $Mg_3VO_4)_2$ $LiVO_3$	650–800	9–12	Medium-high	Negative	V_2O_5 volatilization, atmosphere control needed	[125, 129]
Tungstate	$MgWO_4$, $ZnWO_4$, $NiWO_4$, $CoWO_4$	850–950	15–18	Medium-high	Near zero	Higher T_s than vanadate/tellurate	[130]
Molybdate	$ZnMoO_4$, $MgMoO_4$	800–900	12–15	Medium	Positive	Moderate $Q\times f$, MoO_3 volatility	[131, 132]
Borate-based ceramics	$Zn_3B_2O_6$, $Mg_3B_2O_6$	750–850	7–10	Medium	Positive	Lower $Q\times f$ than oxide ceramics	[133, 134]

4.3 Cold sintering process (CSP)

As introduced historically in Section 3.5,CSP represents a paradigm shift in ceramic processing by enabling densification at remarkably low temperatures. This section provides a detailed mechanistic analysis of CSP, including the roles of the transient liquid phase, dissolution-precipitation, congruent/incongruent behavior, post-annealing strategies, and the critical issue of residual hydroxyl groups that affect microwave dielectric performance. Ceramic materials are known for their high melting temperatures due to strong ionic and/or covalent bonding. This necessitates high firing temperatures (typically exceeding 1,000 °C for oxides) and long dwell times (several hours) to achieve dense samples. However, most ceramics are fabricated by sintering powders at temperatures between 50% and 75% of their melting point. While this approach can achieve theoretical densities exceeding 95%, it also makes the sintering

process energy intensive. An additional challenge arises when ceramics contain volatile elements like Pb, Bi, Na, K, and Li. During high-temperature firing, these elements can evaporate, leading to stoichiometric variations in the final material [135-139]. To maintain the desired composition, various techniques are applied during the preparation process. For example, excess lead oxide is added to lead-based systems to achieve the desired composition and high-density samples [140, 141]. Researchers have employed several techniques to reduce sintering temperature and time consumption, including flash sintering [142], two-step sintering [143], spark plasma sintering [144], and microwave-assisted sintering [145]. All the mentioned sintering methods involve a diffusive mass transfer process to densify the ceramic samples. Sintering is driven by the thermodynamic principle of minimizing surface energy. As temperature increases, atoms diffuse and migrate to reduce surface area. This can cause the forming of necks between particles. This densification process reduces porosity and can lead to grain growth. The ultra-low sintering technique known as "cold sintering" was proposed by a research group of C. Randall. This term serves to distinguish it from traditional sintering methods, which necessitate high temperatures.[16]. The technique is a low-temperature consolidation method (temperature below 400 °C) used to fabricate materials and their composites by applying transient solvents with the assistant of external pressure which is much lower than the traditional high-temperature sintering process (temperature >1000 °C) [64]. The densification of ceramics by this technique is achieved through a dissolution-precipitation mechanism which depends on several factors, such as solvent type, applied pressure, temperature, and processing time [146-148]. The schematic diagram of cold sintering process is shown in Fig. 12.

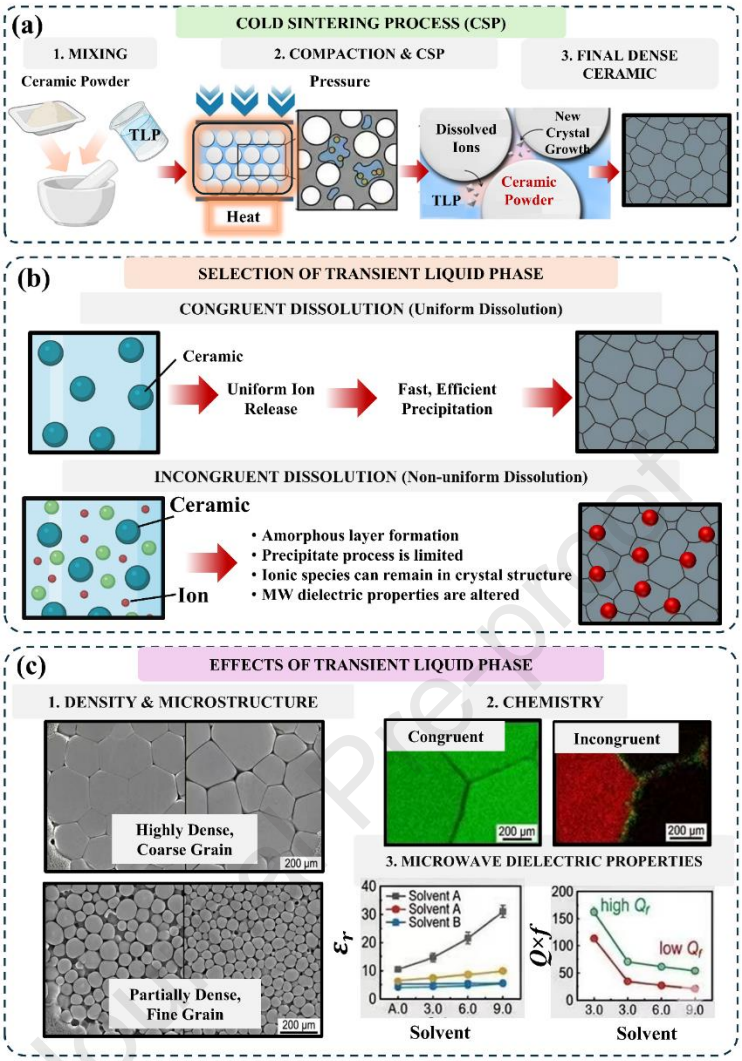

703

704 **Fig. 12** (a) Schematic of CSP mechanism, from powder–solvent mixture to densified ceramic. (b)
705 Diagram highlighting the transient liquid phase selection, distinguishing congruent from
706 incongruent dissolution. (c) Role of the transient liquid phase in promoting densification versus
707 incongruent dissolution, which may introduce defects and affect microwave dielectric properties.

708 Cold sintering technique is very similar to liquid-phase sintering [149]. In conventional
709 liquid-phase sintering, the glass phase is melted at high temperatures. In contrast, ceramic
710 densification is achieved by adding solvents and applying high pressure for cold sintering. The
711 steps of densification can be divided into two main steps. At the first step, it involves particle

712 rearrangement and compaction under external pressure and capillary forces. The presence of a
713 transient solution, elevated temperature, and increased pressure accelerates this process compared
714 to traditional dry pressing. The second stage of sintering involves densification through the filling
715 of voids between grains. In conventional solid-state sintering, mass transport occurs
716 predominantly through solid-state diffusion mechanisms. However, in cold sintering, the lower
717 temperature regime favors dissolution-precipitation as the dominant mass transport mechanism.
718 Dissolution-precipitation is particularly effective for compositionally sensitive ceramics that
719 exhibit congruent dissolution. For systems with limited solubility or incongruent dissolution,
720 densification may still occur, but this can compromise the overall material properties. A
721 representative case is $BaTiO_3$, a prototypical ferroelectric material that exhibits strongly
722 incongruent dissolution in pure water. During conventional cold sintering with water as the
723 transient liquid, Ba^{2+} ions preferentially leach out, leaving behind an amorphous Ti-rich layer that
724 hinders reprecipitation and results in poor densification (~70% relative density) [57]. To
725 overcome this limitation, barium hydroxide octahydrate ($Ba(OH)_2 \cdot 8H_2O$) has been employed as
726 a hydrated flux [150-152]. The excess Ba^{2+} ions in the transient liquid phase shift the local
727 chemical equilibrium, suppress Ba leaching, and promote a more congruent-like dissolution–
728 precipitation pathway. Consequently, a relative density of ~95% and a permittivity exceeding
729 1000 can be achieved at only 150 °C [151]. Nevertheless, this system is not fully congruent; high
730 uniaxial pressure (350 MPa) or subsequent post-annealing (600 °C) remains necessary to attain
731 optimal microwave dielectric properties, highlighting the remaining kinetic barriers [16]. Some
732 representative examples of solubility behavior and its impact on densification and phase purity in
733 CSP are summarized in Table 3.

734 **Table 3** Solubility behavior and its impact on the cold sintering process (CSP).

Ceramic system	Transient liquid phase	Dissolution behavior	Key Observations	Ref.
Li_2MoO_4	Deionized H_2O	Congruent	Complete dissolution and reprecipitation; no secondary phases	[153, 154]
$Na_2Mo_2O_7$	Deionized H_2O	Congruent	Full solubility in water; rapid densification	[56, 155]
K_2MoO_4	Deionized H_2O	Congruent	Similar to Li/Na molybdates	[156]
$LiMgPO_4$	Deionized H_2O	Congruent (Limited solubility)	Moderate solubility; assisted by pressure	[157]
$BaTiO_3$	Deionized H_2O	Incongruent	Ba^{2+} leaches out, forms amorphous Ti-rich layer on particle surfaces	[57]
$BaTiO_3$	$Ba(OH)_2/TiO_2$ Suspension	Congruent	Solvent chemistry adjusted to match Ba/Ti stoichiometry	[150-152]
$Mg_3B_2O_6$	Acetic acid (13.5M)	Congruent	Acid enhances solubility; prevents hydrolysis	[158]
ZnO	Acetic acid (0.5-5M)	Congruent	Acid increases Zn^{2+} solubility; promotes dissolution-precipitation	[146, 149]
ZnO	Deionized H_2O	Incongruent	Very low solubility in water	[159]

For microwave dielectric compounds, the cold sintering technique is proposed to fabricate in both single phase and composite microwave dielectrics. For the single-phase microwave dielectric, molybdate families have been fabricated using deionized water. Li_2MoO_4 which dissolves in deionized water can be densified at room temperature under a pressure of 130 MPa (ρ=87%–93%, ε_r=4.6–5.2 and $Q\times f$=10,200–18,500 GHz) [160]. Other compounds that can be densified using deionized water are, for examples, $Na_2Mo_2O_7$ (ρ=93.7%, ε_r=13.4, $Q\times f$=14,900 GHz), $K_2Mo_2O_7$ (ρ=94.1%, ε_r=9.8, $Q\times f$=16,000 GHz) [56], $(Li,Bi)_{0.5}MoO_4$ (ρ=88.5%, ε_r=33.7,

$Q\times f$=2,300 GHz, τ_f=+184 ppm/°C), $Na_{0.5}Bi_{0.5}MoO_4$ (ρ=85%, ε_r=20.7, $Q\times f$=1,500 GHz, τ_f=+46 ppm/°C) [154], $(Bi_{0.95}Li_{0.05})(V_{0.9}Mo_{0.1})O_4$ (ρ=73%, ε_r=30, $Q\times f$~1300 GHz, τ_f=+61 ppm/°C), K_2MoO_4 (ρ=100%, ε_r=6.37, $Q\times f$=26,500 GHz, τ_f=−70 ppm/°C), $NaBiSrMoO_4$ (ρ=94%, ε_r=15.48, $Q\times f$=18,763 GHz, τ_f=+2.7 ppm/°C) [156], $LiMgPO_4$ (ρ=93%, ε_r=6.5, $Q\times f$=16,000 GHz) [157]. As seen, the microwave dielectric compounds that can be cold sintered are mostly contained molybdenum. However, the high cost of molybdenum can limit the economic benefits of cold sintering.

Zhou *et al.* demonstrated the cold sintering technique for LiF microwave dielectric ceramics using water as the transient liquid phase [161]. The compound normally exhibits a low firing temperature (T_S~800°C). The previously reported the relative density of the conventional sintered LiF is 90.2% with $Q\times f$ value of 73,800 GHz (see Fig. 13 (a-d)) [103]. However, the cold sintered LiF shows the higher relative density around 97%. In that work, optimal microwave dielectric properties were achieved when samples were sintered under a pressure of 600 MPa at 100°C, yielding ε_r=8.56, $Q\times f$=143,000 GHz, and τ_f=−137 ppm/°C [161]. In a separate study, LiF ceramics were also prepared using the cold sintering technique, but notably, with an initial pre-calcination step. Yuan *et al*. reported that the pre-calcination temperature significantly influenced the microstructure and microwave dielectric properties of the final product. The higher $Q\times f$ value could be primarily attributed to improvements in both density and crystallinity. Optimal microwave dielectric properties (ε_r=8.80, $Q\times f$=33300 GHz, and τ_f=+138 ppm/°C) were attained by cold sintering LiF powder that was pre-calcined at 800°C [162].

While these CSP-processed LiF systems already demonstrate impressive $Q\times f$ values compared to many other low-temperature ceramics, when benchmarked against projected sub-THz 6G requirements ($Q\times f$>~200,000 GHz and tan δ in the 10^{-5}–10^{-6} range), it is clear that

CSP-based materials still face a substantial performance gap. This gap motivates the hybrid CSP + post-annealing strategies and solvent-engineering approaches discussed in the following sections.

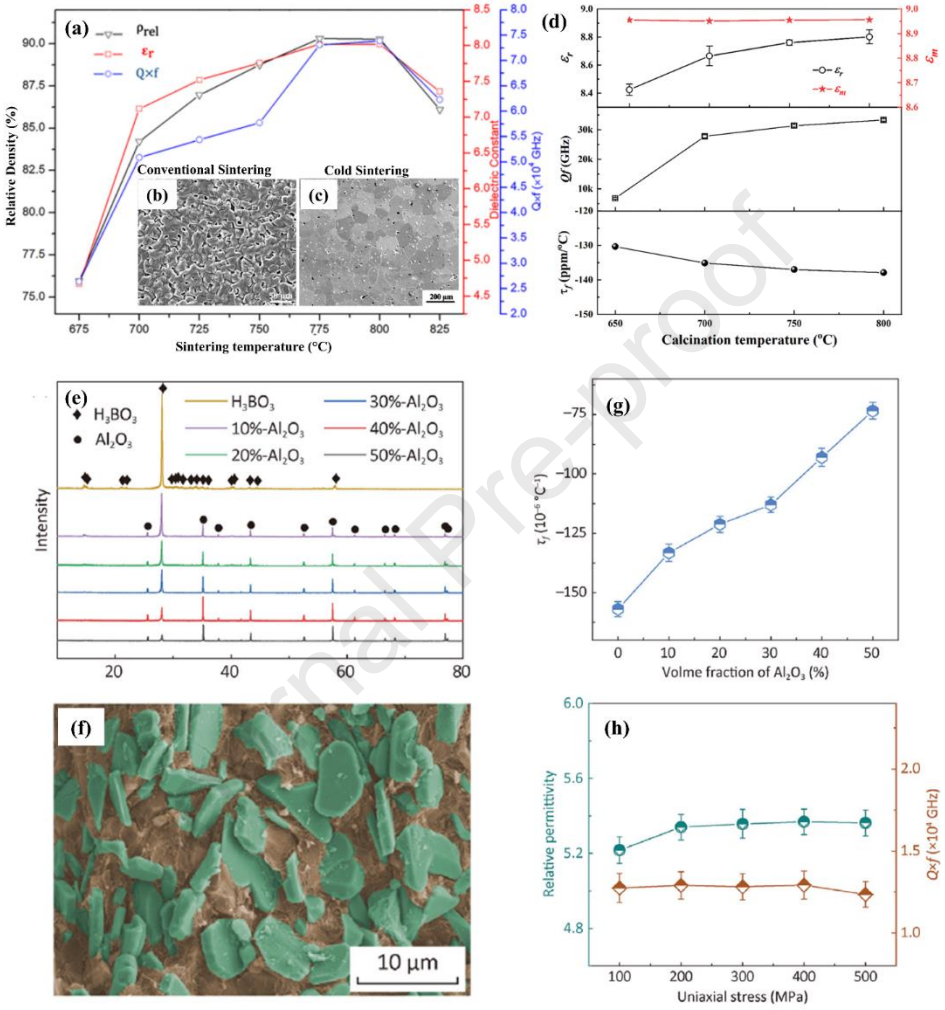

Fig. 13 LiF ceramics prepared by conventional sintering and cold sintering techniques. (a) Relative density and microwave dielectric properties as a function of sintering temperature. (b) Microstructure of conventional sintered LiF ceramics. (c) microstructure of cold sintered LiF ceramics. (d) Microwave dielectric properties as a function of calcination temperature. Adapted from Ref. [103, 162]. Characterization of cold sintered Al_2O_3- H_3BO_3 composite ceramics. (e) XRD patterns showing the phase composition as a function of Al_2O_3 volume fraction. (f)

Scanning electron microscope (SEM) micrograph of the composite with 50 vol% Al_2O_3, showing plate-like Al_2O_3 particles (false-colored green) embedded in the H_3BO_3 matrix. (g) Temperature coefficient of resonant frequency (τ_f) as a function of Al_2O_3 volume fraction. (h) Relative permittivity (ε_r) and quality factor ($Q\times f$) as a function of applied uniaxial stress for the 50 vol% Al_2O_3 composite. Adapted from Ref. [163].

Zeng *et al.* reported the room temperature sintering of Al_2O_3-H_3BO_3 composite ceramic which exhibits negative τ_f. They found that H_3BO_3 facilitates plastic deformation in a deionized water medium, which significantly enhances the densification of Al_2O_3-H_3BO_3 ceramics even under minimal uniaxial stress (100 MPa). The resulting material achieves a high relative density exceeding 96% with good microwave dielectric properties (ε_r=5.37, $Q\times f$=12,924 GHz, and τ_f=−73.42 ppm/°C) (see Fig. 13 (e-h)) [163].

Researchers are exploring alternative materials such as aluminates, titanates, and phosphates. While these materials may have lower solubility, making cold sintering more challenging, they offer potential for lower-cost, high-performance microwave ceramics. It is important to note that while cold sintering can produce fine-grained ceramics, the specific grain size and microstructure can be influenced by factors such as the starting powder size, solvent type, applied pressure, and sintering temperature.

In some cases, cold sintering technique is employed to fabricate ceramic compounds that exhibit limitations when processed through conventional sintering. M. Chi *et al.* prepare $Mg_3B_2O_6$ ceramic by cold sintering at 150 °C using acetic acid as a transient liquid phase followed by post annealing. This ceramic system showed some evaporation and decomposition during the conventional sintering at sintering temperature around 1300°C [134, 164]. Ceramic obtained by cold sintering technique showed the relative density around 80%. After post

799 annealing at 900 °C, the density improved to 91% with good microwave dielectric properties
800 (ε_r=6.37, $Q\times f$=16,686 GHz, and τ_f=−63.74 ppm/°C) [158].

801 Although the cold sintering process provides a promising paradigm of low temperature
802 ceramic processing, its utility for ultra-high Q microwave dielectrics is fundamentally limited by
803 materials science constraints that are inherent to its low-temperature, solution-based mechanism.
804 The low temperature densification mechanism in cold sintering is insufficient to overcome the
805 kinetic limitations for pore elimination and, more critically, for the formation of chemically and
806 structurally pristine grain boundaries. Moreover, inhomogeneity, residual elements from transient
807 liquid phase and microstructural defects are factors that make cold sintering a challenging
808 technique for microwave dielectric ceramics fabrication. Conventional sintering achieves
809 densification predominantly through solid-state diffusion kinetics using high thermal energies.
810 This elevated temperature promotes rapid atomic and vacancies mobility where pore can be
811 eliminated easily. In contrast, the densification process in cold sintering is different. At low
812 temperatures, the rate of atomic diffusion in the solid state is extremely low. Thus, the kinetics of
813 pore elimination in the final stage of sintering are restricted [57]. Incomplete removal of transient
814 liquid phase components or their decomposition products can leave behind nanoscale voids or
815 residues that contribute to porosity. However, for ultra-high Q materials, the most detrimental
816 factors extend beyond simple porosity and lie within the chemistry and structure of the grain
817 boundaries themselves.

818 Firstly, the incomplete removal of the aqueous transient phase, which is fundamental to the
819 CSP mechanism, often leaves residual hydroxyl groups (OH^-) trapped within the ceramic matrix.
820 These polar OH^- groups, particularly concentrated at the grain boundaries, possess a strong
821 dipole moment. When subjected to an oscillating microwave electric field, these dipoles attempt

to reorient, leading to significant dipolar relaxation losses which directly and severely degrade the quality factor. The low processing temperature of CSP is insufficient to drive off these chemically bound species, making this a fundamental challenge. For cold-sintered $Mg_3B_2O_6$ by Chi *et al*. [158], their work clearly shows a broad FTIR absorption band centered at ~3400 cm^{-1} (characteristic of O-H stretching) in the as-cold sintered sample. This band virtually disappears after post-annealing at 900 °C, 3h. Critically, the $Q \times f$ value increases from ~5900 GHz to ~16700 GHz, directly linking the removal of OH^- to the suppression of dielectric loss. For LiF, we also include a similar correlation from Zhou *et al*. [161], where the $Q \times f$ value improves from ~4500 GHz to >111,000 GHz after a 800 °C anneal, which is attributed to the elimination of residual OH^- and other point defects. These representative cases clearly demonstrate that post-annealing in the 400-800 °C range can yield a factor-of-two or greater improvement in $Q \times f$ via the removal of residual OH^- and the healing of grain-boundary defects, as summarized in Table 4. The Effect of post-annealing temperature on the microwave dielectric properties are summarized in Table 4.

Table 4 Effect of post-annealing temperature on the microwave dielectric properties of cold-sintered ceramics (comparison in the 400–800 °C range)

Ceramic system	CSP condition	Annealing condition	$Q \times f$ (GHz)		Key change	Ref.
			As-cold sintered	After annealing		
LiF	150 °C, 250 MPa	800 °C, 2 h	~4500	~111000	$Q \times f$ improves from ~4500 to ~111000 GHz due to OH^- elimination	[165]
$Mg_3B_2O_6$	150 °C, 800 MPa	900 °C, 3 h	~5900	~16700	As-cold sintered sample exhibits strong OH^- band (FTIR), post-annealing at 900 °C removes OH^-	[158]
$Zn_3B_2O_6$	200 °C, 300 MPa	550 °C, 3 h	~6300	21000	Acetic acid transient liquid leaves residual OH^-/acetate; annealing at 550 °C removes	[166]

					these species. Post-annealing also promotes fine grain precipitation between larger grains, forming uniform dense microstructure	
BaF_2	150 °C, 600 MPa	900 °C, 3 h	~53000 (conventional sintered)	~82000	No aqueous solvent used, post-annealing enhances crystallinity and density,	[167]
CaF_2	150 °C, 750 MPa	1,000 °C, 3 h	~26000 (conventional sintered)	~81000	OH^- not relevant, post-annealing eliminates the amorphous grain-boundary phase, leading to clearer grain boundaries, higher crystallinity, and thus higher $Q \times f$.	[168]
TiO_2	300 °C, 350 MPa	1,000 °C, 2 h	~6000 (conventional sintered)	31900	CSP+ post-annealing promotes recrystallization with clear grain boundaries and reduced amorphous phase.	[169]

Secondly, the dissolution-precipitation process can result in the formation of a thin, disordered amorphous phase at the grain boundaries. Unlike the highly ordered, low-loss crystalline grains, this amorphous interfacial layer disrupts long-range lattice periodicity, increases phonon scattering, and introduces a continuum of energy states that dissipate microwave energy. This structurally imperfect "glue" between grains acts as an intrinsically lossy medium, placing a ceiling on the achievable $Q \times f$ value, regardless of the bulk crystal quality.

As known, the dielectric permittivity of air is around 1 ($\varepsilon_r \sim 1$). The presence of such porosity, along with these chemically and structurally defective grain boundaries, leads to a reduction in the overall effective permittivity (ε_r) of the material and an increase in dielectric loss. Even a small volume of pores, coupled with lossy interfacial phases, can substantially elevate the total loss. Furthermore, pores can store moisture or other impurities that can increase the dielectric loss [170].

While the low sintering temperature can significantly affect the microwave dielectric properties, the selection of an appropriate transient liquid phase is also crucial. This is because various ceramic compounds exhibit differing solubilities, thereby requiring distinct transient liquid phases for effective cold sintering. If the ceramic compounds undergo incongruent dissolution, amorphous layers can be formed on the particle surfaces which limited the precipitation process [57]. This phenomenon mainly occurs in perovskite and spinel compounds which are hardly soluble in water. The formation of amorphous layers perturbs the overall stoichiometry of the system. Moreover, this amorphous layer makes the mass transport between liquid and solid interface more difficult thus impedes the nucleation or precipitation [57]. It is suggested that, nanoparticles provide more lattice sites which facilitate the precipitation process [171]. A study by H. Guo demonstrated the use of a $Ba(OH)_2/TiO_2$ aqueous suspension instead of pure water to prevent the incongruent phenomenon for the cold sintering of $BaTiO_3$ [172]. However, the impurity phase such as $BaCO_3$ occurs. This $BaCO_3$ phase is possibly formed because the cold sintering process was done in an ambient environment where Ba can react to CO_2 in the atmosphere. The present of $BaCO_3$ affects the electrical properties. Some studies have used acidic and/or basic solutions to fabricate microwave dielectric ceramics, such as NaOH solution, NaOH-KOH flux, acetic acid, oxalic acid, hydrochloric acid, or formic acid [150, 151, 173, 174]. After the cold sintering process, some ionic species, such as K^+, Na^+, and Cl^-, may remain in the crystal structure. This substitutional incorporation consequently influences the material's dielectric response. When cations or anions of different sizes are substituted, whether on A-site or B-site, the bond length and bond strength are altered [175]. This can result in both its dielectric permittivity (ε_r), quality factor and temperature coefficient of resonance frequency (τ_f) [176-178].

Due to the low temperature processing, the cold sintering process has potential for co-sintering microwave dielectric ceramics with other components such as polymer, metal, or other nanoparticles forming composite materials and functionally graded materials. This process enables the integration of ceramics with polymers or other ceramics without thermal degradation. A composite between $Na_2Mo_2O_7$ microwave dielectric with polyetherimide (PEI) cold sintered at 120 °C for 20 minutes using DI water can achieve a high relative density in the range 94%-98% [155]. Li_2MoO_4 composited with PTFE represented relative density from 92%-98% after cold sintered at 120°C for 15-20 minutes. It is showed that as the concentration of PTFE increases, the temperature coefficient of resonant frequency is closer to zero (see Fig. 14) [179].

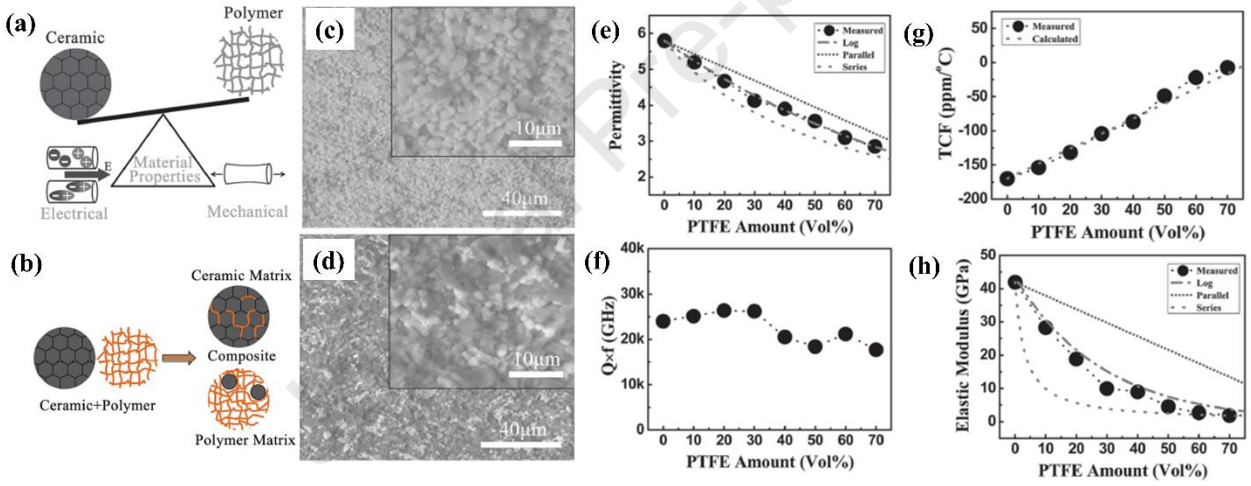

Fig. 14 (a) Effects of ceramic/polymer ratio on the properties of Li_2MoO_4 composited with PTFE. (b) IIllustration of different amount of ceramic/polymer. (c) Microstructures of cold sintered ceramic-polymer Li_2MoO_4 composited with PTFE at composition of $90Li_2MoO_4$-10PTFE and (d) $40Li_2MoO_4$-60PTFE. (e) Permittivity, (f) quality factor, (g) temperature coefficient of resonant frequency. (h) Elastic modulus as a function of PTFE concentration [179].

Despite its revolutionary potential in temperature reduction, a critical analysis reveals that CSP currently faces significant performance trade-offs when compared to established LTCC and

emerging ultra-low temperature co-fired ceramic (ULTCC) technologies. While CSP enables densification at unparalleled low temperatures (<200°C), the resulting microwave dielectric properties, particularly the quality factor, often lag behind. For instance, cold-sintered LiF and molybdate-based systems typically exhibit $Q \times f$ values in the range of 10000–25000 GHz, with exceptional cases reaching up to ~143000 GHz under optimized conditions [160, 161]. However, these values are generally lower than those achieved by state-of-the-art LTCC and ULTCC systems, which consistently deliver $Q \times f$>40000 GHz and can exceed 100000 GHz [57, 180]. This performance gap is primarily attributed to the fundamental mechanisms of CSP: the incomplete removal of the transient liquid phase (often water) leaves residual hydroxyl (OH^-) groups, and the low-thermal-energy process promotes the formation of disordered amorphous phases at grain boundaries. These features act as sources for dipolar relaxation and phonon scattering, respectively, fundamentally limiting the achievable dielectric loss at microwave frequencies.

Overcoming these intrinsic limitations is the central focus of current CSP research. A promising strategy involves multi-stage processing, where a low-temperature cold sintering step is followed by a controlled, moderate-temperature post-annealing step (*e.g.*, 400 °C–800 °C). This hybrid approach aims to leverage CSP for initial densification and shaping, while the subsequent thermal treatment provides the necessary energy to drive off residual volatile species and facilitate grain boundary crystallization, thereby significantly improving the $Q \times f$ value [69, 158]. Furthermore, research is actively exploring advanced solvent systems beyond deionized water, including non-aqueous or chemically reactive transient phases that can promote congruent dissolution and minimize the formation of undesirable amorphous intermediates. The integration of CSP with other energy sources, such as microwave-assisted cold sintering, also presents an

intriguing pathway to enhance reaction kinetics at the particle-liquid interface. The ultimate goal is to engineer a CSP-based workflow that can produce ceramics with microstructures and properties comparable to high-temperature methods, thus unlocking its full potential as a truly disruptive and sustainable manufacturing technology for next-generation electronic devices. To provide a holistic overview, the key characteristics, advantages, and limitations of the three primary low-temperature sintering strategies discussed in this section are comparatively summarized in Table 5.

CC

Table 5. A comparative analysis of the primary strategies for low-temperature sintering of microwave dielectric ceramics, highlighting their respective mechanisms, typical performance ranges, and key challenges.

Parameter	Sintering aids (*e.g.*, Glass Additives)	Intrinsic low-T_S compounds (*e.g.*, Li-based)	Cold sintering process (CSP)
Typical sintering temperature	850 °C–950 °C	800 °C–950 °C	<200 °C (initial densification) + post-annealing (400 °C–900 °C)
Primary mechanism	Liquid-phase sintering	Enhanced solid-state diffusion	Pressure-assisted dissolution-precipitation
Typical $Q\times f$ (GHz)	40000–80000	50000–100000+	10000–30000 (can be higher)
Key advantage	Cost-effective, widely applicable	High $Q\times f$, intrinsic low loss	Unparalleled T reduction, Polymer/Metal Compatible
Primary limitation	Potential secondary phases, residual glass is lossy	Li volatilization, higher cost of some precursors	Lower $Q\times f$ (residual OH^-), Limited material systems

Future outlook	Multi-component glass design, glass-ceramics	Anion substitution (F^-), high-entropy designs	Hybrid processing (post-annealing), solvent engineering

While these academic advancements in sintering aids, intrinsic materials, and cold sintering demonstrate immense promise in the laboratory, their translation to high-volume manufacturing introduces a complex interplay of performance, cost, and reliability. The ultimate success of these materials is not judged by their properties alone, but by their ability to be integrated into robust, scalable production processes. The next section will therefore shift focus from the laboratory to the factory floor, exploring how industry leaders are navigating these challenges and commercializing low-temperature technologies through proprietary innovations and strategic material design.

4.4 Unified Process-Structure-Property Framework

The three low-temperature sintering strategies, sintering aids, intrinsically low-T_s compounds, and CSP, each achieve densification through distinct mechanisms, yet they converge on the same microstructure-property objectives: high density, clean grain boundaries, and minimal extrinsic losses (see Fig. 15). This unified lens allows direct comparison of trade-offs: sintering aids offer the widest compositional flexibility but at the cost of residual glass-related loss; intrinsic low-T_s compounds achieve higher $Q \times f$ (often >80000 GHz) but are largely limited to Li-rich chemistries; CSP enables unparalleled temperature reduction (<300 °C) but currently sacrifices $Q \times f$ unless a controlled post-anneal is applied. The following sections build on this framework to analyze industrial viability and future research directions.

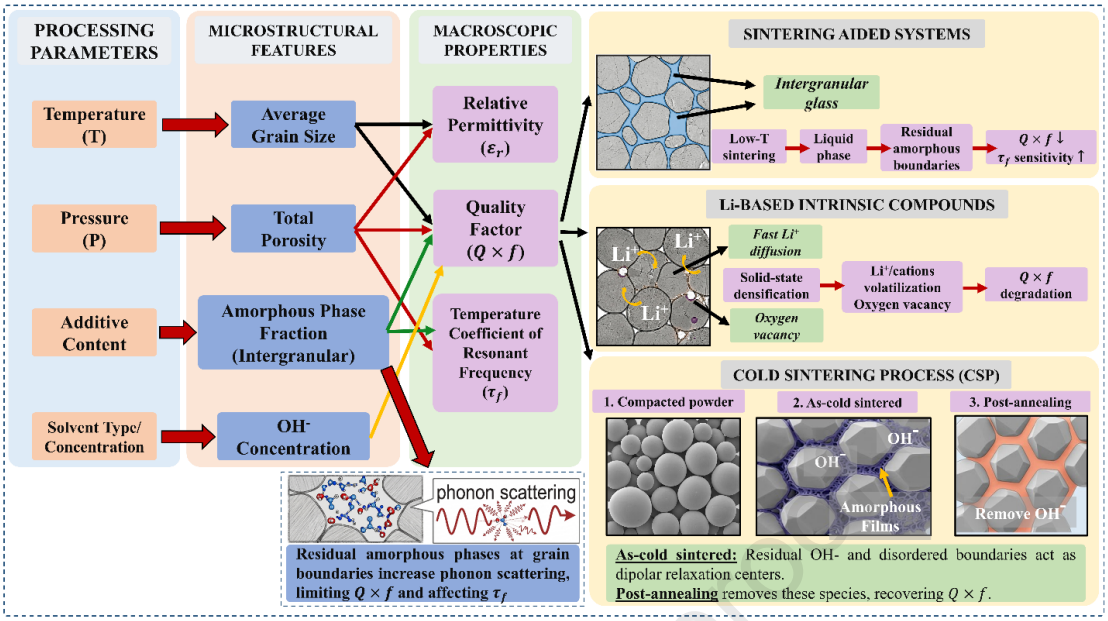

945

946 **Fig. 15** Unified conceptual diagram linking processing, microstructure, and macroscopic
947 properties in microwave dielectric ceramics.

948 To complement this conceptual framework, an Ashby-type plot (Fig. 16) compiles
949 representative $Q \times f$ values as a function of sintering temperature for LTCC/sintering-aid systems,
950 intrinsic low-T_s/ULTCC compounds, and CSP-processed ceramics. This quantitative overview
951 highlights the distinct performance windows of each strategy and visualizes how CSP combined
952 with post-annealing can partially close the gap towards LTCC/ULTCC, while still falling short of
953 the projected sub-THz 6G requirements.

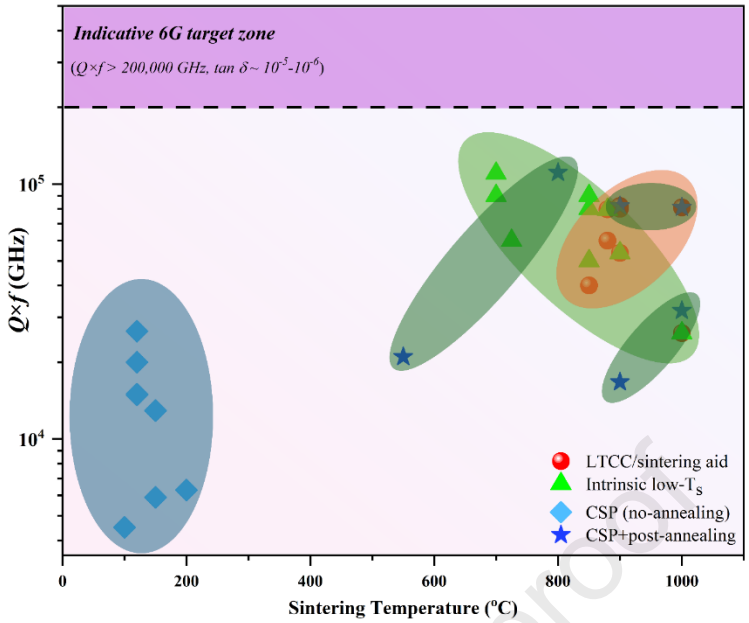

954

955 **Fig. 16** Ashby-type plot of sintering temperature versus $Q \times f$ for representative low-temperature
956 microwave dielectric systems. Data points are taken from selected LTCC/sintering--aid
957 compositions, intrinsic low-T_s/ULTCC compounds, and CSP-processed ceramics (with and
958 without post-annealing), using values compiled in Tables 2–4. Shaded regions indicate typical
959 performance windows for each strategy, highlighting the trade-off between sintering temperature
960 and achievable $Q \times f$ and the current gap to sub-THz 6G targets.

961 **5. Industrial Case Studies**

962 The translation of academic breakthroughs in low-temperature microwave dielectric
963 ceramics to high-volume manufacturing is a complex endeavor, fraught with technical, economic,
964 and intellectual property challenges. While academic studies often prioritize record-low sintering
965 temperatures or exceptionally high $Q \times f$ values, industrial LTCC development is fundamentally
966 application-driven. Commercial systems must balance electrical performance with multilayer
967 processability, thermal management, mechanical robustness, and long-term operational stability.
968 Consequently, different industrial players have adopted distinct material-design philosophies and
969 processing strategies depending on the targeted frequency regime and packaging requirements.

Within the unified process–structure–property framework developed in Section 4.4, these industrial case studies can be viewed as distinct optimization choices along the axes of residual glass content, interface stability, and processing window.

5.1 Industry Leaders and Core Technologies

Murata Manufacturing has long focused on low-loss, mechanically robust LTCC systems based on controlled crystalline phase assemblages rather than highly glass-rich formulations. A cornerstone of their technology, disclosed in patents like EP2397452B1, is a unique quartz-alumina-fresnoite ($Ba_2TiSi_2O_8$) microstructure [181]. This design enables co-firing with Ag/Cu electrodes below 1050°C while maintaining low permittivity ($\varepsilon_r \leq 10$) and low loss ($\tan \delta < 0.001$). The innovation lies in the controlled crystallization of the fresnoite phase, which enhances thermal conductivity and mechanical strength, making these materials ideal for demanding applications like millimeter-wave automotive radar (77–81 GHz) [182]. The primary challenge remains silver migration, which Murata mitigates through crystalline barrier phases and surface passivation [183]. Such crystallized systems are particularly attractive for millimeter-wave RF modules and automotive radar applications because they minimize excessive residual glass phases that can degrade dielectric performance at high frequencies. However, this approach requires precise control of phase evolution during firing and introduces relatively narrow processing windows for large-scale multilayer manufacturing.

Samsung Electro-Mechanics (SEMCO), in contrast, has concentrated heavily on dimensional stability and multilayer registration control. Patented LTCC architectures employ combinations of plate-like and globular ceramic particles within glass-assisted sintering matrices to suppress *x-y* shrinkage and improve alignment precision in multilayer structures [184]. This approach is vital for the high-yield production of fine-line (>30 layers) RF substrates for 5G,

993 enabling tight inter-layer registration (<15 μm) required for complex 3D structures with
994 embedded cavities and passives [185]. TDK Corporation targets the IoT and high-frequency filter
995 markets with tunable BaO-TiO_2-SiO_2 glass-ceramic composites (ε_r=6-15) designed for sintering
996 below 900°C [186]. Their foundational patents (*e.g.*, JP S51143898A) [187] and subsequent
997 innovations focus on proprietary sintering additives (*e.g.*, MnO_2, Nd_2O_3) that promote liquid-
998 phase sintering while -preserving high quality factors ($Q \times f$ > 40,000 GHz) [184]. Like Murata,
999 TDK grapples with silver migration and humidity-related degradation, which they address with
1000 protective surface passivation layers. Such materials remain commercially relevant for sub-6
1001 GHz communication modules, IoT devices, and RF filters because they provide a practical
1002 balance among dielectric performance, manufacturability, and cost. However, residual amorphous
1003 phases and liquid-phase sintering routes may limit performance under mm-Wave conditions and
1004 increase susceptibility to humidity-related degradation or interfacial instability.

1005 Vibrantz Technologies (formerly Ferro Electronic Materials) has specifically targeted
1006 high-frequency 5G applications requiring ultra-low dielectric loss and enhanced thermal
1007 management. Commercial LTCC tape systems such as A6M-E and M7 are designed for operation
1008 in the 10-60 GHz range and emphasize low insertion loss, stable dielectric behavior, high thermal
1009 conductivity, and mechanical robustness [188]. Based on a magnesium-silicate composition, this
1010 system achieves an extremely low loss tangent (tan δ<0.0003 at 10 GHz) and high thermal
1011 conductivity (λ>4 $W \cdot m^{-1} \cdot K^{-1}$) after sintering at 850 °C. This demonstrates a clear industry trend
1012 towards developing specialized material systems optimized for specific frequency bands and
1013 performance targets, rather than a one-size-fits-all approach.

1014 Despite targeting similar low-temperature co-firing applications, these industrial strategies
1015 differ substantially in their optimization priorities, processing philosophies, and targeted

operating frequency ranges. Murata-type crystallized systems prioritize dielectric stability and mechanical reliability for demanding high-frequency environments, whereas SEMCO emphasizes dimensional precision and multilayer manufacturability. TDK-type glass-ceramic systems remain attractive for scalable and cost-sensitive applications, while Vibrantz focuses explicitly on ultra-low-loss performance for emerging mm-Wave and advanced 5G packaging technologies.

5.2 Analysis and Emerging Trends

The comparative industrial landscape reveals that no universal LTCC material platform currently satisfies all requirements for next-generation wireless communication systems. Instead, industrial development is increasingly application-specific, with different material systems emerging for sub-6 GHz infrastructure, mm-Wave RF modules, automotive radar, heterogeneous integration, and prospective 6G packaging technologies.

For sub-6 GHz applications and IoT devices, conventional glass-ceramic LTCC systems remain commercially dominant because cost efficiency, multilayer scalability, and moderate dielectric performance are prioritized over achieving the lowest possible dielectric loss. In contrast, mm-Wave applications operating above ~24 GHz impose significantly stricter requirements on dielectric loss, thermal conductivity, conductor-interface stability, and dimensional precision. Under these conditions, crystallized low-glass systems and highly optimized low-loss composites become increasingly attractive.

This trend is strongly reflected in recent industrial patents and emerging ultra-low-temperature co-fired ceramic (ULTCC) systems. Recent developments increasingly move away from conventional silicate-rich LTCC chemistry toward molybdates [189], tungstates [190], vanadates [191], and chemically engineered composite systems capable of densification below ~700 °C. Lower processing temperatures not only reduce manufacturing energy consumption,

but also mitigate thermally activated interfacial diffusion and conductor migration, thereby improving compatibility with Ag, Cu, and potentially even Al metallization.

At the same time, the industrial emphasis is gradually shifting from merely lowering sintering temperature toward holistic optimization of process-structure-property relationships. Future commercial competitiveness will likely depend on simultaneously balancing dielectric loss, shrinkage behavior, thermal transport, multilayer integration capability, reliability, and manufacturing yield rather than maximizing a single dielectric parameter alone.

Table 6 Comparative positioning of representative industrial LTCC strategies for high-frequency applications

Industrial route	Main strategy	Key advantage	Main limitation	Most suitable application
Murata-type crystallized LTCC	Controlled crystalline phase assemblage	High dielectric stability and mechanical robustness	Narrow processing window	77-81 GHz automotive radar, high-reliability mmWave RF modules
SEMCO dimensional-control LTCC	Platelet-assisted shrinkage control	Excellent multilayer registration	Glass-assisted loss/reliability trade-offs	High-density 24-40 GHz RF substrates and embedded passive architectures
TDK glass-ceramic LTCC	Glass-assisted low-temperature densification	Scalable and cost-effective manufacturing	Residual glass-related dielectric limitations	Sub-6 GHz 5G modules, IoT devices, RF filters
Vibrantz/Ferro low-loss LTCC	Ultra-low-loss RF packaging system	Excellent mm-Wave dielectric performance	Higher process/material complexity	24-60 GHz 5G mmWave packaging

				and high-speed RF interconnect
Emerging ULTCC systems	Ultra-low-temperature densification	Reduced interfacial diffusion and lower thermal budg	Limited industrial maturity	Prospective 6G sub-THz and heterogeneous integration platform

The comparative analysis indicates that no single LTCC platform is universally optimal across all 5G and 6G frequency regimes. Conventional glass-ceramic LTCC systems remain the most practical solution for sub-6 GHz communication modules due to their scalability and cost efficiency. However, as operating frequencies move toward the FR2 mm-Wave regime (>24 GHz), dielectric loss, conductor-interface stability, and thermal management become increasingly critical, favoring crystallized low-glass systems and specialized ultra-low-loss LTCC platforms. For automotive radar operating at 77–81 GHz, mechanically robust crystallized systems appear more advantageous than highly glass-rich formulations because of their superior thermal and dimensional stability. Meanwhile, emerging ULTCC systems are considered among the most promising candidates for future 6G and sub-THz applications due to their lower thermal budgets and improved compatibility with advanced metallization and heterogeneous integration schemes, particularly when combined with appropriate metallization and packaging strategies.

5.3 Critical Manufacturing Barriers and Future Outlook

Despite substantial progress, several critical barriers continue to limit the broader commercialization of advanced LTCC and ULTCC technologies, particularly for high-frequency 5G mm-Wave and prospective 6G applications.

- **Interface Stability:** Conductor-related degradation remains one of the most persistent reliability challenges in co-fired ceramic systems. Silver migration, interfacial diffusion,

and chemically induced dielectric degradation become increasingly severe as operating frequencies move toward the mm-Wave and sub-THz regime. In conventional glass-rich LTCC systems, residual amorphous phases may accelerate ionic diffusion and interfacial instability during long-term operation. Consequently, industrial strategies are evolving beyond passive diffusion barriers toward intrinsically compatible low-temperature chemistries, reduced-glass or glass-free crystallized systems, and ultra-low-temperature processing routes that minimize thermally activated diffusion processes. This trend is particularly important for future heterogeneous integration schemes involving Ag, Cu, and potentially Al metallization.

- **Dimensional Control:** As integration density increases, maintaining dimensional precision during co-firing becomes increasingly difficult. High-density RF substrates operating in the FR2 mm-Wave regime require extremely tight interlayer registration, controlled shrinkage behavior, and defect-free multilayer architectures. Even minor dimensional variations can significantly affect impedance matching, insertion loss, and signal integrity at high frequencies. These requirements are driving continued innovation in tape-casting formulations, particle morphology engineering, lamination protocols, and real-time process monitoring. In particular, digital-twin-assisted manufacturing and AI-enabled process optimization are emerging as promising approaches for improving manufacturing reproducibility and yield in complex multilayer LTCC systems.
- **Cost vs. Performance:** Although LTCC technologies provide substantial advantages in integration density, thermal stability, and high-frequency performance, manufacturing costs remain significantly higher than those of conventional polymer-based substrates such as FR-4. This economic barrier becomes particularly important in cost-sensitive

commercial 5G infrastructure and consumer electronics markets. As a result, current industrial efforts increasingly focus on reducing firing temperatures, simplifying multilayer fabrication routes, and replacing expensive or scarce raw materials with lower-cost alternatives. The growing interest in molybdate-, tungstate-, and vanadate-based ULTCC systems reflects not only dielectric-performance considerations, but also broader economic and sustainability pressures associated with large-scale manufacturing.

Overall, the industrial trajectory of low-temperature microwave dielectric ceramics is shifting from general-purpose LTCC formulations toward application-specific material platforms optimized for distinct frequency windows and packaging requirements. Conventional glass-ceramic LTCC systems are expected to remain commercially dominant for sub-6 GHz communication modules and IoT applications due to their scalability and cost efficiency. In contrast, crystallized low-glass systems and ultra-low-loss composite LTCC platforms are becoming increasingly attractive for FR2 mm-Wave applications because of their improved dielectric stability and thermal reliability. For future 6G and sub-THz technologies, emerging ULTCC and glass-free or low-glass crystalline systems appear particularly promising due to their reduced thermal budgets, lower interfacial diffusion, and compatibility with heterogeneous integration architecture.

Moreover, the enormous compositional and processing parameter space associated with LTCC and ULTCC materials makes conventional trial-and-error optimization increasingly inefficient. The industrial challenges discussed above, from controlling conductor diffusion to achieving zero-shrinkage multilayer integration, highlight the growing need for predictive, data-driven materials design approaches. Consequently, computational modeling, high-throughput screening, and artificial intelligence-assisted materials discovery are expected to play increasingly

important roles in accelerating the development of next-generation microwave dielectric ceramics for advanced 5G and 6G communication systems.

6. Cross-disciplinary approaches

Artificial intelligence (AI) and computational modeling have emerged as powerful tools for accelerating the discovery and design of new ceramic materials. By using machine learning algorithms, researchers can analyze numerous experimental and theoretical data to determine trends, correlations, and potential material candidates. This data-driven approach significantly reduces the time and cost of traditional methods. By employing machine learning algorithms such as random forests, neural networks, and Bayesian optimization, researchers can rapidly screen thousands of candidate chemistries for targeted dielectric properties (*e.g.*, ε_r, $Q \times f$, τ_f). Additionally, computational modeling techniques, such as DFT and molecular dynamics simulations, can be used to predict the structural, electronic, and dielectric properties of materials, enabling the design of tailored materials with desired properties.

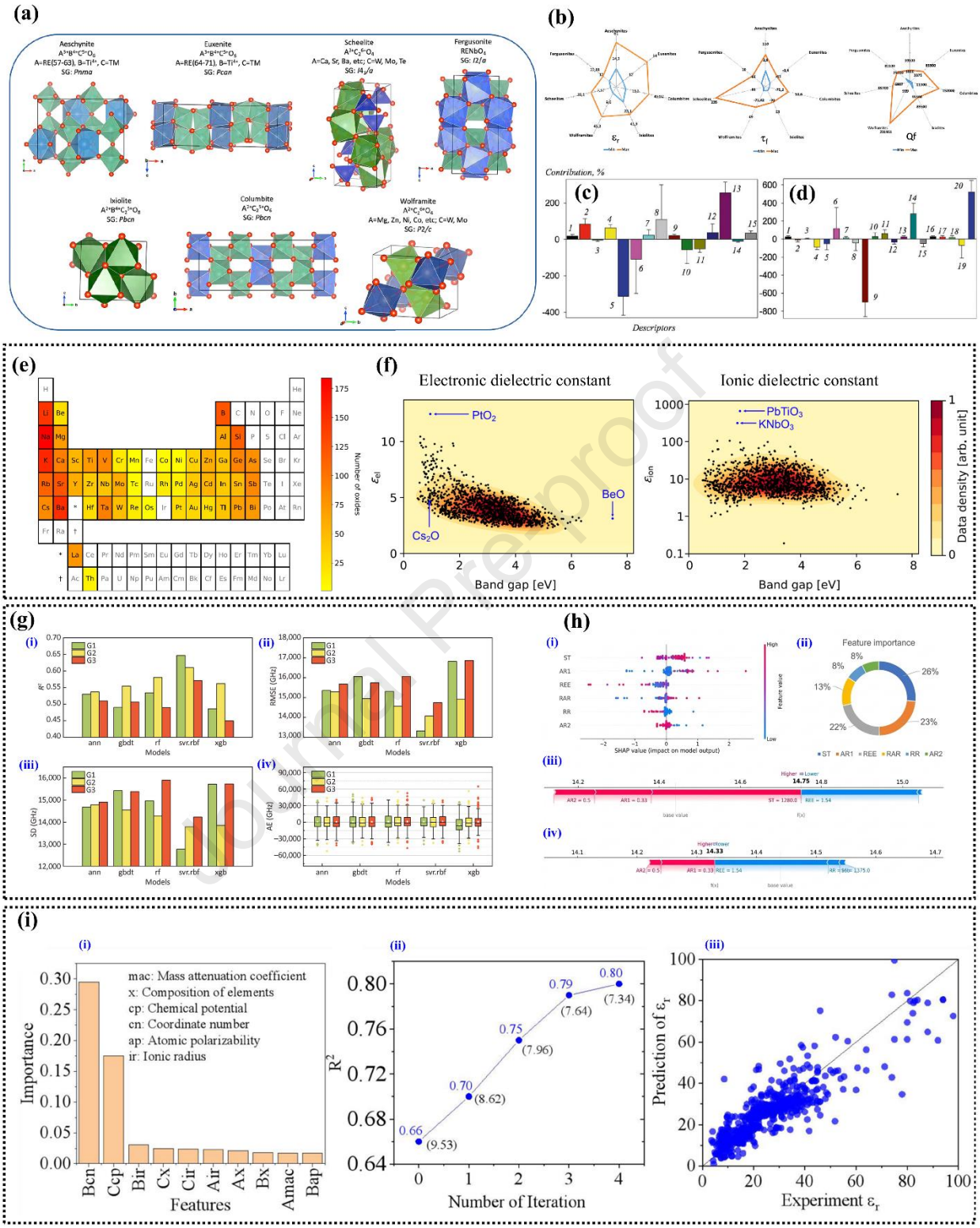

Fig. 17 A summary of data-driven and computational approaches for accelerating the design and understanding of microwave dielectric ceramics. (a) Crystal structures and (b) property ranges

(ε_r, $Q\times f$, τ_f) for seven common families of microwave dielectric ceramics from experimental datasets. (c,d) Contribution analysis of various descriptors to ε_r for aeschynites/euxenites and columbites/ixiolites/wolframites, respectively, highlighting the significant impact of processing parameters alongside intrinsic properties (adapted from Kireeva *et al*. [192]). (e) The distribution of cation species within a large-scale computational database of ~1200 oxides generated via first-principles calculations. (f) Computationally derived distributions showing the distinct behaviors of the electronic ($\varepsilon_{\mathrm{el}}$) and ionic ($\varepsilon_{\mathrm{ion}}$) contributions to the dielectric constant as a function of the material's band gap (adapted from Takahashi *et al*. [193]). (g) A methodological comparison of different machine learning algorithms and feature engineering strategies for predicting the challenging quality factor ($Q\times f$) property in ABO_4-type ceramics, evaluated by (i) R^2, (ii) RMSE, (iii) standard deviation, and (iv) absolute error (adapted from Mo *et al*. [194]). (h) An example of explainable AI (XAI) using SHAP analysis for rock-salt structures, showing (i) the swarm plot of feature impacts, (ii) the overall feature importance, and (iii, iv) force plots explaining the prediction for individual samples (adapted from Liu *et al*. [195]). (i) An illustration of an interpretable "white-box" model development using the SISSO method, showing (i) initial feature importance ranking, (ii) the iterative improvement of model accuracy (R^2), and (iii) the final high-fidelity correlation between the model's predictions and experimental ε_r values (adapted from Sheng *et al*. [121]).

The application of computational and ML techniques in microwave dielectric ceramics has rapidly matured from initial feasibility studies to the generation of sophisticated, physically interpretable design principles, as summarized in Fig. 17. The synergy between high-throughput computation, advanced ML algorithms, and interpretable methods provides a powerful toolkit for navigating the complex materials landscape required for next-generation wireless technologies.

A foundational step in this data-driven paradigm involves building robust models from extensive experimental datasets. Kireeva *et al*. [192] exemplified this by analyzing data for seven distinct structural families, including aeschynites and wolframites (Fig. 17 (a-b)). A key innovation in their work was the holistic inclusion of processing parameters (e.g., sintering temperature and time) as crucial descriptors, demonstrating that ML can decode the complex interplay between composition, structure, and synthesis pathways. The contribution analysis (Fig. 17 (c-d)) highlights that these processing-related features have a significant impact on the final dielectric properties, bridging the gap between theoretical composition and real-world material performance. Notably, several of the most influential descriptors identified in these studies-such as sintering temperature, dwell time, and defect-related structural metrics-map directly onto the process-structure-property axes discussed in Section 4.4, reinforcing the mechanistic framework developed earlier in this review.

To overcome the inherent noise in experimental data, a complementary strategy is to generate large, self-consistent datasets using high-throughput first-principles calculations. Takahashi *et al*. [193] pursued this computational route, constructing a database of ~1200 metal oxides. Their work provided a deeper physical insight by separately modeling $\varepsilon_{\mathrm{el}}$ and $\varepsilon_{\mathrm{ion}}$ contributions to the relative permittivity. As shown in Fig. 17f, they confirmed the inverse correlation between ε_{el} and the band gap, while revealing that the much larger $\varepsilon_{\mathrm{ion}}$ has a far more complex relationship, underscoring the power of computation to deconstruct a property into its fundamental components.

Building on these approaches, ML has been applied to predict specific and challenging properties. The quality factor ($Q \times f$) is notoriously difficult to model due to its sensitivity to subtle defects and lattice anharmonicity. Mo *et al.* [194] tackled this by developing a predictive model

for ABO_4-type ceramics, demonstrating through systematic algorithm and feature selection that support vector regression (SVR) could achieve high accuracy in predicting $Q \times f$ (Fig. 17g). As ML models become more sophisticated, attention has shifted towards improving their interpretability. Liu *et al.* [195] employed explainable AI (XAI) using SHapley Additive explanations (SHAP) for rock-salt structured ceramics. Their analysis (Fig. 17h) moved beyond "black-box" predictions by definitively quantifying the importance of each feature, identifying sintering temperature, atomic ratio, and electronegativity as the most critical factors, and explaining how they influence the prediction for any individual sample.

The ultimate goal is the creation of "white-box" models that yield explicit, physically meaningful formulas. Sheng *et al*. [121] achieved this using the Sure Independence Screening and Sparsifying Operator (SISSO) method. Their work not only generated an interpretable model with high fidelity ($R^2 \sim 0.8$) but also proposed a novel strategy to merge datasets of different component numbers. By iteratively building a physically transparent descriptor, as shown in Fig. 17i, their approach represents the frontier of data-driven materials science: using ML not just to predict, but to discover the underlying physical laws governing material properties.

6.1 Cross-Study Comparison of Model Performance

To enable direct comparison across different ML studies, Table 7 summarizes key works on microwave dielectric ceramics, including dataset sizes, algorithms, target properties, and quantitative performance metrics. As shown, the R^2 values for $Q \times f$ prediction typically lie between 0.78 and 0.81, indicating room for improvement before industrial adoption (where $R^2 >$ 0.95 is often desired). Notably, the XGBoost model for τ_f prediction achieved an R^2 of 0.7799, identifying molecular dielectric polarizability (p_m), tolerance factor (t), ionic volume (V_i), and relative molecular mass (m) as the most critical features [188]. For ε_r prediction in rock-salt

systems, a high R^2 of 0.9376 was achieved using only six key features, with sintering temperature, atomic ratio, and electronegativity contributing approximately 71% to the prediction accuracy [12]. The SISSO approach, while sacrificing some accuracy (R^2 ~ 0.8), provides an interpretable, closed-form equation for ε_r that can be used without running the ML model itself [190]. This comparison also highlights a clear research frontier: closing the gap between current model performance and the reliability levels required for industrial LTCC/ULTCC and CSP process control.

Table 7 Cross-study comparison of machine learning models for microwave dielectric ceramics

Target property	Dataset size	Model(s)	Best performance	Key features identified	Ref.
ε_r, $Q\times f$, τ_f	~300 (7 structural families)	Random Forest, etc.	Contribution analysis of processing parameters	Ts and time as crucial descriptors	[192]
$Q\times f$ (ABO_4-type)	164	SVR, RF, XGBoost, etc	SVR (RBF): R^2=0.8115, RMSE=8,362 GHz	Structural features, 35 input descriptors	[194]
ε_r, τ_f (multiple systems)	254 (for ε_r)	RF, GBR, SVR, etc	ε_r: RMSE=4.84; τ_f: RMSE=21.86	32 intrinsic chemical, structural, and thermodynamic features	[196]
ε_r (ternary/quaternary oxides)	1,419	SISSO (white-box)	R^2≈0.8 (quaternary)	Derived explicit physical formula	[121]

				p_m (molecular polarizability), t	[197]
τ_f (ABO_3-type)	104	XGBoost, RF, SVR, etc.	XGBoost: R^2=0.7799, RMSE=15.75 ppm/°C	(tolerance factor), V_i, m	
ε_r (rock-salt)	Not specified	XGBoost + INFO optimization	R^2=0.9376, MAE=0.5249	T_S, atomic ratio, electronegativity (~71% contribution)	[195]

6.2 Current challenges and future directions for ML in microwave dielectrics

Despite significant progress, several critical challenges remain.

- Data scarcity: Experimental datasets in MWDC research are typically limited to 100–300 samples, which is small by ML standards. This scarcity constrains model generalizability and increases the risk of overfitting. Several strategies are being pursued to mitigate this issue: (i) NLP-based data mining from the literature, Wang *et al.* constructed a pipeline to extract normalized property data from approximately 12,900 dielectric ceramics articles, achieving micro-F1 scores exceeding 90% for sentence classification and relation extraction [198]; (ii) generative virtual sample generation, data augmentation techniques can artificially expand small datasets; (iii) transfer learning, pre-training models on related tasks with larger datasets; and (iv) active learning, iteratively selecting the most informative samples for experimental validation [199, 200].
- Lack of benchmark datasets: Unlike computer vision (e.g., ImageNet), the MWDC community lacks standardized, open-access benchmark datasets for fair model comparison. MatBench, developed by the Materials Project, offers curated benchmarking tasks for general materials properties (band gaps, elastic moduli, formation energies, etc.) but does not yet include microwave-specific properties such as ε_r, $Q\times f$, or τ_f [200]. The field would greatly benefit from community-driven efforts to establish such benchmarks.

- Prediction-experiment validation gap: Many ML studies achieve high accuracy on held-out literature data, but their predictions are rarely validated through actual synthesis and measurement. This gap arises from differences in synthesis protocols, measurement conditions, and the inherent noise in literature-compiled data. Encouragingly, recent studies have begun to address this issue. For rock-salt ceramics, the ML model's predictions were experimentally validated on two different material compositions ($LiMg_8AlO_{10}$ and Li_2SnO_3-doped Li_3MgNbO_5), confirming its predictive capability beyond the training distribution [195]. Moreover, closed-loop autonomous experimentation systems that combine ML prediction with automated synthesis and characterization are emerging as a powerful solution to close the feedback loop and accelerate materials discovery [199].
- Bridging the gap: The ultimate goal is to integrate AI, high-throughput computation, and autonomous experimentation into a unified workflow. By using AI to guide computational simulations, which in turn inform nanoscale materials design, the development timeline could be reduced from years to months. Several research groups are already pursuing such integrated platforms, and their success will be instrumental in delivering the next generation of low-temperature microwave dielectrics for 6G and beyond.

The synergy between AI-driven discovery, high-throughput computation, and advanced synthesis not only promises to accelerate the development of high-performance materials but also enables a more efficient and targeted approach to manufacturing. This optimization of resources and reduction in experimental waste naturally aligns with broader global goals. Beyond pure performance, the drive towards low-temperature processing is fundamentally linked to the critical

imperatives of sustainability and economic viability, which will be discussed in the following section.

7. Sustainability and economic impact

7.1 Energy consumption reduction

The transition from conventional high-temperature sintering to low-temperature approaches represents a paradigm shift in ceramic manufacturing sustainability. Traditional microwave dielectric ceramics require sintering temperatures above 1000 °C, with some systems demanding temperatures as high as 1400 °C for cordierite-based materials [201, 202]. In stark contrast, recent advances in low-temperature sintering have demonstrated remarkable temperature reductions. Ultra-low temperature sintering of molybdate-based ceramics can achieve full densification at temperatures as low as 550 °C–600 °C [202], representing energy savings of up to 50% compared to conventional processing [201].

A quantitative comparison of energy consumption across different sintering techniques, compiled by J. Andrews, reveals dramatic differences [203]. Conventional solid-state sintering of $BaTiO_3$ consumes 2800 $kJ \cdot g^{-1}$, while liquid-phase sintering consumes 2000 $kJ \cdot g^{-1}$. Field-assisted sintering, microwave sintering, and fast firing consume 1050 540, and 130 $kJ \cdot g^{-1}$, respectively. In striking contrast, CSP consumes only 30 $kJ \cdot g^{-1}$, representing a 98.9% reduction relative to conventional solid-state sintering. This dramatic saving is achieved by combining a transient liquid phase (typically water) with applied uniaxial pressure at temperatures mostly below 300 °C. However, as discussed in Section 4.3, these dramatic energy savings must be balanced against the current limitations in $Q \times f$ and microstructural perfection for ultra-high-Q applications.

For ULTCC systems, the Fraunhofer Institute for Ceramic Technologies and Systems states that ULTCCs can be sintered at very low temperatures of 400 °C to 700 °C, making their

manufacturing process very energy-efficient [204]. The NAT-ULTCC project further quantifies that reducing the sintering temperature from 850–1000 °C down to below 600 °C lowers energy consumption in the sintering phase by at least 30% [205]. A techno-economic analysis by T. Ibn-Mohammed *et al.* (2019) concluded that CSP offers the lowest capital cost, the best return on investment, and the most considerable combined energy and emission savings among the methods examined [183].

7.2 Carbon Footprint Reduction

Ultra-low temperature co-fired ceramics processed at 470 °C represent a breakthrough in sustainable manufacturing, achieving properties suitable for high-frequency applications while operating within temperature ranges accessible to renewable heating technologies [206]. The NAT-ULTCC project's ≥30% energy reduction target, when combined with the replacement of precious-metal electrodes (Ag, Au) by base metals (Al), further lowers both material cost and embodied carbon. It must be noted, however, that the concept of fully "carbon-neutral" ceramic manufacturing remains a forward-looking target rather than a current reality. The transition will require not only low-temperature processing but also widespread adoption of renewable-electricity heating, hydrogen-based burners, or carbon-capture technologies, as highlighted in recent roadmaps for the European ceramic industry [207].

The dramatic reduction in energy consumption afforded by low-temperature sintering directly translates to lower operational CO_2 emissions, especially when the electricity used is sourced from renewable generation. T. Ibn-Mohammed *et al.* estimated, using marginal abatement cost curve methods, that cold sintering can achieve substantial CO_2 savings per ton of ceramic produced compared with conventional solid-state and liquid-phase sintering, although

the exact saving depends on the specific ceramic composition, production scale, and local energy mix [183].

7.3 Economic benefits and cost reduction

The economic advantages of low-temperature sintering have been quantitatively analyzed by T. Ibn-Mohammed *et al.* [183]. Using marginal abatement cost curves, they showed that cold sintering offers the lowest capital cost and the best return on investment among all sintering techniques compared. Energy-efficient sintering technologies can reduce production costs through decreased fuel consumption, shortened processing cycles, and reduced equipment maintenance.

Low-temperature compatible silver metallization systems enable cost-effective electrode integration in LTCC applications, eliminating the need for expensive platinum or palladium conductors, substantially reducing metallization costs for LTCC and ULTCC manufacturing [188].

7.4 Life-cycle comparison of sintering strategies

To provide a quantitative comparison, Table 8 summarizes key metrics for the four sintering strategies discussed in this review. This table draws exclusively on LTCC/ULTCC/CSP-specific literature, not on generic ceramic statistics.

Table 8 Comparative life-cycle assessment (LCA) metrics for low-temperature sintering strategies.

Sintering strategy	Typical T_S (°C)	Relative energy consumption (Compared to conventional sintering)	CO_2 saving potential	Ref
Conventional	1200–1600	100% (baseline, 2800 kJ·g^{-1})	-	[203]
Sintering aids/LTCC	850–950	~50%–70% of baseline	Moderate; avoids high-temp. volatilization	[183]
Intrinsic low- T_S ***(ULTCC)***	400–700	≤30% of baseline*	Significant; enables Al co-firing	[205]
Cold sintering (CSP)	<300 (Plus post-annealing)	≤1.1% of baseline**	Largest; applicable to many compositions	[203]

** Based on NAT-ULTCC project target of ≥30% energy reduction vs. LTCC baseline.*

*** Based on CSP energy consumption of 30 kJ·g⁻¹ vs. 2,800 kJ·g⁻¹ for conventional sintering.*

7.5 Future Sustainability Outlook

Comprehensive life-cycle assessments for LTCC substrates have identified the co-firing step as the dominant environmental hotspot, which low-temperature strategies directly address [208]. The convergence of low-temperature sintering technologies with renewable energy systems and circular economy principles positions microwave dielectric ceramics manufacturing for substantial sustainability improvements. Government initiatives supporting green manufacturing, including the European Green Deal and various national decarbonization strategies, provide policy frameworks encouraging adoption of energy-efficient ceramic processing technologies.

Advanced manufacturing concepts like energy-aware 6G networks emphasize the importance of sustainable materials and processing technologies, creating market demand for environmentally responsible microwave components. The integration of artificial intelligence and machine learning in ceramic processing optimization further enhances the economic and

environmental benefits of low-temperature sintering by enabling precise control of processing parameters and reducing material waste.

In principle, Cold sintering processes demonstrate particular promise for carbon capture integration, potentially enabling atmospheric CO_2 utilization in ceramic precursor materials while achieving room-temperature consolidation. This approach represents a paradigm shift from traditional ceramic manufacturing, transforming the industry from a carbon emitter to a potential carbon sink [209].

This transformation toward sustainable ceramic manufacturing represents not only an environmental imperative but also a competitive advantage for manufacturers adopting low-temperature processing technologies. The combination of reduced energy consumption, lower production costs, improved material properties, and enhanced market positioning creates a compelling case for industry-wide adoption.

8. Future trends and research directions

8.1 The next frequency frontier: from millimeter-Wave to Terahertz

The convergence of low-temperature sintering technologies (LTCC, ULTCC, and cold sintering) with the demanding specifications of 5G/6G communication systems represents the most critical trajectory for microwave dielectric ceramics research. As 5G networks transition to millimeter-wave frequencies (24–71 GHz) and 6G explores sub-terahertz bands (100–300 GHz), low-temperature co-fireable ceramics enable the miniaturization, cost reduction, and high-density integration essential for massive MIMO antenna arrays, small-cell base stations, and phased-array transceivers [55].

8.2 Advancements in low-temperature Co-fired technologies

Addressing the formidable challenges of the millimeter-wave and terahertz frontier requires a multi-pronged approach to materials processing. The following section details the technological advancements across three critical tiers of low-temperature co-firing technologies. We begin by examining the breakthroughs that have pushed conventional LTCC into the 5G millimeter-wave domain. Subsequently, we explore the "next frontier" of ULTCC and the CSP, which promise to overcome the fundamental limitations of LTCC by enabling co-integration with a wider range of materials and drastically reducing the manufacturing energy footprint

8.2.1 LTCC technology breakthroughs for millimeter-wave 5G

Traditional LTCC implementations were historically limited to operating frequencies below 10 GHz due to material loss and conductor constraints. However, recent innovations in proprietary dielectric compositions, distributed filter topologies, and advanced conductive pastes have extended LTCC capabilities to millimeter-wave frequencies exceeding 40 GHz, with commercial filters now available for 5G FR2 bands (n257, n258, n260, n261) operating at 26 – 28 GHz and 37- 40 GHz. These LTCC components achieve footprints 75% smaller than thin-film-on-alumina alternatives at one-quarter the cost, while maintaining superior environmental robustness through internally shielded structures that prevent detuning after board assembly [210]. For massive MIMO architectures requiring thousands of antenna elements, LTCC-based wideband patch antennas demonstrate impedance bandwidths exceeding 20% at Ka-band (28 GHz) with compact multilayer structures ($4.88\times4.88\times1.036$ mm^3) suitable for dense array integration. High-performance millimeter-wave front-end modules co-integrate filters, couplers, and transmission lines on LTCC substrates sintered at 850°C-900°C with silver electrodes, achieving insertion losses below 2 dB and return losses exceeding 15 dB across 24-30 GHz bands [211].

8.2.2 Ultra-Low and Cold Sintering: The Next Frontier

Ultra-low temperature co-fired ceramics (ULTCC, T_S~400 °C–700 °C) and cold sintering processes (CSP, T_S<200°C) address fundamental limitations of conventional LTCC by enabling co-firing with aluminum electrodes (melting point 660 °C), eliminating silver migration issues, and dramatically reducing energy consumption [154, 162]. The ULTCC6G-EPac project specifically targets energy-efficient electronic packaging for 6G systems through the development of ULTCC materials with sintering temperatures below 550°C while maintaining ε_r = 6-12, $Q\times f >$ 40,000 GHz, and $|\ \tau_f\ | <$ 30 ppm/°C [162, 212]. Recent molybdate-based ULTCC systems demonstrate exceptional promise for 5G/6G applications. $Na_5Tm_{0.91}Y_{0.03}Yb_{0.06}(MoO_4)_4$ ceramics sintered at 600 °C achieve ε_r=7.82, $Q\times f$=34,752 GHz, and τ_f =-71.9 ppm/°C, with low sintering temperatures enabled by the liquid-phase formation during processing [154]. $LiGaW_2O_8$ ceramics sinter at 870 °C with ε_r~14.4, $Q\times f$ ~33,500 GHz, suitable for 5G antenna substrates. Li_2MoO_4-based systems achieve full densification at 540 °C with silver and aluminum electrode compatibility, positioning them as prime candidates for next-generation multilayer devices [153, 202, 213]. Cold sintering at temperatures below 200 °C represents the ultimate low-temperature paradigm, with successful demonstrations of C0G multilayer ceramic capacitors and microwave dielectric resonators fabricated at 120 °C–180 °C [212]. SrF_2-based dielectric resonator antennas cold-sintered at 140 °C and post-annealed at 450°C resonate at 24.5 GHz with outstanding S_{11} performance, proving the viability of cold sintering for millimeter-wave 5G applications [162, 212]. Cold-sintered MgO-based composites (MgO-TiO_2, MgO-Na_2MoO_4) achieve relative densities >95% at 200 °C with subsequent post-annealing at 600–800 °C optimizing microwave properties to $Q\times f$>50,000 GHz [180].

8.3 The Multifunctional Design Imperative for 6G and Beyond

The evolution toward 6G and beyond demands a paradigm shift in materials design, moving beyond the historical focus on optimizing the dielectric triad (ε_r, $Q \times f$, τ_f) in isolation. Deployment in practical systems, particularly aerospace platforms, high-power base stations, and portable devices, requires a holistic, multifunctional design framework that concurrently addresses competing requirements. As conceptually summarized in Fig. 18, next-generation dielectric ceramics must simultaneously exhibit lightweight design, high thermal conductivity, robust mechanical strength, and seamless integration with metal electrodes. This section delves into the specific challenges and emerging material strategies for achieving this multifunctional performance in low-temperature sinterable systems.

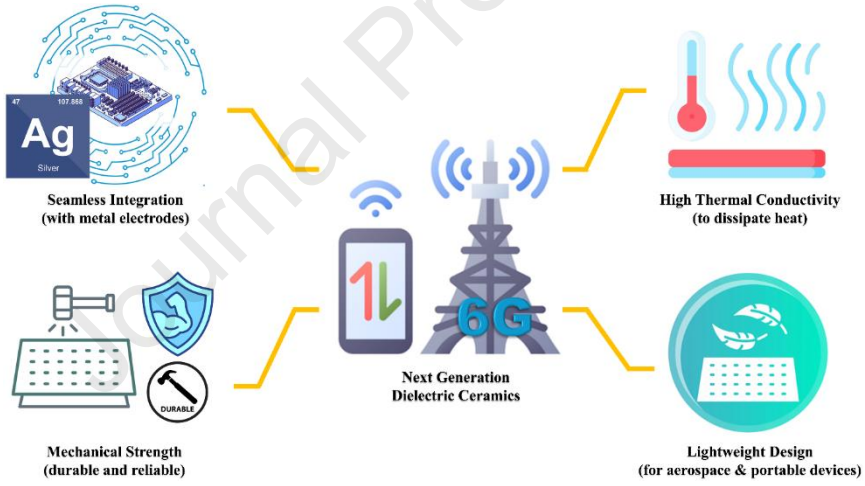

Fig. 18 A holistic design approach for next-generation microwave dielectric ceramics for 6G and beyond. Future research must move beyond optimizing only dielectric properties and holistically address key multifunctional requirements, including lightweight design for aerospace and portable applications, high thermal conductivity for heat dissipation in high-power devices, robust mechanical strength for durability, and seamless integration with metal electrodes for cost-effective manufacturing.

8.3.1 Lightweight, high-performance ceramics for mm-wave/THz

The progression toward 6G sub-terahertz frequencies (100–300 GHz) demands ultra-low-loss materials ($\tan\delta < 10^{-5}$, $Q\times f$>200,000 GHz) while simultaneously addressing weight constraints for aerospace-mounted 6G nodes and satellite constellations. Low-temperature sintered ceramics offer unique advantages: reduced grain growth during shorter thermal exposure preserves dense, defect-free microstructures that minimize scattering losses at terahertz frequencies [55].

$Na_5RE(MoO_4)_4$ systems (RE=Y, Yb) sintered at 570 °C–600 °C exhibit $Q\times f$ values up to 56800 GHz with densities below 4.5 g/cm^3, positioning them as lightweight candidates for frequency-agile 6G antenna substrates requiring tunable ε_r (ε_r~7–9) for beam-steering applications. Magnesium-based low-temperature ceramics (MgO, $Mg_3B_2O_6$, $MgTiO_3$) achieve densities of 2.8–3.2 g/cm^3–40% lighter than conventional alumina substrates, while maintaining $Q\times f$>60,000 GHz at sintering temperatures below 900 °C with LiF or V_2O_5 fluxes [180, 202].

8.3.2 Co-Firing Compatibility and 3D Integration

Low-temperature regimes fundamentally enable seamless co-firing with low-cost silver and copper electrodes, eliminating the platinum/palladium requirements of high-temperature ceramics and reducing metallization costs by 60%–80%. ULTCC systems co-fired at 500 °C–650 °C with silver demonstrate no interfacial reactions or Ag diffusion beyond 5 μm depths, maintaining stable electrical contact and preventing secondary phase formation that degrades dielectric properties [214].

Three-dimensional integration via LTCC/ULTCC enables vertical stacking of antenna arrays, filters, power dividers, and passives within compact multilayer modules, critical for space-constrained 5G small cells and 6G reconfigurable intelligent surfaces (RIS). Ten-layer LTCC modules with embedded cavities, vias, and microstrip circuits achieve component densities

exceeding 200 elements/cm^3 while maintaining inter-layer registration tolerances below 15 μm through co-sintering at 850 °C–900 °C [210].

Cold sintering uniquely permits hybrid ceramic–polymer composites and ceramic-metal cermets by avoiding thermal degradation of organic phases, enabling multifunctional structures combining electromagnetic performance with mechanical damping, thermal spreading, or embedded sensing capabilities [162, 212].

8.4 AI-Accelerated Discovery of Low-Temperature Dielectric Ceramics

The vast compositional space of low-temperature sinterable systems, spanning molybdates, tungstates, vanadates, fluorides, borates, and their composites, exceeds manual exploration capacity. Machine learning-guided materials design trained on existing LTCC/ULTCC databases can predict sintering temperatures, ε_r, $Q\times f$, and τ_f from composition and structure descriptors, accelerating identification of novel low-temperature ceramics meeting 6G specifications [215].

High-entropy ceramic (HEC) strategies applied to low-temperature regimes offer simultaneous optimization of multiple properties through configurational disorders. Rare-earth-doped molybdate HECs (*e.g.*, $Na_5(Tm, Y, Yb)(MoO_4)_4$) demonstrate that multi-element substitution tunes τ_f from −101 to −71.9 ppm/°C while lowering sintering temperatures and improving $Q\times f$, suggesting a rich design space for AI exploration [202, 216].

Autonomous robotic synthesis platforms integrating low-temperature solid-state reactions (T<800 °C), in-situ phase analysis, and microwave resonator testing could screen 50–100 ULTCC/CSP compositions per week, two orders of magnitude faster than conventional research workflows. Digital twin frameworks for LTCC manufacturing enable real-time prediction of sintering shrinkage, warpage, and electrical performance, reducing prototype iterations and time-to-market for 6G components by 40%–60% [217]. The key scientific challenges, advanced

solutions, and targeted applications for each low-temperature sintering strategy are systematically summarized in Table 9. Below, we elaborate on several high-priority directions that will shape the next decade of research.

8.5 Vision: low-temperature ceramics as eenablers of sustainable 6G

The future trajectory of microwave dielectric ceramics for 6G is not a simple extrapolation of past achievements; it demands a paradigm shift towards a holistic integration of low-temperature processing, multifunctional performance, and sustainable manufacturing. The era of optimizing dielectric properties in isolation is over. To successfully enable next-generation technologies, we must concurrently address the competing demands of electrical performance, thermal management, mechanical robustness, and seamless co-integration.

To synthesize the complex landscape discussed throughout this review and provide a clear path forward, Table 9 presents a strategic roadmap for the field.

Table 9 A Strategic Roadmap for Low-Temperature Microwave Dielectric Ceramics: Challenges, Opportunities, and Future Directions.

Sintering strategy	Key scientific/technical challenges	Key opportunities & advanced solutions	Future directions & target applications (6G and beyond)
Sintering aids / glass additives	- Residual amorphous phase limiting $Q \times f$ - Secondary phase formation - Precise composition control	- **Glass-ceramic design:** Develop crystallizable glasses that become part of the functional phase. - **Multi-component glass engineering (via CALPHAD/ML):** Predict optimal glass compositions to	- Cost-effective LTCC for massive MIMO antenna arrays (Sub-6 GHz & low mm-Wave). - High-volume substrate manufacturing.

		minimize reactions and melting point. - **Nanoscale Coating:** Apply sintering aids as thin, uniform coatings instead of mixed powders.	
Intrinsically Low-T Compounds	- Li/Na volatilization during sintering - Limited material families discovered - Fine-tuning τ_f to near-zero can be difficult	- **High-Entropy Design:** Stabilize crystal structures and tune properties by introducing configurational disorder. - **Anion Substitution (F^-, N^{3-}):** Weaken lattice bonds to further reduce sintering temperature. - **AI-Accelerated Discovery:** Screen new, stable low-energy compounds (*e.g.*, novel tellurates, vanadates).	- High-performance ULTCC for mm-Wave/Sub-THz filters and resonators ($Q \times f$>100000 GHz). - Lightweight ceramics for aerospace and satellite communications.
Cold Sintering Process (CSP)	- **Residual Hydroxyls (OH^-):** The primary source of dielectric loss, severely limiting $Q \times f$. -Amorphous/ defective grain boundaries - Limited material solubility in common solvents.	- **Hybrid Processing (Post-Annealing):** Use CSP for shaping, followed by a moderate-temperature anneal (400 °C-800 °C) to remove OH^- and crystallize boundaries. - **Advanced Solvent Engineering:** Explore non-aqueous or chemically reactive transient liquids to promote congruent dissolution.	- **Co-integration with Polymers/Metals:** Fabricate 3D heterogeneous packages with embedded components (e.g., Al electrodes). - Flexible/wearable electronics. - Sustainable manufacturing for next-gen green electronics.

	- Microwave/Field-Assisted CSP: Enhance kinetics at the particle-liquid interface.

It systematically outlines the persistent scientific challenges, key technological opportunities, and targeted future applications for each of the three primary low-temperature sintering strategies. This roadmap crystallizes the critical research frontiers that must be conquered to unlock the full potential of these materials.

Building upon this strategic foundation, the vision for the next decade of research and development can be distilled into several concrete, ambitious goals. These goals represent the collective mission to transform low-temperature microwave ceramics from mere passive components into foundational enablers of an energy-efficient, cost-effective, and environmentally sustainable 6G communication infrastructure. The key milestones for this vision include:

- Sub-600°C sintering for all major device classes (resonators, filters, antennas, capacitors) to enable aluminum electrode co-firing and 50% energy reduction [180, 216].
- Ultra-low loss at mm-wave/THz ($Q \times f$>100,000 GHz, $\tan\delta$ <10^{-4}) through crystalline, low-porosity microstructures achievable via cold sintering + controlled post-annealing [202, 213].
- Lightweight architectures (ρ<3.5 g/cm^3) using magnesium-, sodium-, and lithium-based chemistries compatible with aerospace 6G nodes [158, 210].
- Thermal conductivity enhancement (λ>10 W·m^{-1}·K^{-1}) via low-temperature-compatible nitride/carbide fillers for high-power massive MIMO [180, 218].
- 3D heterogeneous integration of ceramics, semiconductors, and passives through LTCC/ULTCC co-sintering below 700 °C [214].

This paradigm shift positions low-temperature microwave ceramics not merely as passive components but as transformative enablers of energy-efficient, cost-effective, and environmentally sustainable 6G communication infrastructure capable of supporting terabit-per-second data rates, ubiquitous connectivity, and global digital equity.

9. Conclusions

The development of high-performance microwave dielectric ceramics requires both excellent intrinsic properties and low-temperature densification. Traditional high-temperature sintering is energy-intensive and causes stoichiometric variations, while also requiring additional processing steps for metal electrode integration. Three main strategies have been developed to lower sintering temperatures. The use of sintering aids, especially multi-component glasses such as borosilicate-based systems, offers a cost-effective route, but careful glass selection is crucial to avoid secondary phases and degraded $Q \times f$. Alternatively, intrinsically low-sintering-temperature compounds, particularly Li-based rock-salt, spinel, and olivine systems, achieve excellent microwave properties at 850–950 °C through fast Li^+ diffusion and weak Li–O bonds. Partial anion substitution (*e.g.*, O^{2-} by F^-) further reduces processing temperatures without sacrificing performance. CSP represents a paradigm shift, enabling densification at ultra-low temperatures (<300 °C) via a dissolution-precipitation mechanism. While molybdate-based systems densify successfully with deionized water, molybdenum cost drives the search for alternative affordable materials such as aluminates, titanates, and phosphates. Understanding the interplay between CSP processing parameters (solvent, pressure, temperature, time) and microstructure (grain size, residual OH^-, amorphous phases) is essential for tailoring properties.

In summary, sintering aids, intrinsically low-T_s materials, and CSP each offer distinct advantages and limitations. The optimal choice depends on the specific frequency band, co-firing

requirements, and manufacturing constraints. This review provides a critical, comparative framework to guide future material selection and processing design, as further elaborated in the strategic roadmap (Table 9).

10. References

[1] M.T. Sebastian, Chapter one – Introduction, in: M.T. Sebastian (Ed.), Dielectric Materials for Wireless Communication, Elsevier, Amsterdam, 2008, pp. 1-10.

[2] M.T. Sebastian, R. Ubic, H. Jantunen, Low-loss dielectric ceramic materials and their properties, International Materials Reviews 60 (2015) 392-412.

[3] M.D. Hill, D.B. Cruickshank, I.A. Macfarlane, Perspective on ceramic materials for 5G wireless communication systems, Applied Physics Letters 118 (2021) 120501.

[4] M.T. Sebastian, H. Jantunen, Low loss dielectric materials for LTCC applications: a review, Int. Mater. Rev. 53 (2008) 57-90.

[5] W.W. Cho, K. Kakimoto, H. Ohsato, High-Q microwave dielectric $SrTiO_3$-doped $MgTiO_3$ materials with near-zero temperature coefficient of resonant frequency, Japanese Journal of Applied Physics 43 (2004) 6221-6224.

[6] A. Feteira, K. Sarma, N.M. Alford, I.M. Reaney, D.C. Sinclair, Microwave dielectric properties of gallium-doped hexagonal barium titanate ceramics, Journal of the American Ceramic Society 86 (2003) 511-513.

[7] M. Li, A. Feteira, M. Mirsaneh, S. Lee, M.T. Lanagan, C.A. Randall, D.C. Sinclair, Influence of nonstoichiometry on extrinsic electrical conduction and microwave dielectric loss of $BaCo_{1/3}Nb_{2/3}O_3$ ceramics, Journal of the American Ceramic Society 93 (2010) 4087-4095.

[8] R. Muhammad, Y. Iqbal, C.R. Rambo, H. Khan, Research trends in microwave dielectrics and factors affecting their properties: a review, International Journal of Materials Research 105 (2014) 431-439.

[9] P. Pulphol, W. Vittayakorn, T. Bongkarn, T. Kolodiazhnyi, S. Pongampai, T. Maluangnont, N. Vittayakorn, The tuning of temperature stability in ultralow loss (Ba/Sr) zirconate microwave dielectric, Ferroelectrics 601 (2022) 59-69.

[10] K.P. Surendran, M.T. Sebastian, P. Mohanan, M.V. Jacob, The effect of dopants on the microwave dielectric properties of $Ba(Mg_{0.33}Ta_{0.67})O_3$ ceramics, Journal of Applied Physics 98 (2005) 094114.

[11] M.R. Varma, R. Raghunandan, M.T. Sebastian, Effect of dopants on microwave dielectric properties of $Ba(Zn_{1/3}Ta_{2/3})O_3$ ceramics, Japanese Journal of Applied Physics 44 (2005) 298.

[12] V.L. Gurevich, A.K. Tagantsev, Intrinsic dielectric loss in crystals, Advances in Physics 40 (1991) 719-767.

[13] A.K. Tagantsev, Phonon mechanisms of intrinsic dielectric loss in crystals, in Ferroelectric Ceramics, Basel, N. Setter and E. L. Colla, Eds., 1993//1993: Birkhäuser Basel, pp. 127-145.

[14] Q. Pang, Y. Li, F. Yang, Z. Liu, X. Li, H. Cheng, S. Sun, Y. Chen, G. Wang, Microstructure and crystal structure dependence of microwave dielectric properties of non-stoichiometric $(Sr_{0.7}Ca_{0.3})_z(Zr_{0.95}Ti_{0.05})O_3$ perovskite ceramics, Ceramics International 49 (2023) 8598-8606.

[15] S. Chen, T. He, Y. Li, X. Li, Y. Zhuang, X. Wang, Y. Liu, X. Liu, Significantly reduced intrinsic dielectric constant and loss of nano-silica by direct fluorination, Ceramics International 49 (2023) 22816-22825.

[16] X.H. Ma, S.H. Kweon, S. Nahm, C.Y. Kang, S.J. Yoon, Y.S. Kim, Synthesis and microwave dielectric properties of $Bi_2Ge_3O_9$ ceramics for application as advanced ceramic substrate, Journal of the European Ceramic Society 37 (2017) 605-610.

[17] L. Pan and G. Zhu (Eds.), Book Perovskite Materials, IntechOpen, Place, 2016.

[18] H. Ohsato, Microwave dielectrics with perovskite-type structure, (2016) doi: 10.5772/61718 .

[19] T. Kolodiazhnyi, P. Pulphol, W. Vittayakorn, N. Vittayakorn, Giant suppression of dielectric loss in $BaZrO_3$, Journal of the European Ceramic Society 39 (2019) 4144-4148.

[20] P. Pulphol, N. Vittayakorn, W. Vittayakorn, and T. Kolodiazhnyi, Dielectric relaxation behavior of $BaZrO_3$ ceramics at low temperature, Ceramics International 46 (2020) 24488-24494.

[21] T. Kolodiazhnyi, Origin of extrinsic dielectric loss in 1:2 ordered, single-phase $BaMg_{1/3}Ta_{2/3}O_3$, Journal of the European Ceramic Society 34 (2014) 1741-1753.

[22] I.M. Reaney, P.L. Wise, I. Qazi, C.A. Miller, T.J. Price, D.S. Cannell, D.M. Iddles, M.J. Rosseinsky, S.M. Moussa, M. Bieringer, L.D. Noailles, R.M. Ibberson, Ordering and quality factor in $0.95BaZn_{1/3}Ta_{2/3}O_3$–$0.05SrGa_{1/2}Ta_{1/2}O_3$ production resonators, Journal of the European Ceramic Society 23 (2003) 3021-3034.

[23] S. Kawashima, M. Nishida, I. Ueda, H. Ouchi, $Ba(Zn_{1/3}Ta_{2/3})O_3$ ceramics with low dielectric loss at microwave frequencies, Journal of the American Ceramic Society 66 (1983) 421-423.

[24] P.K. Davies, A. Borisevich, M. Thirumal, Communicating with wireless perovskites: cation order and zinc volatilization, Journal of the European Ceramic Society 23 (2003) 2461-2466.

[25] C.W. Ahn, H.J. Jang, S. Nahm, H.M. Park, H.J. Lee, Effects of microstructure on the microwave dielectric properties of $Ba(Co_{1/3}Nb_{2/3})O_3$ and $(1-x)Ba(Co_{1/3}Nb_{2/3})O_3$–$xBa(Zn_{1/3}Nb_{2/3})O_3$ ceramics, Journal of the European Ceramic Society 23 (2003) 2473-2478.

[26] W. Wang, M. Shehbaz, X. Wang, C. Du, D. Xu, Z.Q. Shi, M.A. Darwish, H.S. Qiu, B.B. Jin, T. Zhou, Y.W. Chen, Q.X. Liang, M.R. Zhang, D. Zhou, Low-permittivity and low-temperature cofired $BaSO_4$–BaF_2 microwave dielectric ceramics for high-reliability packaged electronics, ACS Applied Materials & Interfaces 15 (2023) 51453-51461.

[27] D. Zhou, C. A. Randall, L.X. Pang, H. Wang, J. Guo, G.Q. Zhang, X.G. Wu, L. Shui, X. Yao, Microwave dielectric properties of Li_2WO_4 ceramic with ultra-low sintering temperature, Journal of the American Ceramic Society 94 (2011) 348-350.

[28] D. Zhou, C.A. Randall, H. Wang, L.X. Pang, X. Yao, Microwave dielectric ceramics in Li_2O–Bi_2O_3–MoO_3 system with ultra-low sintering temperatures, Journal of the American Ceramic Society 93 (2010) 1096-1100.

[29] D. Zhou, H. Wang, L.X. Pang, X. Yao, X.G. Wu, Microwave dielectric characterization of a Li_3NbO_4 ceramic and its chemical compatibility with silver, Journal of the American Ceramic Society 91 (2008) 4115-4117.

[30] H. Zhou, X. Chen, L. Fang, D. Chu, H. Wang, A new low-loss microwave dielectric ceramic for low temperature cofired ceramic applications, Journal of Materials Research 25 (2010) 1235-1238.

[31] H. Palneedi, P. Sharief, S.M. Hong, J.W. Kim, M. Uzair, S.C. Jeon, J. Guo, Densification and grain growth in ceramics fabricated by cold sintering: a review on the effect of process parameters, Journal of the American Ceramic Society 109 (2026) e70268.

[32] C. Liu, M. Xu, X. Kang, J. Guo, B. Zhang, H. Wang, X. Xu, H. Jin, H. Wang, Advances in low-temperature Co-fired ceramics for next-generation electronics applications, Advanced Materials n/a (2026) e17514.

[33] H.W. Chen, H. Su, H.W. Zhang, T.C. Zhou, B.W. Zhang, J.F. Zhang, X.L. Tang, Low-temperature sintering and microwave dielectric properties of $(Zn_{1-x}Co_x)_2SiO_4$ ceramics, Ceramics International 40 (2014) 14655-14659.

[34] D.H. Yeon, Y.H. Jo, V.S. Saji, D.H. Kang, Y.S. Cho, Crystallization behavior and microwave dielectric characteristics of ZnO-$(La, Nd)_2O_3$-B_2O_3-based dielectrics, Journal of Electroceramics 23 (2009) 127-132.

[35] D. Thomas, M.T. Sebastian, Temperature-compensated $LiMgPO_4$: a new glass-free low-temperature cofired ceramic, Journal of the American Ceramic Society 93 (2010) 3828-3831.

[36] S.B. Narang, S. Bahel, Low loss dielectric ceramics for microwave applications : a review, Journal of Ceramic Processing Research 11 (2010) 6.

[37] L.L. Yuan, J.J. Bian, Microwave dielectric properties of the lithium containing compounds with rock salt structure, Ferroelectrics 387 (2009) 123-129.

[38] A. Ali, A. Zaman, S.A.A. Aldulmani, M. Abbas, M. Mushtaq, K. Bashir, M. Amami, K. Althubeiti, Structural evolution and microwave dielectric properties of $Ba_{(1-x)}Sr_{(x)}Ti_{(4)}O_{(9)}$, ($0 \le x \le 0.06$) ceramics, ACS Omega 7 (2022) 2331-2336.

[39] W. Wong-Ng, R.S. Roth, T.A. Vanderah, H.F. Mcmurdie, Phase equilibria and crystallography of ceramic oxides, Journal of Research of the National Institute of Standards and Technology 106 (2001) 1097-134.

[40] A. Ali, A. Zaman, S.A.A. Aldulmani, M. Abbas, M. Mushtaq, K. Bashir, M. Amami, K. Althubeiti, Structural evolution and microwave dielectric properties of $Ba_{1-x}Sr_xTi_4O_9$, ($0 \le x \le 0.06$) ceramics, ACS Omega 7 (2022) 2331-2336.

[41] S.F. Wang, Y.C. Hsu, J.P. Chu, C.H. Wu, Hexagonal $Ba(Ti_{1-x}Mn_x)O_3$ ceramics: microstructural evolution and microwave dielectric properties, Applied Physics Letters 88 (2006)

[42] S.I. Hirano, T. Hayashi, A. Hattori, Chemical processing and microwave characteristics of $(Zr,Sn)TiO_4$ microwave dielectrics, Journal of the American Ceramic Society 74 (1991) 1320-1324.

[43] C.L. Wang, H.Y. Lee, F. Azough, R. Freer, The microstructure and microwave dielectric properties of zirconium titanate ceramics in the solid solution system $ZrTiO_4$–$Zr_5Ti_7O_{24}$, Journal of Materials Science 32 (1997) 1693-1701.

[44] K. Wakino, K. Minai, H. Tamura, Microwave characteristics of $(Zr, Sn)TiO_4$ and BaO-PbO-Nd_2O_3-TiO_2 dielectric resonators, Journal of the American Ceramic Society 67 (1984) 278-281.

[45] P.K. Davies, H. Wu, A.Y. Borisevich, I.E. Molodetsky, L. Farber, Crystal chemistry of complex perovskites: new cation-ordered dielectric oxides, Annual Review of Materials Research 38 (2008) 369-401.

[46] I.M. Reaney, D. Iddles, Microwave dielectric ceramics for resonators and filters in mobile phone networks, Journal of the American Ceramic Society 89 (2006) 2063-2072.

[47] K.P. Surendran, M.T. Sebastian, Low loss dielectrics in $Ba[(Mg_{1/3}Ta_{2/3})_{1-x}Ti_x]O_3$ and $Ba[(Mg_{1-x}Zn_x)_{1/3}Ta_{2/3}]O_3$ systems, Journal of Materials Research 20 (2005) 2919-2926.

[48] M.S. Venkatesh, G.S.V. Raghavan, An overview of microwave processing and dielectric properties of agri-food materials, Biosystems Engineering 88 (2004) 1-18.

[49] H. Ohsato, Research and development of microwave dielectric ceramics for wireless communications, Journal of the Ceramic Society of Japan 113 (2005) 703-711.

[50] Y.C. Liou, K.H. Tseng, T.C. Chung, Effect of dopants on synthesis of $BaTi_4O_9$ and $Ba_2Ti_9O_{20}$ ceramics prepared by reaction-sintering process, Journal of the European Ceramic Society 27 (2007) 3027-3032.

[51] L.W. Chu, G.H. Hsiue, Y.J. Chiang, K.S. Liu, I. N. Lin, Ultra-fine $Ba_2Ti_9O_{20}$ microwave dielectric materials synthesized by chemical process, Journal of the European Ceramic Society 24 (2004) 1781-1785.

[52] Z. Wang, X. Yao, L. Zhang, CeO_2-modified $BiNbO_4$ microwave ceramics sintered under atmosphere, Ceramics International 30 (2004) 1329-1333.

[53] F. Liu, J. Li, Y. Sun, Y. Tang, L. Fang, Tuning τf and improving structure stability in Nd_2O_3 microwave dielectric ceramics with Eu^{3+} substitution, Ceramics International 51 (2025) 7370-7376.

[54] M.D. Hill, D.B. Cruickshank, I.A. Macfarlane, Perspective on ceramic materials for 5G wireless communication systems, Applied Physics Letters 118 (2021)

[55] G.Q. He, J.C. Miao, F.F. Wu, W. Wang, J. Bao, J.P. Jiang, D.W. Liu, M.A. Darwish, T. Zhou, D.M. Xu, S. Xia, K.B. Tan, D. Zhou, Advancements in microwave dielectric ceramics with K20 for 5G/6G communication systems: a review, Journal of Materials Chemistry C 13 (2025) 15746-15766.

[56] J. Guo, H. Guo, A.L. Baker, M.T. Lanagan, E.R. Kupp, G.L. Messing, C.A. Randall, Cold sintering: a paradigm shift for processing and integration of ceramics, Angewandte Chemie International Edition 55 (2016) 11457-11461.

[57] H. Guo, A. Baker, J. Guo, C.A. Randall, Cold sintering process: a novel technique for low-temperature ceramic processing of ferroelectrics, Journal of the American Ceramic Society 99 (2016) 3489-3507.

[58] A. Galotta and V.M. Sglavo, The cold sintering process: a review on processing features, densification mechanisms and perspectives, Journal of the European Ceramic Society 41 (2021) 1-17.

[59] M.R. Gongora-Rubio, P. Espinoza-Vallejos, L. Sola-Laguna, J.J. Santiago-Avilés, Overview of low temperature co-fired ceramics tape technology for meso-system technology (MsST), Sensors and Actuators A: Physical 89 (2001) 222-241.

[60] R. Peng, Y. Li, H. Su, Y. Lu, M. Chen, W. Du, B. Liao, Experiment and calculation: the Li(Zn, Mn)PO_4 solid solution ceramics with low dielectric constant, high quality factor, and low densification temperature, Journal of Alloys and Compounds 842 (2020) 155709.

[61] O. Renoult, J.P. Boilot, F. Chaput, R. Papiernik, L.G. Hubert-Pfalzgraf, M. Lejeune, Sol–gel processing and microwave characteristics of $Ba(Mg_{⅓}Ta_{⅔})O_3$ dielectrics, Journal of the American Ceramic Society 75 (1992) 3337-3340.

[62] C.H. Lu, C.C. Tsai, Homogeneous precipitation synthesis and sintering behavior of microwave dielectrics: $Ba(Mg_{1/3}Ta_{2/3})O_3$, Materials Science and Engineering: B 55 (1998) 95-101.

[63] S.J.L. Kang, 14 - Basis of liquid phase sintering, in: S.J.L. Kang (Ed.), Sintering, Butterworth-Heinemann, Oxford, 2005, pp. 199-203.

[64] W.D. Kingery, Densification during sintering in the presence of a liquid phase. I. Theory, Journal of Applied Physics 30 (1959) 301-306.

[65] P.V. Bijumon, M.T. Sebastian, Influence of glass additives on the microwave dielectric properties of $Ca_5Nb_2TiO_{12}$ ceramics, Materials Science and Engineering: B 123 (2005) 31-40.

[66] J. Majling, V. Figusch, F. Hanic, V. Wiglasz, J. Ĉorba, Crystal data and thermal expansion of tricalciumborate, Materials Research Bulletin 9 (1974) 1379-1382.

[67] A.R. West, Phase equilibria in the system Li_2O-CaO-SiO_2, Journal of the American Ceramic Society 61 (1978) 152-155.

[68] P.V. Bijumon, P. Mohanan, M.T. Sebastian, High dielectric constant low loss microwave dielectric ceramics in the $Ca_5Nb_{2-x}Ta_xTiO_{12}$ system, Materials Letters 57 (2003) 1380-1384.

[69] Y. Bisht, A. Pullanchiyodan, D.R. Lekshmi, M. Thirumal, Microwave dielectric properties of (1-x)$Ba(Mg_{1/3}Ta_{2/3})O_3$–(x)$Ba(Mg_{1/8}Ta_{3/4})O_3$ ceramics synthesized by one pot metathesis process, Ferroelectrics 558 (2020) 92-103.

[70] K.P. Surendran, M.T. Sebastian, P. Mohanan, R.L. Moreira, A. Dias, Effect of nonstoichiometry on the structure and microwave dielectric properties of $Ba(Mg_{0.33}Ta_{0.67})O_3$, Chemistry of Materials 17 (2005) 142-151.

[71] E. Ringdalen, M. Tangstad, Softening and melting of SiO_2, an important parameter for reactions with quartz in Si production, in: R.G. Reddy, P. Chaubal, P.C. Pistorius, U. Pal (Ed.), Advances in Molten Slags, Fluxes, and Salts: Proceedings of the 10th International Conference on Molten Slags, Fluxes and Salts, Springer International Publishing, Washington, 2016 pp. 43-51.

[72] J.M. Wu, H.L. Huang, Microwave properties of zinc, barium and lead borosilicate glasses, Journal of Non-Crystalline Solids 260 (1999) 116-124.

[73] P. Zhang, J. Liao, Y. Zhao, X. Zhao, M. Xiao, Effects of B_2O_3 addition on the sintering behavior and microwave dielectric properties of $Li_3Mg_2NbO_6$ ceramics, Journal of Materials Science: Materials in Electronics 28 (2017) 686-690.

[74] W. Wang, C. Liu, L. Shi, G. Wang, H. Zhang, W. Xu, H. Zhang, Effects of Li_2O–B_2O_3–SiO_2–CaO–Al_2O_3 glass addition on the sintering behavior and microwave dielectric properties of $Li_3Mg_2NbO_6$ ceramics, Applied Physics A 125 (2019) 602.

[75] P. Zhang, X. Zhao, Y. Zhao, Effects of MBS addition on the low temperature sintering and microwave dielectric properties of $Li_3Mg_2NbO_6$ ceramics, Journal of Materials Science: Materials in Electronics 27 (2016) 6395-6398.

[76] K.H. Felgner, T. Müller, H.T. Langhammer, H.P. Abicht, Investigations on the liquid phase in barium titanate ceramics with silica additives, Journal of the European Ceramic Society 21 (2001) 1657-1660.

[77] K.P. Surendran, P. Mohanan, M.T. Sebastian, The effect of glass additives on the microwave dielectric properties of $Ba(Mg_{1/3}Ta_{2/3})O_3$ ceramics, Journal of Solid State Chemistry 177 (2004) 4031-4046.

[78] T. Takada, S.F. Wang, S. Yoshikawa, S.J. Jang, R.E. Newnham, Effect of glass additions on BaO–TiO_2–WO_3 microwave ceramics, Journal of the American Ceramic Society 77 (1994) 1909-1916.

[79] T. Takada, S.F. Wang, S. Yoshikawa, S.J. Jang, R.E. Newnham, Effects of glass additions on $(Zr,Sn)TiO_4$ for microwave applications, Journal of the American Ceramic Society 77 (1994) 2485-2488.

[80] D.W. Kim, J.R. Kim, S.H. Yoon, K.S. Hong, C.K. Kim, Microwave dielectric properties of low-fired $Ba_5Nb_4O_{15}$, Journal of the American Ceramic Society 85 (2002) 2759-2762.

[81] Y.H. Zhang, Q.Q. Liu, H.T. Wu, Low-temperature sintering and microwave dielectric properties of H_3BO_3-doped $Li_2Mg_3Ti_{0.95}(Mg_{1/3}Nb_{2/3})_{0.05}O_6$ ceramics, Ceramics International 44 (2018) 17526-17529.

[82] P. Zhang, Y. Hua, W. Xia, L. Li, Effect of H_3BO_3 on the low temperature sintering and microwave dielectric properties of $Li_2ZnTi_3O_8$ ceramics, Journal of Alloys and Compounds 534 (2012) 9-12.

[83] B. Heng, L. Ding, D. Wang, C. Tong, H. Zhu, L. Wang, Y. Hou, Q. Zhang, Low-temperature sintering and microwave dielectric properties of H_3BO_3-added $0.8BaSi_2O_5$–$0.2Ba_3(VO_4)_2$ composite ceramics, Journal of Materials Science: Materials in Electronics 35 (2024) 429.

[84] X. Chen, H. Zhou, L. Fang, D. Chu, C. Li, R. Guo, H. Wang, Microwave dielectric properties and its compatibility with silver electrode of $LiNb_{0.6}Ti_{0.5}O_3$ with B_2O_3 and CuO additions, Journal of Materials Science: Materials in Electronics 22 (2011) 371-375.

[85] J. Zhu, J. Liu, Y. Zeng, Low temperature sintering and microwave dielectric properties of Li_2O–$3ZnO$–$5TiO_2$ ceramics doped with V_2O_5, Journal of Materials Science: Materials in Electronics 29 (2018) 14455-14461.

[86] P. Yan, X. Wang, Z. Cheng, Z. Chen, H. Su, Low-temperature co-firing of $Co_{1.1}Zn_{0.9}TiO_4$ microwave dielectric ceramics by doping with H_3BO_3, Ceramics International 50 (2024) 9931-9936.

[87] D.W. Kim, K.S. Hong, C.S. Yoon, C.K. Kim, Low-temperature sintering and microwave dielectric properties of $Ba_5Nb_4O_{15}$–$BaNb_2O_6$ mixtures for LTCC applications, Journal of the European Ceramic Society 23 (2003) 2597-2601.

[88] C. Zhang, H. Qiu, and Z.X. Xiong, Low-temperature sintering of $Ba_5(Nb_{1-x}V_x)_4O_{15}$ ceramics with H_3BO_3, Key Engineering Materials 368-372 PART 1 (2008) 132-135.

[89] C. Zhang, F. Xiao, H. Qiu, Low temperature sintering of $Ba_5(Nb_{1-x}Sb_x)_4O_{15}$ microwave dielectric ceramics, Electronic Components and Materials 26 (2007) 55.

[90] H. Zhou, H. Wang, M. Zhang, H. Yang, Microwave dielectric properties and compatibility with silver of low-fired $Ba_5Nb_4O_{15}$ ceramics by $BaCu(B_2O_5)$ addition, Journal of Materials Research 25 (2010) 1793-1798.

[91] J. Tang, Y. Wang, M. Deng, F. Zou, H. Yang, D. Liu, Crystal structure, bonding features, and improved low-firing microwave dielectric properties of $Ba_5Nb_4O_{15}$ ceramic, Ceramics International 51 (2025) 25623-25631.

[92] J.R. Kim, D.W. Kim, H.S. Jung, K.S. Hong, Low-temperature sintering and microwave dielectric properties of $Ba_5Nb_4O_{15}$ with ZnB_2O_4 glass, Journal of the European Ceramic Society 26 (2006) 2105-2109.

[93] J.Y. Qiu, C.S. Tu, S.T. Huang, Y. Li, P.Y. Chen, C.S. Chen, R. Montecillo, K.C. Feng, Microwave dielectric and structural characteristics in Li_2O-B_2O_3-SiO_2 glass ceramics, Ceramics International 51 (2025) 22925-22931.

[94] E. Apel, C. Van't Hoen, V. Rheinberger, W. Höland, Influence of ZrO_2 on the crystallization and properties of lithium disilicate glass-ceramics derived from a multi-component system, Journal of the European Ceramic Society 27 (2007) 1571-1577.

[95] W.P. Gong, T. Chen, Z.P. Jin, Thermodynamic calculation of the ZrO_2-TiO_2 phase diagram and the microwave dielectric property, 21 (2001) 93-95.

[96] L. Ueberricke, T. Murata, H. Ikeda, S. Nakane, J. Deubener, Crystal growth in oxide melts—From CALPHAD thermodynamic modeling to statistical prediction, Acta Materialia 273 (2024) 119960.

[97] L.G. Van Uitert, Melting-point relations for simple halides and oxides, Journal of the American Ceramic Society 64 (1981) 544-548.

[98] P. Wang, M. Zhu, Y. Chen, F. Xie, N. Xiao, B. Hou, W. Lu, F. Jiang, W. Zheng, Low loss and low temperature sintering of $Li_3Mg_2NbO_6$ ceramics for LTCC applications, Materials Research Express 6 (2019) 086313.

[99] C.F. Xing, J.X. Bi, H.T. Wu, Effect of Co-substitution on microwave dielectric properties of $Li_3(Mg_{1-x}Co_x)_2NbO_6$ ($0 \le x \le 0.10$) ceramics, Journal of Alloys and Compounds 719 (2017) 58-62.

[100] S. Chen, X. Hu, W. Bao, Z. Wang, Q. Yang, L. Nie, X. Zhang, J. Zhang, Y. Jiang, Y. Han, C. Wan, J. Xie, Y. Yu, W. Liu, Low-sintering-temperature garnet oxides by conformal sintering-aid coating, Cell Reports Physical Science 2 (2021) 100569.

[101] R.D. Shannon, Revised effective ionic radii and systematic studies of interatomic distances in halides and chalcogenides, Acta Crystallographica Section A 32 (1976) 751-767.

[102] D. Szwagierczak, B. Synkiewicz-Musialska, J. Kulawik, E. Czerwińska, N. Pałka, Ultra-low temperature cofired ceramics based on Li2WO4 as perspective substrate materials for terahertz frequencies, Journal of Advanced Ceramics 12 (2023) 526-538.

[103] X.Q. Song, K. Du, J. Li, X.K. Lan, W.Z. Lu, X.H. Wang, W. Lei, Low-fired fluoride microwave dielectric ceramics with low dielectric loss, Ceramics International 45 (2019) 279-286.

[104] J. Yang, R. Liu, X. Xiong, J. Chen, H. Li, Low-temperature sintering and microwave dielectric properties of LiF-doped $Zn_{1.8}SiO_{3.8}$ ceramics, Ceramics International 51 (2025) 13545-13553.

[105] P. Zhang, M. Yang, M. Xiao, Z. Zheng, Sintering behavior and microwave dielectric properties of $Li_2Mg_3Ti(O_{1-x/2}F_x)_6$ ($0.06 \le x \le 0.15$) ceramics for LTCC application, Materials Chemistry and Physics 236 (2019) 121805.

[106] X. Chu, J. Jiang, J. Wang, Y. Wu, L. Gan, T. Zhang, A new high-Q×f Li_4NbO_4F microwave dielectric ceramic for LTCC applications, Ceramics International 47 (2021) 4344-4351.

[107] Z. Zhang, L. Fang, H. Xiang, M. Xu, Y. Tang, H. Jantunen, C. Li, Structural, infrared reflectivity spectra and microwave dielectric properties of the $Li_7Ti_3O_9F$ ceramic, Ceramics International 45 (2019) 10163-10169.

[108] S. George, M.T. Sebastian, Synthesis and microwave dielectric properties of novel temperature stable high Q, $Li_2ATi_3O_8$ (A=Mg, Zn) ceramics, Journal of the American Ceramic Society 93 (2010) 2164-2166.

[109] Y. Tang, L. Fang, H. Zhou, Q. Liu, H. Zhang, Microwave dielectric properties and chemical compatibility with silver electrode of low-fired $Li_2Cu_{0.2}Mg_{0.8}Ti_3O_8$ ceramic, Ceramics International 39 (2013) 8503-8506.

[110] M.M. Haque, M. Huq, M.A. Hakim, Influence of CuO and sintering temperature on the microstructure and magnetic properties of Mg–Cu–Zn ferrites, Journal of Magnetism and Magnetic Materials 320 (2008) 2792-2799.

[111] A. Kan, H. Ogawa, H. Ohsato, J. Sugishita, Influence of M (M=Zn and Ni) substitution for Cu on microwave dielectric characteristics of Yb2Ba($Cu_{1-x}M_x$)O_5 solid solutions, Japanese Journal of Applied Physics 40 (2001) 5774.

[112] J. Zhang and R. Zuo, Effect of ordering on the mMicrowave dielectric properties of spinel-structured $(Zn_{1-x}(Li_{2/3}Ti_{1/3}))_2TiO_4$ ceramics, Journal of the American Ceramic Society 99 (2016) 3343-3349.

[113] D.K. Kwon, M.T. Lanagan, T.R. Shrout, Microwave dielectric properties and low-temperature cofiring of $BaTe_4O_9$ with aluminum metal electrode, Journal of the American Ceramic Society 88 (2005) 3419-3422.
[114] M. Udovic, M. Valant, D. Suvorov, Phase formation and dielectric characterization of the Bi_2O_3–TeO_2 system prepared in an oxygen atmosphere, Journal of the American Ceramic Society 87 (2004) 591-597.
[115] G. Subodh, M.T. Sebastian, Glass-free $Zn_2Te_3O_8$ microwave ceramic for LTCC applications, Journal of the American Ceramic Society 90 (2007) 2266-2268.
[116] M. Yu, Y. Tang, J. Li, W. Fang, L. Duan, L. Fang, Microwave dielectric properties and chemical compatibility with alumina electrode of two novel ultra-low temperature firing $ATeMoO_6$ (A=Mg, Zn) ceramics, Ceramics International 46 (2020) 25619-25625.
[117] Y. Tang, H. Li, J. Li, H. Xiang, L. Fang, Microwave dielectric properties of $Li_3A_3Te_2O_{12}$ (A=Y, Yb) garnets for low temperature cofired ceramic technologies, Journal of the European Ceramic Society 42 (2022) 2248-2253.
[118] K.R. Park, S. Kim, N.V. Myung, S.O. Kang, Y.H. Choa, Simple electrochemical synthesis of ultra-long silver telluride nanotubes, RSC Advances 5 (2015) 29782-29785.
[119] M. Valant, D. Suvorov, Chemical compatibility between silver electrodes and low-firing binary-oxide compounds: conceptual study, Journal of the American Ceramic Society 83 (2000) 2721-2729.
[120] M. Nakayama, M. Kotobuki, H. Munakata, M. Nogami, K. Kanamura, First-principles density functional calculation of electrochemical stability of fast Li ion conducting garnet-type oxides, Physical Chemistry Chemical Physics 14 (2012) 10008-10014.
[121] Y. Sheng, Y. Wu, C. Jiang, X. Cui, Y. Mao, C. Ye, W. Zhang, Interpretable model of dielectric constant for rational design of microwave dielectric materials: a machine learning study, Journal of Materials Informatics 5 (2025) 7.
[122] H. Hu, Y. Wang, C. Cai, P. Zhang, X. Chen, R. Xiang, H. Li, $BaMnV_2O_7$：a novel microwave dielectric ceramic for LTCC applications, Ceramics International 47 (2021) 31506-31511.
[123] H. Cao, L. Chen, B. Li, A new microwave dielectric ceramic $Zn_2V_2O_7$ with low sintering temperature, Materials Letters 326 (2022) 132924.
[124] C. Yin, C. Li, G. Yang, L. Fang, Y. Yuan, L. Shu, J. Khaliq, $NaCa_4V_5O_{17}$: a low-firing microwave dielectric ceramic with low permittivity and chemical compatibility with silver for LTCC applications, Journal of the European Ceramic Society 40 (2020) 386-390.
[125] P.J. Tseng, C.F. Tseng, W.H. Chang, B.Z. Huang, C.H. Han, Microwave dielectric properties and bond characteristics of glass-free low permittivity $LiVO_3$ ULTCC ceramics, Ceramics International 50 (2024) 39202-39211.
[126] Q. Du, Y. Tang, J. Li, W. Fang, A. Yang, J. Chen, L. Fang, A low-ε_r and high-Q microwave dielectric ceramic Li_2SrSiO_4 with abnormally low sintering temperature, Journal of the European Ceramic Society 41 (2021) 7678-7682.
[127] H. Jantunen, R. Rautioaho, A. Uusimäki, S. Leppävuori, Compositions of $MgTiO_3$-$CaTiO_3$ ceramic with two borosilicate glasses for LTCC technology, Journal of the European Ceramic Society 20 (2000) 2331-2336.
[128] J.J. Bian, Y.F. Dong, New high Q microwave dielectric ceramics with rock salt structures: $(1-x)Li_2TiO_3+xMgO$ system ($0\leq x\leq 0.5$), Journal of the European Ceramic Society 30 (2010) 325-330.
[129] H. Ogawa, A. Yokoi, R. Umemura, A. Kan, Microwave dielectric properties of $Mg_3(VO_4)_2$–$_xBa_3(VO_4)_2$ ceramics for LTCC with near zero temperature coefficient of resonant frequency, Journal of the European Ceramic Society 27 (2007) 3099-3104.
[130] R.C. Pullar, S. Farrah, N.M. Alford, $MgWO_4$, $ZnWO_4$, $NiWO_4$ and $CoWO_4$ microwave dielectric ceramics, Journal of the European Ceramic Society 27 (2007) 1059-1063.

[131] W. Bian, X. Lu, Y. Wang, H. Zhu, T. Chen, S. Ta, Q. Zhang, Correlations between structure and microwave dielectric properties of Co doped $MgMoO_4$ ceramics, Ceramics International 46 (2020) 22024-22029.
[132] E.S. Kim, C.J. Jeon, P.G. Clem, Effects of crystal structure on the microwave dielectric properties of ABO_4 (A=Ni, Mg, Zn and B=Mo, W) ceramics, Journal of the American Ceramic Society 95 (2012) 2934-2938.
[133] X.G. Wu, H. Wang, Y.H. Chen, D. Zhou, Synthesis and microwave dielectric properties of $Zn_3B_2O_6$ ceramics for substrate application, Journal of the American Ceramic Society 95 (2012) 1793-1795.
[134] U. Došler, M.. Kržmanc, B. Jančar, D. Suvorov, A high-Q microwave dielectric material based on $Mg_3B_2O_6$, Journal of the American Ceramic Society 93 (2010) 3788-3792.
[135] Y.H. Lee, J.H. Cho, B.I. Kim, D.K. Choi, Piezoelectric properties and densification based on control of volatile mass of potassium and sodium in $(K_{0.5}Na_{0.5})NbO_3$ ceramics, Japanese Journal of Applied Physics 47 (2008) 4620.
[136] Y. Wu, G. Wang, Z. Jiao, Y. Fan, P. Peng, X. Dong, High electrostrictive properties and energy storage performances with excellent thermal stability in Nb-doped $Bi_{0.5}Na_{0.5}TiO_3$-based ceramics, RSC Advances 9 (2019) 21355-21362.
[137] X. Huang, Y. Lu, Z. Song, K. Rui, Q. Wang, T. Xiu, M. E. Badding, Z. Wen, Manipulating Li_2O atmosphere for sintering dense $Li_7La_3Zr_2O_{12}$ solid electrolyte, Energy Storage Materials 22 (2019) 207-217.
[138] M.H. Lee, D.J. Kim, J.S. Park, S.W. Kim, T.K. Song, M.H. Kim, W.J. Kim, D. Do, I.K. Jeong, High-performance lead-free piezoceramics with high Curie temperatures, Advanced Materials 27 (2015) 6976-6982.
[139] W. Sakamoto, N. Makino, B.Y. Lee, T. Iijima, M. Moriya, T. Yogo, Influence of volatile element composition and Mn doping on the electrical properties of lead-free piezoelectric $(Bi_{0.5}Na_{0.5})TiO_3$ thin films, Sensors and Actuators A: Physical 200 (2013) 60-67.
[140] C. Duran, S. Trolier-Mckinstry, G.L. Messing, Processing and electrical properties of $0.5Pb(Yb_{1/2}Nb_{1/2})O_3$-$0.5PbTiO_3$ ceramics, Journal of Electroceramics 10 (2003) 47-55.
[141] D. Pérez-Mezcua, M.L. Calzada, I. Bretos, J. Ricote, R. Jiménez, L. Fuentes-Cobas, R. Escobar-Galindo, D. Chateigner, R. Sirera, Influence of excesses of volatile elements on structure and composition of solution derived lead-free $(Bi_{0.50}Na_{0.50})_{1x}Ba_xTiO_3$ thin films, Journal of the European Ceramic Society 36 (2016) 89-100.
[142] M. Yu, S. Grasso, R. Mckinnon, T. Saunders, M.J. Reece, Review of flash sintering: materials, mechanisms and modelling, Advances in Applied Ceramics 116 (2017) 24-60.
[143] N.J. Lóh, L. Simão, C.A. Faller, A. De Noni, O.R.K. Montedo, A review of two-step sintering for ceramics, Ceramics International 42 (2016) 12556-12572.
[144] Z. Shen, Z. Zhao, H. Peng, M. Nygren, Formation of tough interlocking microstructures in silicon nitride ceramics by dynamic ripening, Nature 417 (2002) 266-269.
[145] T. Ebadzadeh, M. Valefi, Microwave-assisted sintering of zircon, Journal of Alloys and Compounds 448 (2008) 246-249.
[146] J. Guo, R. Floyd, S. Lowum, J.P. Maria, T.H. De Beauvoir, J.H. Seo, C.A. Randall, Cold sintering: progress, challenges, and future opportunities, Annual Review of Materials Research 49 (2019) 275-295.
[147] X. Zhao, J. Guo, K. Wang, T.H. De Beauvoir, B. Li, C.A. Randall, Introducing a ZnO-PTFE (polymer) nanocomposite varistor via the cold sintering process, Advanced Engineering Materials 20 (2018) 1700902.
[148] W.D. Kingery, J.M. Woulbroun, F.R. Charvat, Effects of applied pressure on densification during sintering in the presence of a liquid phase, Journal of the American Ceramic Society 46 (1963) 391-395.
[149] D. Wang, L. Li, J. Jiang, Z. Lu, G. Wang, K. Song, D. Zhou, I.M. Reaney, Cold sintering of microwave dielectric ceramics and devices, Journal of Materials Research 36 (2021) 333-349.

[150] T. Okazaki, T. Sada, K. Tsuji, Y. Fujioka, C.A. Randall, $BaTiO_3$-based composites provide new opportunities enabled with the cold sintering process, Japanese Journal of Applied Physics (2023)

[151] T. Sada, K. Tsuji, A. Ndayishimiye, Z. Fan, Y. Fujioka, C.A. Randall, High permittivity $BaTiO_3$ and $BaTiO_3$-polymer nanocomposites enabled by cold sintering with a new transient chemistry: $Ba(OH)_2{\cdot}8H_2O$, Journal of the European Ceramic Society 41 (2021) 409-417.

[152] T. Sada, K. Tsuji, A. Ndayishimiye, Z. Fan, Y. Fujioka, C.A. Randall, Highly reliable $BaTiO_3$-polyphenylene oxide nanocomposite dielectrics via cold sintering, Advanced Materials Interfaces 8 (2021) 2100963.

[153] Y. Ji, K. Song, X. Luo, B. Liu, H. Barzegar Bafrooei, D. Wang, Microwave dielectric properties of $(1\text{-}x)Li_2MoO_4$–xMg_2SiO_4 composite ceramics fabricated by cold sintering process, Frontiers in Materials Volume 6 - 2019 (2019)

[154] D. Wang, D. Zhou, S. Zhang, Y. Vardaxoglou, W.G. Whittow, D. Cadman, I.M. Reaney, Cold-sintered temperature stable $Na_{0.5}Bi_{0.5}MoO_4$–Li_2MoO_4 microwave composite ceramics, ACS Sustainable Chemistry & Engineering 6 (2018) 2438-2444.

[155] J. Guo, N. Pfeiffenberger, A. Beese, A. Rhoades, L. Gao, A. Baker, K. Wang, A. Bolvari, C.A. Randall, Cold sintering $Na_2Mo_2O_7$ ceramic with poly(ether imide) (PEI) polymer to realize high-performance composites and integrated multilayer circuits, ACS Applied Nano Materials 1 (2018) 3837-3844.

[156] A.R.H. Alzakree, C.H. Wang, M. Shehbaz, W. Wang, M.A. Darwish, T. Zhou, D.M. Xu, C. Du, D. Zhou, Microwave dielectric properties of temperature-stable $(Na_{0.5}Bi_{0.5})MoO_4$–$SrMoO_4$ ceramics sintered at ultra-low temperature, Journal of the American Ceramic Society 108 (2025) e20504.

[157] D. Wang, J. Chen, G. Wang, Z. Lu, S. Sun, J. Li, J. Jiang, D. Zhou, K. Song, I.M. Reaney, Cold sintered $LiMgPO_4$ based composites for low temperature co-fired ceramic (LTCC) applications, Journal of the American Ceramic Society 103 (2020) 6237-6244.

[158] M. Chi, Y. Liu, J. Zhao, C. Dong, X. Luo, D. Wang, B. Liu, M. Mao, F. Shi, and K. Song, $Mg_3B_2O_6$ microwave dielectric ceramics fabricated by combining cold sintering with post-annealing process, Journal of the American Ceramic Society 106 (2023) 285-292.

[159] K. Aicher, T. Berger, U. Aschauer, O. Diwald, Activation and cold sintering of commercial ZnO powders: compaction-induced oxide reduction, Journal of the European Ceramic Society 46 (2026) 117769.

[160] H. Kähäri, M. Teirikangas, J. Juuti, H. Jantunen, Dielectric properties of lithium molybdate ceramic fabricated at room temperature, Journal of the American Ceramic Society 97 (2014) 3378-3379.

[161] M.F. Zhou, Y. Jiang, B. Liu, K.X. Song, F. Shi, Cold sintering optimized LiF microwave dielectric ceramics for the development of dielectric resonator antennas at 5G millimeter-wave band, Journal of Materials Science: Materials in Electronics 33 (2022) 20012-20020.

[162] J.P. Yuan, N. Chen, C.C. Hu, B. Liu, K.X. Song, Enhanced microwave dielectric properties in one-step cold sintered LiF ceramics via pre-calcination treatment, Ceramics International 50 (2024) 51625-51630.

[163] Z. Zeng, J. Cheng, X. Xu, H. Wang, Y. Lu, L. Sun, N. Chen, X. Li, B. Zhang, H. Wang, Room-temperature densified Al_2O_3-H_3BO_3 ceramics with excellent microwave dielectric properties and thermal conductivity for chip packaging, Journal of Materiomics 11 (2025) 101069.

[164] T. Zhou, Y. Liu, K. Song, L. Xue, P. Xu, A. Khesro, D. Wang, B. Liu, M. Mao, F. Shi, S. Sun, New low-ε_r, temperature stable $Mg_3B_2O_6$-$Ba_3(VO_4)_2$ microwave composite ceramic for 5G application, Journal of the American Ceramic Society 104 (2021) 3818-3822.

[165] B. Liu, L. Li, K.X. Song, M.M. Mao, Z. Lu, G. Wang, L. Li, D. Wang, D. Zhou, A. Feteira, I.M. Reaney, Enhancement of densification and microwave dielectric properties in LiF ceramics via a cold sintering and post-annealing process, Journal of the European Ceramic Society 41 (2021) 1726-1729.

[166] C. Li, Y. Liu, M. Chi, X. Luo, B. Liu, M. Mao, H.B. Bafrooei, G. Wang, E. Taheri-Nassaj, K. Song, ULTCC post-annealing cold sintering densification process, microwave dielectric properties of $Zn_3B_2O_6$ ceramics, Materials Today Communications 33 (2022) 104997.
[167] D.H. Jin, B. Liu, K.X. Song, K.W. Xu, Y.H. Huang, C.C. Hu, Y.Y. Hu, Boosting densification and microwave dielectric properties in cold sintered BaF_2 ceramics for 5.8 GHz WLAN applications, Journal of Alloys and Compounds 886 (2021) 161141.
[168] B. Liu, K. Sha, M.F. Zhou, K.X. Song, C.C. Hu, C. Lu, Cold sintering assisted CaF_2 microwave dielectric ceramics for C-band antenna applications, Journal of the European Ceramic Society 42 (2022) 5698-5704.
[169] E. Zhao, J. Hao, X. Xue, M. Si, J. Guo, H. Wang, Rutile TiO_2 microwave dielectric ceramics prepared via cold sintering assisted two step sintering, Journal of the European Ceramic Society 41 (2021) 3459-3465.
[170] C. Liu, L. Zhang, J. Peng, W. Qu, B. Liu, H. Xia, J. Zhou, Dielectric properties and microwave heating characteristics of sodium chloride at 2.45 GHz, 32 (2013) 587-596.
[171] C. Burda, X. Chen, R. Narayanan, M.A. El-Sayed, Chemistry and properties of nanocrystals of different shapes, Chemical Reviews 105 (2005) 1025-1102.
[172] H. Guo, J. Guo, A. Baker, C.A. Randall, Hydrothermal-assisted cold sintering process: a new guidance for low-temperature ceramic sintering, ACS Applied Materials & Interfaces 8 (2016) 20909-20915.
[173] T. Sada, Z. Fan, A. Ndayishimiye, K. Tsuji, S.H. Bang, Y. Fujioka, C.A. Randall, In situ doping of $BaTiO_3$ and visualization of pressure solution in flux-assisted cold sintering, Journal of the American Ceramic Society 104 (2021) 96-104.
[174] N. Salidkul, S. Pinitsoontorn, Cold sintering process for densification of Fe_3O_4 ceramic magnets with improved properties, Ceramics International 50 (2024) 10873-10880.
[175] X. Wen, H. Xiang, X. Mo, Q. Li, Y. Tang, L. Fang, Crystal structure, bond valence, thermal and microwave dielectric properties of $Y_{3+x}Ga_{5-x}O_12$ ceramics, Ceramics International 51 (2025) 7069-7074.
[176] Y. Zhang, J. Chen, J. Chen, Y. Zhou, X. Wu, Y. Tang, L. Fang, H. Xiang, Crystal structure, phase compositions and microwave dielectric properties of $Gd_{1-x}Ca_xV_{1-x}Mo_xO_4$ ceramics, Ceramics International 51 (2025) 20124-20130.
[177] X. Mo, H. Xiang, Q. Li, Y. Tang, L. Fang, Chemical bond characteristics, phase evolution and microwave dielectric properties of $Sm_{3-x}Ca_xGa_{5-x}Zr_xO_{12}$ ceramics with ultra-low loss, Journal of the European Ceramic Society 45 (2025) 117143.
[178] X. Gu, Y. Tang, J. Chen, P. Qing, N. Zhang, S. Zhang, L. Fang, Tuning microwave dielectric properties of low-temperature sintered $Ca_{1-x}(Li_{0.5}Eu_{0.5})_xMoO_4$ ($0 \leq x \leq 0.5$) ceramics by the strong rattling effect of Li^+, Journal of the European Ceramic Society 45 (2025) 117149.
[179] J. Guo, S.S. Berbano, H. Guo, A.L. Baker, M.T. Lanagan, C.A. Randall, Cold sintering process of composites: bridging the processing temperature gap of ceramic and polymer materials, Advanced Functional Materials 26 (2016) 7115-7121.
[180] B. Zhao, X. Chen, N. Chen, X. Xu, Y. Lu, J. Cheng, H. Wang, Low-temperature-sintered MgO-based microwave dielectric ceramics with ultralow loss and high thermal conductivity, Journal of the American Ceramic Society 106 (2023) 1159-1169.
[181] T. Katsube, Sintered body of low temperature cofired ceramic (LTCC) and multilayer ceramic substrate, EP2397452B1, 17.05.2017.
[182] L. Murata Manufacturing Co., "Murata value report 2024," in "Murata Value Report (Integrated Report)," Murata Manufacturing Co., Ltd., Kyoto, Japan, Integrated report Apr 1, 2023–Mar 31, 2024 2024.
[183] T. Ibn-Mohammed, C.A. Randall, K.B. Mustapha, J. Guo, J. Walker, S. Berbano, S.C.L. Koh, D. Wang, D.C. Sinclair, I.M. Reaney, Decarbonising ceramic manufacturing: a techno-economic analysis of energy efficient sintering technologies in the functional materials sector, Journal of the European Ceramic Society 39 (2019) 5213-5235.

[184] E.A. Blum; E.J.P. Lelong, Method for LTCC zero *X–Y* shrinkage., PCT/IB2004/003305, 2025.
[185] K. Yin, P. Deng, Sub-6G LTCC RF front-end microsystem, CN 114006629 A, 2022.
[186] P. Ltd., "LTCC technology overview," PRFI Ltd., The Plextek Building, London Road, Great Chesterford, Saffron Walden, CB10 1NY, UK, echnical Report / Technology Overview Sheet Code 0629 2022.
[187] O. Otani, H. Tanaka, R. Shibata, K. Furukawa, H. Masumura, S. Fujiwara, Dielectric ceramic composition, JPS51143898A, Dec. 10, 1976.
[188] E.S. Tormey, P. Marley, C. Ma, J. Maloney, Y. Yang, O.W. Brown, S. Sridharan, M7 LTCC-silver system and related dielectric compositions for high frequency applications, US 2022/0119315 A1, 2022
[189] N. Joseph, J. Varghese, M. Teirikangas, T. Vahera, H. Jantunen, Ultra-low-temperature cofired ceramic substrates with low residual carbon for next-generation microwave applications, ACS Applied Materials & Interfaces 11 (2019) 23798-23807.
[190] B. Wang, X. Song, Low-loss perovskite-based ultra-low-temperature sintered microwave dielectric ceramic material, and its preparation method and application, CN 108911746 A, 2018
[191] L. Fang, J. Deng, Y. Tang, Low-temperature sinterable microwave dielectric ceramic Li_2MoO_4 and its preparation method, CN 103145419 B, 2014-07-02.
[192] N. Kireeva, V.P. Solov'ev, Machine learning analysis of microwave dielectric properties for seven structure types: the role of the processing and composition, Journal of Physics and Chemistry of Solids 156 (2021) 110178.
[193] A. Takahashi, Y. Kumagai, J. Miyamoto, Y. Mochizuki, F. Oba, Machine learning models for predicting the dielectric constants of oxides based on high-throughput first-principles calculations, Physical Review Materials 4 (2020) 103801.
[194] L. Mo, J. Qin, M. Ma, Z. Liu, Machine learning assisted $Q\times f$ value prediction of ABO_4-type microwave dielectric ceramics, Journal of Materiomics 11 (2025) 100926.
[195] Z. Liu, C. Qian, X. Yang, Machine learning-driven dielectric constant prediction for rock-salt structured microwave dielectric ceramics, Journal of Alloys and Compounds 1044 (2025) 184460.
[196] J. Qin, Z. Liu, M. Ma, Y. Li, Machine learning approaches for permittivity prediction and rational design of microwave dielectric ceramics, Journal of Materiomics 7 (2021) 1284-1293.
[197] M. Yang, L. Mo, J. Qin, F. Zhang, M. Ma, Y. Li, Z. Liu, Machine learning assisted τ_f value prediction of ABO_3-type microwave dielectric ceramics, Journal of Materiomics 12 (2026) 101117.
[198] X. Wang, W. Zhang, W. Zhang, Dielectric ceramics database automatically constructed by data mining in the literature, J Chem Inf Model 64 (2024) 5931-5943.
[199] A.G. Kusne, H. Yu, C. Wu, H. Zhang, J. Hattrick-Simpers, B. Decost, S. Sarker, C. Oses, C. Toher, S. Curtarolo, A.V. Davydov, R. Agarwal, L.A. Bendersky, M. Li, A. Mehta, I. Takeuchi, On-the-fly closed-loop materials discovery via Bayesian active learning, Nature Communications 11 (2020) 5966.
[200] A. Dunn, Q. Wang, A. Ganose, D. Dopp, A. Jain, Benchmarking materials property prediction methods: the Matbench test set and Automatminer reference algorithm, npj Computational Materials 6 (2020) 138.
[201] Y.T. Huang, T.H. Hsu, C.L. Huang, Low-loss and ultra-low temperature sintering microwave dielectrics of pure and Ag-modified $K_2Mg_2(MoO_4)_3$ ceramics, Journal of the European Ceramic Society 42 (2022) 7004-7009.
[202] Y.B. Chen, S. Xiong, Raman spectra and microwave dielectric properties of $Na_5Tm_{1-x}(Y_{1/3}Yb_{2/3})_x(MoO_4)_4$ ceramics with ultra-low sintering temperature, Scientific Reports 15 (2025) 6644.
[203] J. Andrews, D. Button, I.M. Reaney, Advances in cold sintering, Johnson Matthey Technology Review 64 (2020) 219-232.

[204] F.I.F.C.T.A.S. Ikts. "ULTCC ceramics (Ultra Low Temperature Co-fired Ceramics)." https://www.ikts.fraunhofer.de/en/departments/electronics_microsystems_biomedicine/hybrid_micro_systems/Microsystems_LTCCHTCC/ultcc_ceramics.html (accessed 2026-05-08.

[205] T.U. Berlin. "NAT-ULTCC (Sustainable ULTCC Multilayer Ceramics for a Green Future)." https://www.tu.berlin/en/iit/research/projects/nat-ultcc (accessed 2026-05-08.

[206] M. Olszewska-Placha, J. Varghese, D. Szwagierczak, M. Birgit, S. Ziesche, J. Rudnicki, B. Synkiewicz-Musialska, Bulk glass-ceramic composites and ULTCC substrates for microwave and millimetre-wave applications, Materials Research Bulletin 177 (2024) 112862.

[207] M. Alain, Mapping the transition of the EU ceramic industry to carbon neutrality, European Commission, Petten, 2026, JRC144122.

[208] M. Franz, M. Weilguni, Life cycle inventories of LTCC substrates, Proceedings of the 2011 34th International Spring Seminar on Electronics Technology (ISSE), Slovakia, 2011, doi: 10.1109/ISSE.2011.6053939.

[209] A. Ndayishimiye, M.Y. Sengul, T. Sada, S. Dursun, S.H. Bang, Z.A. Grady, K. Tsuji, S. Funahashi, A.C.T. Van Duin, C.A. Randall, Roadmap for densification in cold sintering: chemical pathways, Open Ceramics 2 (2020) 100019.

[210] M. Lahti, K. Kautio, M. Karppinen, K. Keränen, J. Ollila, P. Karioja, Review of LTCC technology for millimeter waves and photonics, INTL JOURNAL OF ELECTRONICS AND TELECOMMUNICATIONS 66 (2020) 361-367.

[211] B. Sheng, S. Liao, and Q. Xue, LTCC-based wideband patch antenna for 5G millimeter-wave applications, 2024 International Conference on Microwave and Millimeter Wave Technology (ICMMT) 1 (2024) 1-3.

[212] D. Wang, D. Zhou, K. Song, A. Feteira, C.A. Randall, I.M. Reaney, Cold-sintered C0G multilayer ceramic capacitors, Advanced Electronic Materials 5 (2019) 1900025.

[213] X. Wang, H. Su, Z. Cheng, F. Qiao, X. Yang, Y. Chen, M. Qu, X. Tang, Low-temperature sintering behavior and microwave dielectric properties of $LiGaW_2O_8$ ceramic materials in LTCC technology, Ceramics International 51 (2025) 42196-42200.

[214] Z. Chen, S. Xu, H. Zhu, W. Feng, W. Che, Q. Xue, High-performance millimeter-wave front-end module using LTCC technology, 2022 23rd International Conference on Electronic Packaging Technology (ICEPT) (2022) 1-5.

[215] H.R.O. Rocha, R. Roukos, S. Abou Dargham, J. Romanos, D. Chaumont, J.A.L. Silva, H. Wörtche, Optimizing a machine learning design of dielectric properties in lead-free piezoelectric ceramics, Materials & Design 243 (2024) 113053.

[216] L. Ma, L. Jiang, J. Duan, Q. Du, K. Wei, H. Li, Enhanced microwave performance in spinel dielectric ceramics using entropy strategy for 5G/6G communication devices, Chemical Engineering Journal 503 (2025) 158159.

[217] N.J. Szymanski, B. Rendy, Y. Fei, R.E. Kumar, T. He, D. Milsted, M.J. Mcdermott, M. Gallant, E.D. Cubuk, A. Merchant, H. Kim, A. Jain, C.J. Bartel, K. Persson, Y. Zeng, G. Ceder, An autonomous laboratory for the accelerated synthesis of novel materials, Nature 624 (2023) 86-91.

[218] Y. Jia, T.D. Ajayi, B.H. Wahls, K.R. Ramakrishnan, S. Ekkad, C. Xu, Multifunctional ceramic composite system for simultaneous thermal protection and electromagnetic interference shielding for carbon fiber-Reinforced polymer composites, ACS Applied Materials & Interfaces 12 (2020) 58005-58017.

2115